

AD-A184 697

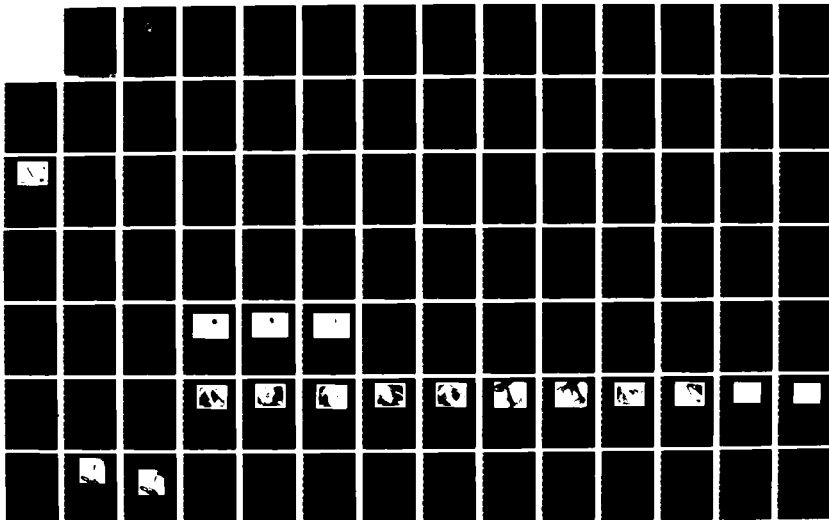
DETERMINATION OF THE ORIGIN OF SELF-PUMPED PHASE  
CONJUGATION IN BARIUM TITANATE(U) NAVAL POSTGRADUATE  
SCHOOL MONTEREY CA T R MOORE JUN 87

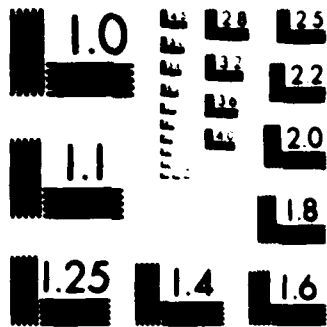
1/2

UNCLASSIFIED

F/G 28/2

NL





MICROCOPY RESOLUTION TEST CHART  
NATIONAL BUREAU OF STANDARDS-1963-A

AD-A184 697

NAVAL POSTGRADUATE SCHOOL  
Monterey, California

2

OTIC FILE COPY



THESIS

DETERMINATION OF THE ORIGIN OF  
SELF-PUMPED PHASE CONJUGATION IN  
BARIUM TITANATE

by

Thomas R. Moore

June 1987

Thesis Advisor

Donald E. Walters

Approved for public release; distribution is unlimited.

87 9 23 236



SEP 25 1987

A

206

AD A104 697

REPORT DOCUMENTATION PAGE

1a REPORT SECURITY CLASSIFICATION <b>UNCLASSIFIED</b>		1b. RESTRICTIVE MARKINGS	
2a SECURITY CLASSIFICATION AUTHORITY		3 DISTRIBUTION/AVAILABILITY OF REPORT Approved for public release; distribution is unlimited	
2b DECLASSIFICATION/DOWNGRADING SCHEDULE		5 MONITORING ORGANIZATION REPORT NUMBER(S)	
4 PERFORMING ORGANIZATION REPORT NUMBER(S)		7a. NAME OF MONITORING ORGANIZATION Naval Postgraduate School	
6a. NAME OF PERFORMING ORGANIZATION Naval Postgraduate School	6b OFFICE SYMBOL (if applicable) 61	7b. ADDRESS (City, State, and ZIP Code) Monterey, California 93943-5000	
6c. ADDRESS (City, State, and ZIP Code) Monterey, California 93943-5000		9 PROCUREMENT INSTRUMENT IDENTIFICATION NUMBER	
8a NAME OF FUNDING/SPONSORING ORGANIZATION	8b OFFICE SYMBOL (if applicable)	10 SOURCE OF FUNDING NUMBERS	
8c ADDRESS (City, State, and ZIP Code)		PROGRAM ELEMENT NO	PROJECT NO
		TASK NO	WORK UNIT ACCESSION NO
11 TITLE (Include Security Classification) DETERMINATION OF THE ORIGIN OF SELF-PUMPED PHASE CONJUGATION IN BARIUM TITANATE			
12 PERSONAL AUTHOR(S) Moore, Thomas R.			
13a TYPE OF REPORT Master's Thesis	13b TIME COVERED FROM _____ TO _____	14 DATE OF REPORT (Year, Month, Day) 1987 June	15 PAGE COUNT 98
16 SUPPLEMENTARY NOTATION			
17 COSATI CODES		18 SUBJECT TERMS (Continue on reverse if necessary and identify by block number)	
FIELD	GROUP	Phase-conjugation, Barium Titanate, Photorefractors	
	SUB-GROUP	Stimulated Photorefractive Scattering	
19 ABSTRACT (Continue on reverse if necessary and identify by block number)			
<p style="text-align: center;">Barium titanate</p> <p>When a beam of extraordinarily polarized light is directed through a poled, single crystal of <math>\text{BaTiO}_3</math> it fans in the direction of the optic axis. This thesis research investigates the origin of this fanning, or asymmetric self-defocusing, in barium titanate. Experimental observations and theoretical simulation suggest that this phenomenon is due to near forward stimulated photorefractive scattering. Additionally, observations of unique variegated beam patterns during phase conjugation are reported, including internally pumped rings and motion invariant patterns.</p>			
20 DISTRIBUTION/AVAILABILITY OF ABSTRACT <input checked="" type="checkbox"/> UNCLASSIFIED/UNLIMITED <input type="checkbox"/> SAME AS RPT <input type="checkbox"/> DTIC USERS		21 ABSTRACT SECURITY CLASSIFICATION UNCLASSIFIED	
22a NAME OF RESPONSIBLE INDIVIDUAL Donald L. Walters		22b TELEPHONE (Include Area Code) 408 -646-2267	22c OFFICE SYMBOL 61We

Approved for public release; distribution is unlimited.

Determination of the Origin of  
Self-Pumped Phase Conjugation in  
Barium Titanate

by

Thomas R. Moore  
Captain, United States Army  
B.S., Stetson University, 1978

Submitted in partial fulfillment of the  
requirements for the degree of

MASTER OF SCIENCE IN PHYSICS

from the

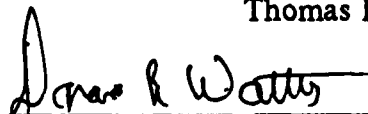
NAVAL POSTGRADUATE SCHOOL  
June 1987

Author:

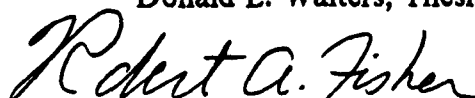


Thomas R. Moore

Approved by:



Donald L. Walters, Thesis Advisor



Robert A. Fisher, Second Reader



K. E. Woehler, Chairman,  
Department of Physics



Gordon E. Schacher,  
Dean of Science and Engineering

## ABSTRACT

When a beam of extraordinarily polarized light is directed through a poled, single crystal of  $\text{BaTiO}_3$  it fans in the direction of the optic axis. This thesis research investigates the origin of this fanning, or asymmetric self-defocusing, in barium titanate. Experimental observations and theoretical simulation suggest that this phenomenon is due to near forward stimulated photorefractive scattering. Additionally, observations of unique variegated beam patterns during phase conjugation are reported, including internally pumped rings and motion invariant patterns.



Accession For	
NTIS GRISI	<input checked="" type="checkbox"/>
DTIC TAB	<input type="checkbox"/>
Unannounced	<input type="checkbox"/>
Justification	

11

## TABLE OF CONTENTS

I.	INTRODUCTION .....	9
II.	BACKGROUND AND THEORY .....	11
	A. INTRODUCTION .....	11
	B. ORIGINS OF THE PHASE-CONJUGATE BEAM .....	11
	1. Four-Wave Mixing .....	13
	2. Scattering .....	16
	C. DISTORTION CORRECTION BY PHASE CONJUGATION .....	19
	D. PHOTOREFRACTORS AND FOUR WAVE MIXING .....	20
	E. STIMULATED PHOTOREFRACTIVE SCATTERING .....	23
	F. BARIUM TITANATE .....	24
	1. The Crystal .....	24
	2. Beam Fanning .....	25
	3. Self Pumped Phase Conjugation .....	29
III.	PSIM: A SIMULATION OF THE PHOTOREFRACTIVE EFFECT IN BARIUM TITANATE .....	31
	A. INTRODUCTION .....	31
	B. THEORY .....	31
	C. THE SIMULATION .....	32
	1. Program Logic .....	32
	2. Limitations .....	33
	D. RESULTS .....	35
	E. DISCUSSION .....	38
IV.	EXPERIMENTS .....	46
	A. INTRODUCTION .....	46
	B. EXPERIMENTAL APPARATUS .....	46
	C. EXPERIMENTAL PROCEDURE .....	47

D.	RESULTS .....	48
V.	ANALYSIS .....	60
A.	DISCUSSION OF RESULTS .....	60
B.	SCATTERING .....	61
C.	SELF PUMPED PHASE CONJUGATION .....	63
VI.	CONCLUSIONS .....	65
APPENDIX A:	INTERNAL BEAM PRODUCTION .....	66
1.	INTRODUCTION .....	66
2.	EXPERIMENTAL APPARATUS .....	67
3.	RESULTS AND ANALYSIS OF DATA .....	70
a.	Experimental variables .....	70
b.	Complex Auxiliary Beam Patterns .....	71
c.	Temporal Effects and Frequency Shifts .....	77
d.	The Free Standing Auxiliary Beam Pattern .....	82
APPENDIX B:	PSIM LISTING .....	85
LIST OF REFERENCES	.....	94
INITIAL DISTRIBUTION LIST	.....	97



## LIST OF FIGURES

2.1	Schematic of the process of four-wave mixing [Ref. 5: p.421] . . . . .	14
2.2	Index grating formation due to the photorefractive effect [Ref. 5] . . . . .	22
2.3	Formation of an optical cavity with a phase conjugate mirror [Ref. 5] . . . . .	23
2.4	BaTiO <sub>3</sub> exhibiting SPPC . . . . .	26
2.5	The process of beam fanning due to photorefraction for a single incident beam [Ref. 27] . . . . .	27
2.6	The process of SPS [Ref. 24] . . . . .	28
3.1	Linear index profile considered as one piece . . . . .	34
3.2	Nonlinear profile with possible divisions . . . . .	35
3.3	PSIM output for profile shown in Figure 3.2 . . . . .	36
3.4	PSIM output for profile shown in Figure 3.2 but broken into five separate pieces . . . . .	37
3.5	Beam fanning resulting in successful SPPC . . . . .	38
3.6	Beam fanning not resulting in successful SPPC . . . . .	39
3.7	Index profile for simulation of beam fanning in BaTiO <sub>3</sub> . . . . .	40
3.8	PSIM output using the index profile of Figure 2.5 . . . . .	41
3.9	PSIM output using the index profile of Figure 3.1 . . . . .	43
3.10	PSIM output for index profile shown in Figure 3.7 . . . . .	44
3.11	Necessary charge distribution and electric field to produce the index profile of Figure 3.7 . . . . .	45
4.1	Experimental Apparatus . . . . .	51
4.2	Dependence of fanning intensity on incident beam diameter . . . . .	52
4.3	Typical dependence of scattered intensity on beam diameter as measured from above for converging light . . . . .	53
4.4	Typical dependence of scattered intensity on beam diameter as measured from above for diverging light . . . . .	54
4.5	Transmitted intensity as a function of beam diameter for diverging light . . . . .	55
4.6	Transmitted intensity as a function of beam diameter for converging light . . . . .	56

4.7a	Photograph of projected spot immediately upon turning on the incident beam .....	57
4.7b	Photograph of projected spot after the onset of beam fanning .....	58
4.7c	Photograph of projected spot in the steady state .....	59
A.1	Experimental Apparatus .....	68
A.2	Normal configuration for BaTiO <sub>3</sub> exhibiting SPPC .....	71
A.3	Effect of placing a knife edge in the incident beam .....	72
A.4	The TIR Ring .....	73
A.5	Determination of the direction of the TIR ring by extraction of light with another crystal .....	74
A.6	The Diamond configuration .....	75
A.7	The Diffuse Diamond configuration .....	76
A.8	Example of lack of reflection of the incident beam within the crystal .....	77
A.9	Example of multiple reflections within the crystal .....	78
A.10	The Diagonals configuration .....	79
A.11	Example of quasi-periodic amplitude oscillations in BaTiO <sub>3</sub> .....	80
A.12	Amplitude oscillations which progressed from those of Figure A.11 .....	81
A.13	BaTiO <sub>3</sub> prior to translation .....	83
A.14	Free standing beams created by translating the crystal ~0.5mm from the configuration of Figure A.13 .....	84

## ACKNOWLEDGEMENTS

I wish to thank my wife for her unfailing support during this research. Without her support, this document would not exist. I also wish to thank Professor Donald Walters and Dr. R. A. Fisher for their encouragement, support and assistance.

Much of the work presented in Appendix A on internal beam production was done in collaboration with the staff of the Los Alamos National Laboratory. In particular much of the theory and many explanations are directly attributable to conversations with Dr. R. A. Fisher. Also, Dr. A. V. Nowak was responsible for most of the apparatus and the discovery of many of the effects. Many of the photographs presented here are from video tapes taken by Dr. Nowak after painstakingly recreating these effects from my notes. His work resulted in better photographs than my own work produced, and consistently contained new and important observations. He is solely responsible for some of the information I will present in Appendix A, and in these cases I have endeavored to give him due credit. Also, Dr. Otis Peterson has graciously loaned me two barium titanate crystals for use in the experimental portion of this work, in addition to much encouragement. I am especially indebted to these men for their help and guidance, and to the management of the Los Alamos National Laboratory for support during this portion of my research.

## I. INTRODUCTION

During the last decade the photorefractive crystal barium titanate ( $\text{BaTiO}_3$ ) has received a large amount of attention within the scientific community. Barium titanate has long been of interest to acousticians and solid state physicists because of its photoacoustic and piezoelectric properties, but only recently have optical physicists become very interested in this crystal. The cause of this sudden and intense interest was the discovery of photorefraction and optical phase conjugation. Originally found in liquids and gases [Ref. 1], optical phase conjugation has the ability to reconstruct a distorted wavefront (sometimes loosely referred to as time reversal). Barium titanate is one of many photorefractive crystals which can exhibit phase conjugation.

There exist a number of intriguing optical properties of single crystals of barium titanate, but by far the most interesting is its ability to phase-conjugate at continuous wave low powers, with no external apparatus. This effect, known as self-pumped phase conjugation (SPPC), is the subject of extensive current investigation. The goal of this research is to determine the origin of self pumped phase conjugation in  $\text{BaTiO}_3$ .

Currently there exist two explanations of the cause of SPPC in  $\text{BaTiO}_3$ . One theory, developed by Feinberg and his students at UCLA [Ref. 2], attributes the production of the phase conjugate reflection to the photorefractive effect via Degenerative Four Wave Mixing (DFWM). According to this theory, an asymmetric change in the index of refraction across the path of an incident beam causes the beam to bend. This bending eventually leads to a geometry which, through two internal reflections (often termed a CAT corner), allows the beam to intersect itself, leading to DFWM. The second theory, originating with Lam and his co-workers at Hughes Research Laboratory [Ref. 3], attributes SPPC to Simulated Photorefractive Scattering (SPS), or Two Wave Mixing, similar to that exhibited in gases and liquids with two frequency disparate input beams of very high powers. With the goal of proving one or the other of these theories, this thesis begins with a general background and theory of phase conjugation as it applies to  $\text{BaTiO}_3$  (Chapter II). Chapter III describes PSIM (Photorefractive SIMulation), a simulation of the phenomenon of beam fanning due to a change in index of refraction within the incident beam path arising from the photorefractive effect. This simulation enables the prediction of the change in index of

refraction and the index profile necessary to account for SPPC with only the photorefractive effect taken into account.

Chapter IV introduces experiments to determine the effect of incident beam size on various crystals of  $\text{BaTiO}_3$ . Chapter V summarizes the results and analyzes the data presented. The conclusion is reached that Stimulated Photorefractive Scattering is responsible for the process of beam fanning which leads to self pumped phase conjugation in  $\text{BaTiO}_3$ . The actual origin of the phase conjugate beam is attributed to both SPS and DFWM.

Additionally, Appendix A contains a summary of the work I did at Los Alamos National Laboratory under the direction of Dr. R. A. Fisher in February and March, 1986. This work describes and catalogs internal beam production in barium titanate during SPPC. Some internal beam patterns not previously reported are introduced and explanations for these phenomena are proposed. The results of the experimental work in the body of this thesis have been submitted for publication to *Optics Letters*. An expanded version of Appendix A was presented at the *XIV International Quantum Electronics Conference (1986)*, and has been submitted for publication in the *Journal of the Optical Society of America B* in collaboration with R. A. Fisher and A. V. Nowak.

## II. BACKGROUND AND THEORY

### A. INTRODUCTION

Optical phase conjugation, first discovered in 1972 [Ref. 1], relies on a specific nonlinear property of a substance to create the formation of the complex conjugate of an incident wave. The reflection involved is not the familiar specular reflection seen in everyday life, but a reflection that retraces the path of the incident beam exactly, regardless of the direction or angle of incidence. The exact retracing of the incident beam path and the formation of the complex conjugate of the incident wavefront are the two unique and most important effects that make phase conjugation both interesting and useful. In barium titanate this phase conjugate beam is directly a result of the photorefractive effect.

### B. ORIGINS OF THE PHASE-CONJUGATE BEAM

The origin of the phase conjugate beam in photorefractors is light which is Bragg scattered by an index grating formed by the light in the material. This process is known as wave mixing. There exists both two-wave mixing (scattering) and four-wave mixing in barium titanate. Both of these processes will be treated theoretically in general terms; the specifics of wave mixing in  $\text{BaTiO}_3$  will be treated later.

To understand the origins of phase conjugation one must begin with the wave equation for a homogeneous, isotropic, time-independent, nonmagnetic and nonconducting dielectric. The polarization term is divided into its linear ( $P_l$ ) and nonlinear ( $P_{nl}$ ) parts, and the linear portion is absorbed into the linear permittivity of the medium,  $\epsilon$ . This leaves the wave equation as:

$$\nabla^2 \mathbf{E} - \epsilon \mu \frac{\partial^2 \mathbf{E}}{\partial t^2} = \mu \frac{\partial^2 \mathbf{P}_{nl}}{\partial t^2}. \quad (2.1)$$

For ease of manipulation an approximation to this equation is made that reduces the second order nonlinear wave equation to a first order equation.<sup>1</sup> This approximation is derived by Fisher and Yariv [Ref. 5: pp. 9-11] and for it to be valid, the envelope of the pulse must not change appreciably during an optical period, hence

---

<sup>1</sup>Some calculations can be made without this approximation but they are quite tedious (e.g. [Ref. 4]).

the term Slowly Varying Envelope Approximation. In making the approximation it is necessary to assume that the electromagnetic waves under consideration are plane waves, and also to extract only the portion of the nonlinear polarization that propagates with the same frequency and wave vector as the modulation function of the electric field. This, referred to as the phase matched portion of the polarization, is given by

$$\mathbf{P}_{nl} \equiv P(z,t) \exp \pm i(\omega t - kz), \quad (2.2)$$

in the wave given by

$$\mathbf{E} \equiv E(z,t) \exp \pm i(\omega t - kz). \quad (2.3)$$

Here the boldface letters (**E** and **P**) are the fields and the conventional letters (E and P) are the field envelopes, which vary little in an optical period and in an optical wavelength. All other terms are ignored because they are not phase matched and therefore cannot couple to the electric field. The Slowly Varying Envelope Approximation, or SVEA, is then invoked. That is:

$$|k^2 E| \gg \left| k \frac{\partial E}{\partial z} \right| \gg \left| \frac{\partial^2 E}{\partial z^2} \right|. \quad (2.4)$$

Fisher and Yariv then show that the wave equation with SVEA becomes a first-order equation relating the envelope functions E and P:

$$\frac{\partial E}{\partial z} + \sqrt{\epsilon \mu} \frac{\partial E}{\partial t} = \pm \frac{i\omega \sqrt{\mu}}{2 \sqrt{\epsilon}} P. \quad (2.5)$$

This result is the SVEA wave equation for a plane wave traveling in the  $+z$  direction, which shows that, given a nonlinear polarization, an electric field can be produced. This development can be generalized to the case of many waves present within a single medium, resulting in the origin of the nonlinear processes that can lead to phase conjugation.

The polarization term can often be written as a power series expansion:

$$P = EX(E) = X^{(1)}E + X^{(2)}E^2 + X^{(3)}E^3 + \dots, \quad (2.6)$$

where  $X(E)$  is the susceptibility of the material in which the wave is traveling. The expansion of the susceptibility in a power series separates the effects of the nonlinear material into distinct groups that categorize nonlinear effects [Ref. 5: p. 13]:

- $X^{(1)}$  - These are the linear properties that are the subject of classical optics and are not directly responsible for nonlinear effects.
- $X^{(2)}$  - The second order effects are in general called three-wave mixing and include: second-harmonic generation, optical rectification, parametric mixing and the Pockels effect.
- $X^{(3)}$  - Third order effects include some of the most popular effects responsible for phase conjugation such as: third-harmonic generation, nondegenerate four-wave mixing, Raman scattering, ac Kerr effect (degenerate four-wave mixing), dc Kerr effect, Brillouin scattering, two photon absorption, dc-induced harmonic generation and Stimulated Photorefractive Scattering.

The two methods of creating a phase-conjugate reflection that are directly applicable to the experimentation described here are scattering and degenerate four wave mixing.

#### 1. Four-Wave Mixing

In 1977 Hellwarth [Ref. 6] showed that it was possible to generate a time-reversed replica of any monochromatic-beam wave pattern. The method employed the interaction of an incident beam with counter-propagating pump waves in a homogeneous, transparent, nonlinear medium (see Figure 2.1). This method, called four-wave mixing, has become one of the most popular methods for phase conjugation because of the almost universal availability of the necessary equipment and proper media.

The description of wave mixing begins with the nonlinear polarization derived from the energy function. As shown by Pepper and Yariv [Ref. 5: pp. 26-33], isolating only the third order term gives

$$P_c^{(3)} = 4X_{12pc}^3 E_1 E_2 E_p \quad (2.7)$$

We consider here degenerate four-wave mixing (DFWM), where  $\omega_1 = \omega_2 = \omega_p = \omega_c$  represents frequencies of the four beams. The subscripts 1 and 2 refer to two strong, precisely counterpropagating pump beams, the subscript p refers to the weak probe beam, and the subscript c refers to the phase-conjugate output wave. It is assumed that the following conditions are met:



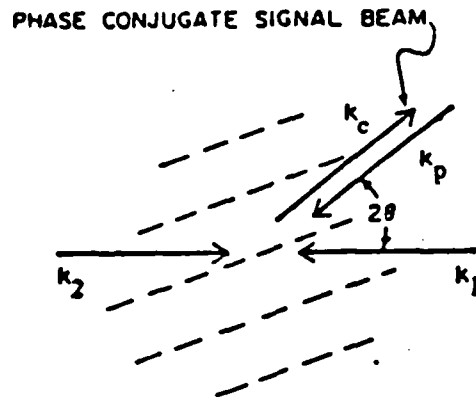


Figure 2.1 Schematic of the process of four-wave mixing [Ref. 5: p.421].

- a) intense (nondepleted) counterpropagating planewave pump beams of equal intensity ( $k_1, k_2$ ),
- b) a weak probe beam ( $k_p$ ),
- c) both the intense pump beams and the weak probe beam are at the same frequency  $\omega$ .

Since the two pump waves are very strong compared to the probe beam they form a standing wave. To obtain the steady-state solutions, we can set

$$\frac{\partial E}{\partial t} = 0. \quad (2.8)$$

So, assuming the SVEA and considering only the phase matched portion of the phase conjugate wave, then from Equation 2.5

$$\frac{\partial E_c}{\partial z} = i \frac{\omega}{2} \frac{\sqrt{\mu}}{\sqrt{\epsilon}} P_c \exp(ik_c \cdot r). \quad (2.9)$$

The nondestructive buildup of the electric field amplitude can occur only if the product of the exponential phase factors in Equation 2.9 and  $P_c$  is small (on the order of zero). If this is not so, then all of the successive contributions will not be in phase to add constructively. This total phase factor is:

$$\exp[-i(\mathbf{k}_1 + \mathbf{k}_2 - \mathbf{k}_p - \mathbf{k}_c) \cdot \mathbf{r}]. \quad (2.10)$$

Since waves 1 and 2 are counterpropagating then,

$$\mathbf{k}_1 + \mathbf{k}_2 = 0. \quad (2.11)$$

Although in practice this may not be exactly so because of nonlinear phase shifts due to unequal pump-wave intensities or non-aligned beams, it is very close [Ref. 5: p. 30]. Therefore the phase factor can be zero only if

$$\mathbf{k}_c = -\mathbf{k}_p. \quad (2.12)$$

Here it is evident that the nonlinearly generated field propagates in the opposite direction of the probe wave.

Assuming that the factor in the exponential of Equation 2.10 is equal to zero, then combining Equation 2.7 and Equation 2.9 yields (within a multiplicative constant) [Ref. 5: p.36]

$$\frac{\partial E_c}{\partial z} = i\omega \frac{\sqrt{\mu}}{\sqrt{\epsilon}} X^3 E_1 E_2 E_p^*. \quad (2.13)$$

This equation was solved concurrently by Yariv and Pepper [Ref. 7] and Bloom and Bjorklund [Ref. 8], and the solution was shown to be:

$$E_p(z) = -i \frac{|k| \sin(|k|z)}{|k| \cos(|k|L)} E_c^*(L) + \frac{\cos[|k|(z-L)]}{\cos(|k|L)} E_p(0), \quad (2.14)$$

$$E_c(z) = \frac{\cos(|k|z)}{\cos(|k|L)} E_c(L) + ik^* \frac{\sin[|k|(z-L)]}{|k| \cos(|k|L)} E_p^*(0). \quad (2.15)$$

Where

$$k^* = \omega \frac{\sqrt{\mu}}{\sqrt{\epsilon}} X^3 E_1 E_2, \quad (2.16)$$

$E_c(L)$  is the amplitude of the conjugate wave at its origin (the phase conjugate mirror), and  $E_p(0)$  is the amplitude of the probe wave at its origin.

In practice, the amplitude of the phase conjugate wave at its origin is zero (i.e.  $E_c(L)=0$ ), so that at the input point ( $z=0$ ) of the probe beam

$$E_c(0) = i \frac{k^*}{|k|} \tan(|k|l) E_p^*(0). \quad (2.17)$$

Equation 2.17 shows that at  $z=0$  (the origin of the probe beam) the reflected field is proportional to the complex conjugate of the incident field. Therefore there exists a phase conjugate reflection.

## 2. Scattering

Phase conjugation by stimulated scattering was first reported by Zel'dovich, Popovichev, Ragul'ski and Faizullov in 1972 [Ref. 1]. As stated by Hellwarth [Ref. 5: p. 171]:

In essence, the nonlinear polarization density, mediated by some driven (Raman-, Brillouin-, etc.) active excitation of the optical medium, couples normal-mode solutions of the linear Maxwell equation so as to create a new set of normal modes in backscattering with, in effect, complex propagation constants representing index change and gain.

For example Stimulated Brillouin Scattering, or SBS, is a direct result of the electrostrictive effect seen in some materials. This effect is seen when the polarizability of a material is a function of pressure. In these materials it is possible for light to be scattered by a sound wave allowing the coupling of a pair of light waves to a pressure wave. Another type of scattering sometimes responsible for phase conjugation is Stimulated Raman Scattering or SRS. SRS is the scattering of light from molecular vibrations or rotations in a gas or liquid, or longitudinal-optical phonons in a solid. In SRS light waves are coupled because of polarizability changes with a molecular coordinate. Of particular importance to this research is Stimulated Photorefractive

Scattering in barium titanate. In SPS it is the photorefractive effect which is responsible for the production of a periodic index of refraction grating; this grating then Bragg scatters light in the backward direction which comprises the phase conjugate beam.

The mathematics involved in all three types of scattering is similar and can be treated together. To this end I outline the work of Hellwarth [Ref. 5: pp. 177-180] and discuss the existence of the phase conjugate wave assuming scalar or symmetric scattering with a monochromatic, multimode, incident wave in a wave guide. The results are largely independent of the nature of the wave guide provided that a specific TEM mode that propagates in the forward direction also propagates in the backward direction.

A wave  $E_1(r)$  may be expressed as:

$$E_1(r) = \sum_m A_m \hat{e}_m \exp[i(k_m z - \beta z)/2], \quad (2.18)$$

where  $\beta$  is the attenuation coefficient,  $\hat{e}_m$  is the normalized transverse-mode pattern, and the propagation constants may vary with wave angular frequency, that is  $k_m = k_m(\nu)$ .

The electric field of the backscattered wave may then be written as [Ref. 5: p.180]

$$E_2 = \sum_n B_n \hat{e}_n \exp[-ik_n z + \beta z/2 - \gamma z/2], \quad (2.19)$$

where  $k_n = k_n(\omega)$ , and  $\gamma$  is used to balance any nonlinear terms from the fields interaction with the medium. If  $\gamma = 0$  in the above equation, then this is the solution to the linear Maxwell equations for a wave in a wave guide.

If in Equation 2.19  $\gamma \neq 0$ , then there is one configuration that allows the  $\gamma$  of one of these modes to have a positive real part significantly greater than that of any other. This means that a single wave (reflection) may dominate the backscattered waves if the necessary conditions are met. The desired result is that

$$E_2(r) = \eta E_1^*(r), \quad (2.20)$$

where  $\eta$  is a constant. Substituting Equations 2.18 and 2.19 into Equation 2.20 gives the polarization density necessary to balance the extra terms in Maxwell's equations that come from the last term in Equation 2.19. According to Hellwarth [Ref. 9] the necessary conditions are satisfied if

$$\gamma k_m(\omega) B_m = \eta \frac{\omega^2}{c^2} \Sigma \iint dx dy \hat{e}_m^* \cdot \hat{e}_{ij} \cdot \hat{e}_n K_{mijn} A_i A_j B_n, \quad (2.21)$$

where

$$K_{mijn} = \int_0^L (1/L) \exp[\Delta k L z] dz, \quad (2.22)$$

and

$$\Delta k = k_m(\omega) + k_i(\nu) - k_j(\nu) - k_n(\omega). \quad (2.23)$$

In Equation 2.21 I have assumed that the scattering considered is the pure scalar or symmetric type, reducing the fourth rank susceptibility tensor to a scalar quantity. This quantity, and all other constants, I have absorbed into  $\eta$ .

The necessary conditions may be determined for special cases, either by exact solution or perturbation methods developed by Hellwarth. These solutions indicate that a backscattered solution that is nearly phase conjugate predominates because it has gain nearly twice that of any other mode, provided that [Ref. 5: p. 177]:

- a. the interaction length is not too long,
- b. the Stokes shift ( $\nu - \omega$ ) is not too large,
- c. the number of guide modes falls within a certain large range, and
- d. the total number of guided modes is not too large.

The solutions that led to these conditions, presented by Hellwarth in 1978 [Ref. 9], unfortunately do not take into account competing nonlinear effects, and therefore are good only to the extent that they predict the major effects observed in experimentation. It is observed that the backscattered wave is not always an exact phase conjugate of the input wave, possibly due to some of these competing effects. These analyses apply equally as well to SPS, SBS and SRS [Ref. 3].

### C. DISTORTION CORRECTION BY PHASE CONJUGATION

Although not immediately applicable to this investigation, the ability of a phase conjugator to correct for phase distortions is one of the primary aspects driving research in this area. As a practical point, this ability is an easy way to determine that any given observed beam is a phase conjugate of another.

It was shown above that, at least for the two cases considered, a wave can be generated propagating directionally opposite to an input wave, with its envelope function proportional to the complex conjugate of the input beam's envelope function. This phase conjugate wave may be considered a separate wave that must satisfy the same wave equation as the input wave. This means that if the wavefront of the input wave is distorted in some way, then the phase conjugate wave will propagate backwards along the same path and its envelope function will remain everywhere the complex conjugate of the input wave's; that is, its wave fronts will coincide with the input wave fronts at every point. Thus a distorted wave front will be restored to its original shape as the phase conjugate wave traverses the distorting medium in the reverse direction. The proof is quite simple, as shown by Fisher and Yariv [Ref. 5: p. 17], and is accomplished by complex conjugating the wave equation for the forward going wave. The result is the equation for the conjugate wave propagating in the opposite direction. So a wave traveling in the opposite direction of the incident wave, with an envelope function the complex conjugate of such a wave, satisfies the same wave equation as the incident wave. This means that the backward going wave will remain everywhere the complex conjugate of the incident wave, and therefore a distorted plane wave will be restored to its original configuration when it is passed back along the same distorting path. This distortion correction capability is the most visible and fascinating effect attributable to phase conjugation at the present time.

An incomplete list of some applications of phase conjugation with emphasis on those currently using barium titanate as the phase-conjugator is [Ref. 5,10,11]:

- a. Holography
- b. Distortion correction
- c. Laser oscillators
- d. Interferometry
- e. Laser beamsteering
- f. Associative memory investigations
- g. Image amplification
- h. Laser coupling

- i. Image addition, subtraction and enhancement
- j. Optical bistability
- k. Automatic pointing and tracking.

#### D. PHOTOREFRACTORS AND FOUR WAVE MIXING

In photorefractive materials the index of refraction changes with incident optical energy. This effect was first discovered in the 1960's [Ref. 12,13] and has since led to the development of optical recording sensitivities comparable to that of the silver halide emulsions used in photography [Ref. 14]. The process involved in the effect is summarized by Feinberg [Ref. 5: p. 418] as follows:

- a. Light causes charge to migrate and separate in a crystalline material.
- b. The separation of charge produces a strong electrostatic field.
- c. The electrostatic field causes a change in the refractive index of the crystal by the linear electro-optic effect.<sup>2</sup>

In the photorefractive effect the important factor in the change in index of refraction is not the intensity of the incident light, but the total energy of the incident radiation; the power only determines the speed of the reaction. Also because of the type of effect concerned, the actual result is dependent on the relative intensity of the incident radiation.

Consider a thin beam of light incident on a photorefractive crystal that is otherwise dark. The light will liberate charge carriers from the lighted area of the crystal and these carriers will then settle back into a place within the crystal structure. If the carriers settle back in the area of the crystal that is lighted they will again be liberated. If, however, the carriers land in a dark area of the crystal, they will stay where they land due to the small dark conductivity of the crystal. Eventually there will be few charge carriers in the lighted area and many in the dark area. This disproportionate distribution creates an electric field between the dark area and the lighted area that creates a change in the index of refraction of the crystal through the linear electro-optic effect.

This process of migration has been aptly described by R. A. Fisher as the flyswatter effect [Ref. 16]. It is as if the charge carriers were flies at a picnic table and the light was a flyswatter suspended from above, slowly swinging across the table top.

---

<sup>2</sup>The linear electro-optic effect is the change in the index of refraction caused by (and proportional to) an applied dc electric field. This effect is seen in crystals that do not exhibit inversion symmetry, such as barium titanate in the tetragonal phase [Ref. 15: p. 275].

Each time a fly lands on the table within the area of the flyswatter's reach, he will immediately fly up as the swatter returns toward him. If, however, the fly lands on the table in an area away from the swatter he will be left alone and will stay on the potato salad. In time therefore, there will be no flies on the table in the area where the flyswatter can reach and many where it cannot. This process effectively pumps the flies to regions on the table which are away from flyswatter.

The model of charge transport described above is known as the hopping model and was first proposed by Chen to explain the change in refractive indices in  $\text{LiNbO}_3$  and  $\text{LiTaO}_3$  [Ref. 17]. There also exists a diffusion model proposed by Amodei [Ref. 18] that may dominate when the spacing between light and dark areas within the crystal is less than one micrometer.

From the flyswatter analogy it is clear that what is important is the optical intensity relative to the ambient. This entire explanation assumes the existence of charge carriers in a crystalline material. In most materials exhibiting the photorefractive effect the origin of the charges is unknown, but it is assumed that they inhabit low-lying traps formed by impurity sites in the crystal. For example, in  $\text{BaTiO}_3$ ,  $\text{Fe}^{2+}$  and  $\text{Fe}^{3+}$  impurities may create the charge carriers as shown by Klein and Schwartz [Ref. 19]. It has also been proposed, and there is extensive evidence to support the theory, that oxygen vacancies are the donors and barium vacancies are the acceptors [Ref. 20]. Whatever the dominant species is, it is assumed that there are a large number of empty receptor sites in the material available to the liberated charge carriers.

If, instead of a single beam, two beams of identical wavelength and equal intensities (one called a pump wave and one called a probe wave) intersect within a photorefractive crystal, the interference pattern they form will cause a periodic optical field to be set up in the region of intersection, resulting in a periodic charge separation. Through the electro-optic effect, a periodic variation in index of refraction will result. This index grating is then able to Bragg scatter a pump wave in the opposite direction to produce a phase conjugate beam. The formation of the index grating is shown in Figure 2.2, adapted from Feinberg [Ref. 5: p. 422].

It is important to note that photorefractive phenomena are not merely four-wave mixing phenomena. Four-wave mixing is a consequence of an index change at some given point at some given time (x,t). Photorefractive phenomena however, are dependent on the history of the medium and are not spatially local effects. That is, the



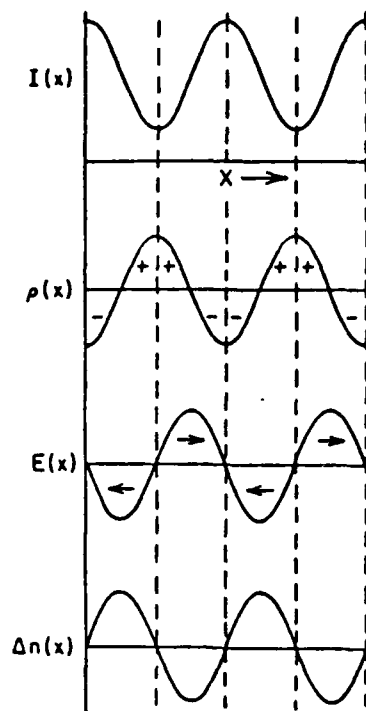


Figure 2.2 Index grating formation due to the photorefractive effect [Ref. 5].

effects at  $(x,t)$  are a consequence of actions at  $(x-\delta x, t-\delta t)$ . This is clearly seen in Figure 2.2.

The top curve of Figure 2.2 shows the intensity as a function of the position along the path of the beam. The second curve is the charge density due to this intensity variation. The electric field intensity is presented in the third curve (note the important  $1/4$  period shift relative to the charge). Finally the variation of the actual index of refraction within the crystal is shown in the last curve.

The spatial shift between the change in index of refraction and the variation in intensity due to the interference pattern (one fourth of the grating period) is an important effect. This happens because the peak of the charge distribution is a center of right-left symmetry, and therefore there can be no electric field at that point. This shift leads to the ability to transfer power from one beam to another, a process known as two-beam coupling. Two-beam coupling, first reported by Staebler and Amodei [Ref. 21], is due to the scattering of one beam into another by Bragg diffraction as they pass through the grating they have mutually produced. The result is that one beam experiences gain at the expense of the other.

One interesting effect of four-wave mixing in photorefractors is seen in the phase conjugate mirror with continuous wave gain. This was first demonstrated by Feinberg in 1980 [Ref. 22] using the configuration shown in Figure 2.3 .

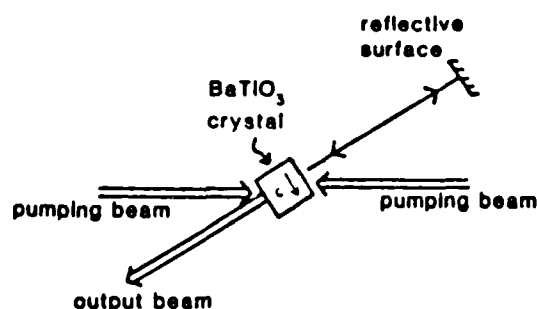


Figure 2.3 Formation of an optical cavity with a phase conjugate mirror [Ref. 5].

In this configuration a phase conjugate mirror (PCM) and an ordinary mirror (M1) can form an optical cavity in which a beam will oscillate. One of the more dramatic demonstrations of this type of oscillation is reported by Feinberg [Ref. 5: p. 436] in a configuration using an ordinary kitchen spatula as one end of the cavity. Just as in any conventional laser oscillator, the oscillations can begin with noise (as little as a single photon) that makes one successful round trip within the cavity. With each additional round trip the system sees gain due to two-beam coupling and in a short period of time a visible CW beam may be observed between the mirror and the phase-conjugator.

#### E. STIMULATED PHOTOREFRACTIVE SCATTERING

The second theory which accounts for phase conjugation in BaTiO<sub>3</sub> was originally proposed by Lam in 1985 [Ref. 3]. Lam proposed that the origin of the phase conjugate beam is two wave mixing or scattering. This process of SPS begins with random inhomogeneities in the photorefractive medium which give rise to noise photons from the Rayleigh scattering of the input beam. In the words of Lam [Ref. 3]:

The noise photons propagating along with [sic] axis of the input beam undergo parametric scattering, resulting in an unidirectional gain. The phase conjugate

wave arises from the component of the scattered wave which experiences the maximum gain.

Later the same year Chang and Hellwarth conclusively demonstrated SPS in  $\text{BaTiO}_3$  [Ref. 23]. To do this they had to index match the surfaces of the crystal to make accessible angles which would not produce the characteristic corner reflection (i.e. the CAT corner) producing DFWM.

Later, Valley [Ref. 24] defined SPS as the selective amplification through the photorefractive effect of optical radiation scattered by medium inhomogeneities. Thus, SPS is a two-wave mixing process in which the incident beam interferes with scattered light to create the necessary grating through the photorefractive effect. As soon as the gain for an individual noise beam exceeds its loss, then that beam will become dominant, increasing the grating strength and hence the backscattered beam gain. This process will continue until a steady state value is reached.

The mathematical equations, as derived by Lam, are of the identical form to those encountered in stimulated scattering in a waveguide (presented above), so the analysis of phase conjugation by SPS has already been addressed.

## F. BARIUM TITANATE

### 1. The Crystal

The experiments reported here were performed with one of the more popular photorefractive crystals capable of creating a phase conjugate reflection. Above the Curie temperature of  $120^\circ\text{C}$ ,  $\text{BaTiO}_3$  is a cubic crystal and therefore centrosymmetrical and non-photorefractive. Between  $5^\circ\text{C}$  and  $120^\circ\text{C}$  however, the crystal is in the polar phase and has a tetragonal symmetry. The axis of fourfold rotation is the optical axis or c-axis. In the tetragonal phase barium titanate is ferroelectric, photorefractive, photoconducting, birefringent, electro-optic, pyroelectric, piezoelectric, photoacoustic and (slightly) electrostrictive. The many possible effects make the crystal itself very difficult to understand, since often the results of the various effects cannot be separated. All results reported here involve  $\text{BaTiO}_3$  in the tetragonal phase.

Since  $\text{BaTiO}_3$  is chemically and mechanically stable at room temperature, it is used extensively in many capacities and is therefore well studied. Jona and Shirane [Ref. 25: pp. 108-215] report extensively on the structure, properties and the effects of temperature, stress and electric fields on barium titanate in the tetragonal phase. Although at the time of printing the photorefractive capabilities were unknown, their

data represent a comprehensive picture of the crystal and forms the basis for analysis of the solid state aspects of barium titanate. More recent but less comprehensive data, emphasizing the optical aspects of  $\text{BaTiO}_3$ , have been compiled by Wemple, et. al. [Ref. 26].

When used as a photorefractor, it is necessary that a single crystal of  $\text{BaTiO}_3$  be used and that the crystal be poled into a single domain. Poling is accomplished by cooling the crystal through the Curie point while an electric field on the order of  $10^3$  V/cm is applied across the optical axis. This poling of the crystal results in an electro-optic tensor which has a very large [42] element. Since the photorefractive effect uses the linear electro-optic effect, it is important to maximize this [42] element. This maximization is accomplished by using extraordinarily polarized light incident at an angle between zero and  $90^\circ$  to the c-axis.

## 2. Beam Fanning

When a beam of extraordinarily polarized light is incident on a poled, single crystal of barium titanate, it is seen to asymmetrically defocus in the direction of the c-axis prior to the onset of phase conjugation. This process, called beam fanning, was first discovered by Feinberg in 1981 [Ref. 27]. Beam fanning is clearly visible in Figure 2.4 (the optic-axis is designated by the arrow). This fanning can be explained by either an asymmetric change in index of refraction within the incident beam path, or by stimulated scattering.

### a. Deflection by Photorefraction

Beam fanning was proposed to be due to an asymmetric change in the index of refraction caused by the photorefractive effect. This process is represented in the curves of Figure 2.5 (from Feinberg [Ref. 27]). The top curve shows the intensity curve of a Gaussian beam. The second curve shows the net charge due to displacement of charge carriers by the incident light. The third curve shows the induced electric field, and the last curve shows the asymmetric change in the index of refraction. It is assumed that at the center, and most intense portion of the beam, the gradient of the index of refraction is greatest. Therefore the center portion of the beam creates the observed effect, and the fanning is induced beginning at that point. In other words, beam fanning begins in the *center* of the beam. This is one of the major discriminating factors and will be referred to later.<sup>3</sup> The second major point to consider

---

<sup>3</sup>Note that even if the intensity profile of the incident beam is not smooth, the top curve of Figure 2.5 represents the envelope that the beam intensity must fall within.

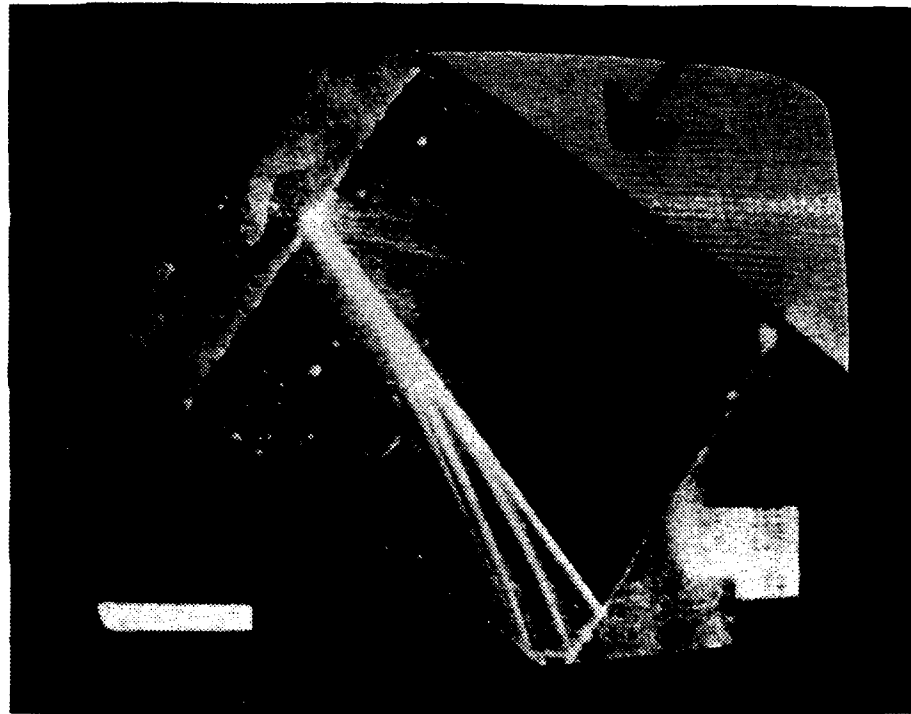


Figure 2.4 BaTiO<sub>3</sub> exhibiting SPPC.

about this theory is that as the diameter of the beam decreases the electric field increases, since the linear distance between charge distributions decreases. Since the photorefractive effect is proportional to the electric field, then beam fanning must increase with a decrease in beam diameter. This is clearly seen by examining the equations describing the electric field and the subsequent refractive index change.

The electrostatic field induced by an incident beam in a photorefractor is given by [Ref. 27]:

$$E(x) = \frac{-2k_B T(\hat{x}x + \hat{y}y)}{e\pi\omega_0^2} \exp[-(x^2 + y^2)/\omega_0^2], \quad (2.24)$$

where  $e$  is the charge of the charge carrier,  $k_B$  is Boltzmann's constant,  $T$  is the temperature of the crystal, and  $\omega_0$  is the incident beam diameter. The change in index of refraction in a crystal of BaTiO<sub>3</sub> for an extraordinary ray due to this field is approximately given by

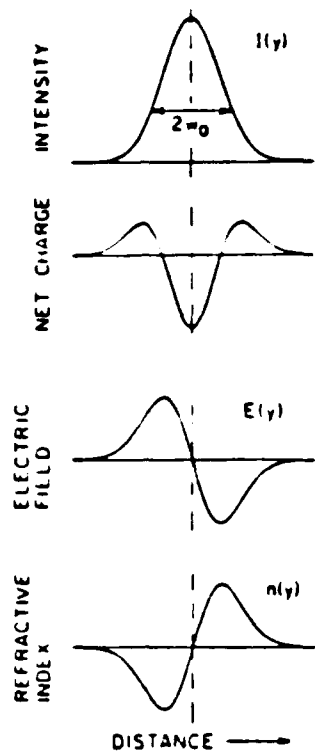


Figure 2.5 The process of beam fanning due to photorefraction for a single incident beam [Ref. 27].

$$n(y) = -[\mathbf{E}(\mathbf{x}) \cdot \hat{\mathbf{y}}] \frac{\cos\theta}{2n(\theta)} (2n_o^2 n_e^2 r_{42} \sin^2\theta), \quad (2.25)$$

where  $n(\theta) = (n_e^2 \cos^2\theta + n_o^2 \sin^2\theta)^{-1/2}$ ,  $\theta$  is the angle the incident beam makes with the non c-axis of the crystal,  $n_o$  is the index of refraction for an ordinary ray,  $n_e$  is the index of refraction of an extraordinary ray, and all terms that do not include the  $r_{42}$  element of the electro-optic tensor have been dropped, since its value exceeds all other elements by an order of magnitude.

Inspection of these equations clearly shows that the change in index of refraction is inversely proportional to the diameter of the incident beam.

#### *a. Near Forward-SPS*

In 1985 Lam proposed that beam fanning is due to an effective nonlinear index of refraction which causes the crystal to behave like a diverging lens [Ref. 3]. This nonlinear index of refraction ( $\sim 10^{-3}$ ) is due to an intensity dependent frequency shift of the incident beam due to the bulk photovoltaic effect. Recently Valley

[Ref. 24] has suggested that beam fanning is actually near forward scattering due to SPS, in an extension of Lam's theory.

As in other types of scattering, SPS is the selective amplification of radiation which is scattered by inhomogeneities in the medium. The amplification is accomplished through the photorefractive effect. This is schematically diagrammed in Figure 2.6.

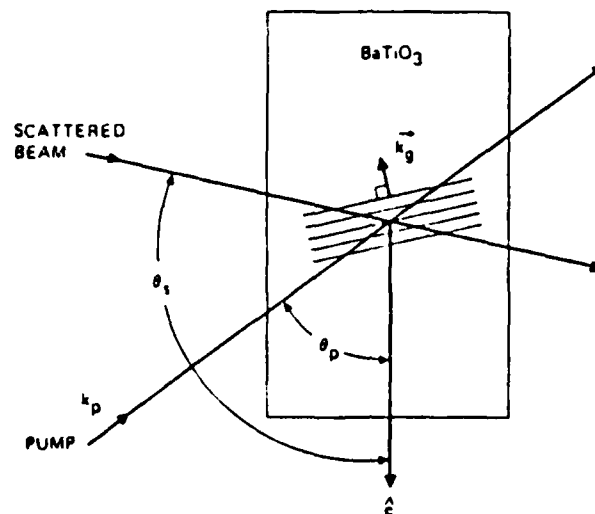


Figure 2.6 The process of SPS [Ref. 24].

In a crystal where one charge carrier dominates, the gain-length product per absorbed energy per volume at turn on is given by [Ref. 24]

$$G_{to} = \frac{k r_{eff} e \mu \tau E_d l_{eff}}{2 n_s [\epsilon \epsilon_0 (1 + E_d / E_m)]}, \quad (2.26)$$

where  $r_{eff}$  is the effective Pockels coefficient for extraordinarily polarized light [Ref. 28],  $k = 2\pi/\lambda$ ,  $e$  is the carrier charge,  $\tau$  is the space charge field and refractive index grating decay rate,  $\epsilon$  is the dielectric constant (which is anisotropic), and

$$E_d / E_m = k_B T k_g^2 \mu \tau / e, \quad (2.27)$$

where  $k_B$  is Boltzmann's constant,  $\mu$  is the carrier mobility (which is also anisotropic) and  $T$  is the temperature of the crystal. Finally,  $l_{\text{eff}}$  is the effective interaction length which Valley models with

$$l_{\text{eff}} = L\{1 - \exp[-\omega_0/(L \sin\theta)]\}, \quad (2.28)$$

where  $L$  is the length of the crystal in the direction bisecting the scattered and incident beam,  $\omega_0$  is the incident beam diameter, and

$$\theta = (\theta_s - \theta_p)/2. \quad (2.29)$$

The important item to note is that the gain-length product is proportional to the effective interaction length given by Equation 2.28. Therefore the amount of scattering due to SPS (both forward and backward) is exponentially dependent on the incident beam diameter in such a way that an increase in beam diameter will increase the scattering, and a decrease in beam diameter will decrease the scattering; this is opposite from that expected by the theory discussed in Section F.2.a above. Also, since SPS is dependent on the interaction of random noise photons with the incident beam, one would expect that beam fanning (near forward-scattering) could commence at the periphery of the beam in addition to the center. This scattering of energy should be more obvious at the edges of the incident beam since the intensity is lower there. Also, any light scattered toward the c-axis from inside the beam would take power from the periphery through two beam coupling, thus adding to the loss of intensity toward the beam edge. Considering these points, if the intensity profile of the incident beam were to be monitored during the fanning process, one should expect to see the intensity diminish from the periphery toward the center. Again this is opposite the effect expected from the prior theory.

### 3. Self Pumped Phase Conjugation

Beam fanning is intricately involved with self-pumped phase conjugation (SPPC). SPPC in  $\text{BaTiO}_3$  was first discovered by Feinberg soon after the discovery of beam fanning [Ref. 2]. According to Feinberg, the process of beam fanning (due to an asymmetric change in index of refraction within the beam path) may result in a portion of the incident beam being bent in such a way that it is internally reflected off the corner of the crystal (see Figure 2.4). This reflected beam then intersects the incident



beam causing a steady state interference pattern. The light and dark areas of the interference pattern cause an index grating (through the photorefractive effect) which then Bragg scatters the incident beam in the process of DFWM, creating a phase conjugate beam. Lam alternatively theorized that the origin of the phase conjugate beam is two-wave mixing (SPS) as described above, and that auxiliary beams were not essential to the process.

Of interest also is the time for phase conjugation to begin in barium titanate. The time to produce self-pumped phase conjugation can vary from a few seconds to tens of minutes depending on the intensity of the incident beam and the configuration used. Because of the typically large time for the onset of phase conjugation in  $\text{BaTiO}_3$ , there is extensive work presently underway to try to decrease it. Some work on changing crystals after growth has been reported [Ref. 20], but the present emphasis is on the doping of the crystals during growth [Ref. 29].

The exact processes involved in beam fanning and phase conjugation are still unresolved in the literature. In the following chapters I will examine these theories as they apply to observed effects and, since in the case of beam fanning there are mutually exclusive indications, I will show that beam fanning must be due solely to near forward SPS.

### III. PSIM: A SIMULATION OF THE PHOTOREFRACTIVE EFFECT IN BARIUM TITANATE

#### A. INTRODUCTION

To investigate the photorefractive effect in barium titanate, I designed a computer simulation which plotted the internal beam pattern within the crystal. This simulation, entitled PSIM (Photorefractive SIMulation), only accounts for the nonlinear photorefractive effect, not for SPS or other competing nonlinear effects. In so doing, I isolated the photorefractive effect from other effects and determined the necessary change in index of refraction across the beam path to account for beam fanning which is typically observed in the laboratory. The source code for PSIM is found in Appendix B.

#### B. THEORY

As discussed above, the photorefractive effect may be solely responsible for the observance of beam fanning, which is in turn responsible for self-pumped phase conjugation [Ref. 2]. The change in index of refraction of a given crystal,  $\Delta n$ , may be given by the equation [Ref. 14]

$$\Delta n(z) = -\left(\frac{1}{2}\right)n^3 r_{\text{eff}} E(z), \quad (3.1)$$

where  $n$  is the index of refraction,  $r_{\text{eff}}$  is the effective Pockels coefficient and  $E(z)$  is the space charge electric field.

Values for  $r_{\text{eff}}$  range generally in the picometers per volt range. Of seven crystals used by Klein and Schwartz [Ref. 19],  $r_{\text{eff}}$  ranged from  $4.2 \times 10^{-12}$  to  $12.0 \times 10^{-12}$  meters per volt. Although these values are very small, the space charge electric field may be very high, on the order of  $10^5$  volts per meter [Ref. 5: p. 418]. Using these values it becomes obvious that the change in index of refraction due to the photorefractive effect in barium titanate may be as high as  $10^{-4}$ . Though not an exact number for any given crystal, this may be accepted as close to an upper bound for  $\Delta n$  (denoted here as  $\Delta n_{\text{max}}$ ) for most of the crystals used. Günter [Ref. 11: p. 226] gives  $\Delta n_{\text{max}}$  as  $2.2 \times 10^{-5}$ , limited by the possible space charge field.

From the above simple calculations it may be assumed that for the photorefractive effect to be solely responsible for self-pumped phase conjugation, the dimensions of any given crystal used must be such that a change in index of refraction on the order of  $10^{-4}$  is sufficient to cause the observed beam fanning. However, as previously mentioned, the gradient of the electric field and hence the index gradient is the important quantity relating to the photorefractive effect. Therefore, the beam size relative to the length of the crystal along the direction of propagation and the intensity profile must also play an important role in SPPC. These factors, in addition to the incident angle, were eventually incorporated into the simulation described here. The resulting simulation was used to determine the minimum change in index of refraction necessary to account for observed beam fanning in any given configuration.

### C. THE SIMULATION

#### 1. Program Logic

The simulation is written in HP basic and designed to run on a Hewlett Packard 300 model computer with at least two megabytes of random access memory. This two dimensional model takes into account only the change in index of refraction across the incident beam path due to the photorefractive effect. The output is a graphic representation of the eventual steady state beam geometry.

The model uses a *brute force* approach to calculate the observed effects which, although time consuming and memory intensive, uses a simple algorithm. The program uses only Snell's law and Huygen's principle to calculate the internal beam pattern. Input into the program is the range of the change of index of refraction across the input beam,  $\Delta n$ , the crystal and beam size (in arbitrary units), the point of entrance of the beam into the crystal, and the angle of incidence of the incident beam relative to the normal. The program computes the mean index of refraction between two input extremes which then corresponds to the normal index of refraction ( $n \sim 2.4$ ). The important factor in the program is the difference between the two extremes,  $\Delta n_{\max}$ . Logically it is this entity which drives the photorefractive effect. Note that the simulation is not concerned with how  $\Delta n_{\max}$  is created.

Once the necessary parameters are entered, the internal angle of the incident beam is calculated and each point on the wavefront is then assigned an index of refraction value that it can impart to the crystal at its location. These points are then grouped into pieces of the wavefront (one to five separate pieces are normally used).

The assigned index value is dependent on  $\Delta n_{\max}$  and an assigned profile which may be varied (more will be said about this profile later). The indices of each point of the wave front are then propagated in a straight line through the crystal, at which time the value of the index of each point in the wavefront is imparted to the corresponding point within the crystal. After completing this process the wavefront is propagated along the same path, allowing each point to move at a speed proportional to the index at the point in the crystal in which it finds itself. After a short time the process of wavefront movement is stopped and the direction of each piece of the wavefront is calculated using Huygen's principle. The original indices of the points within any given piece are then propagated in that new direction, imparting those values along the new path of the piece of the wavefront and the process begins again. The result of many iterations of this algorithm is a graphic output of the steady state internal beam pattern due to the photorefractive effect.

## 2. Limitations

There are several limitations to the model that must be discussed prior to the introduction of results. The first, and major, limitation is that of necessity each point on the wavefront cannot be treated individually. The wavefront must be treated in sections to determine an appropriate direction for a section and this makes the model only an approximation to the actual continuous case. The choice of the number of sections is primarily dependent on the chosen index profile. A profile similar to that shown in Figure 3.1 may be treated as a single piece since the direction of each individual piece will be the same as the direction of the entire wavefront. By contrast compare the profile of Figure 3.2. This profile appears to lend itself to the three pieces shown; however, in using only three pieces the effect around the extremum are minimized and it may be wise to consider the wave in five pieces.

The difference in considering three as opposed to five pieces in the wavefront may be seen in Figures 3.3 and 3.4. In Figure 3.3 the index profile shown in Figure 3.2 was used in three pieces. Note the distinctness of the three discrete sections. Figure 3.4 shows the result of the same profile divided into five sections. It is still easy to note the five individual sections under consideration, however the output is noticeably different. Ideally it would be desirable to have a very large number of pieces used in wavefront calculations. However, the larger the number of pieces, the larger the number of points in the wavefront, and consequently the larger the beam size. To keep the beam/crystal ratio in the proper perspective it is necessary to increase the size of

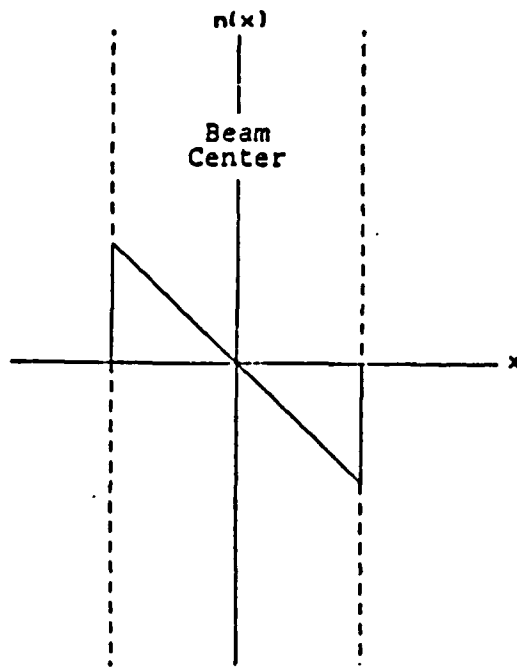


Figure 3.1 Linear index profile considered as one piece.

the crystal whenever increasing the size of the beam, and the maximum crystal size is limited by the available memory. The machine used for this research was limited to two megabytes of random access memory, which allowed for a maximum crystal size of 500 units. To keep appropriate beam/crystal ratios, the beam size used (generally) was between 20 and 40 units and the number of pieces in the wavefront ranged from one to eight, depending on the index profile.

A second limiting factor in the use of this simulation is seen in cases where there is beam crossover. This happens when the index profile has a larger gradient on the side away from the c-axis than it does on the c-axis side. An example of this type of profile can be seen in Figure 3.3. In this case the beam intensity profile is considered to be Gaussian and the more intense section of the beam (i.e. the portion nearest the center) dominates over the weaker section. This ignores any consideration of two beam coupling which would actually occur.

The final major limiting factor is the inability of the model to fully account for a piece of the wavefront which breaks away from the main portion of the incident beam. A case where this happens is seen in Figure 3.3 . In this case the index of

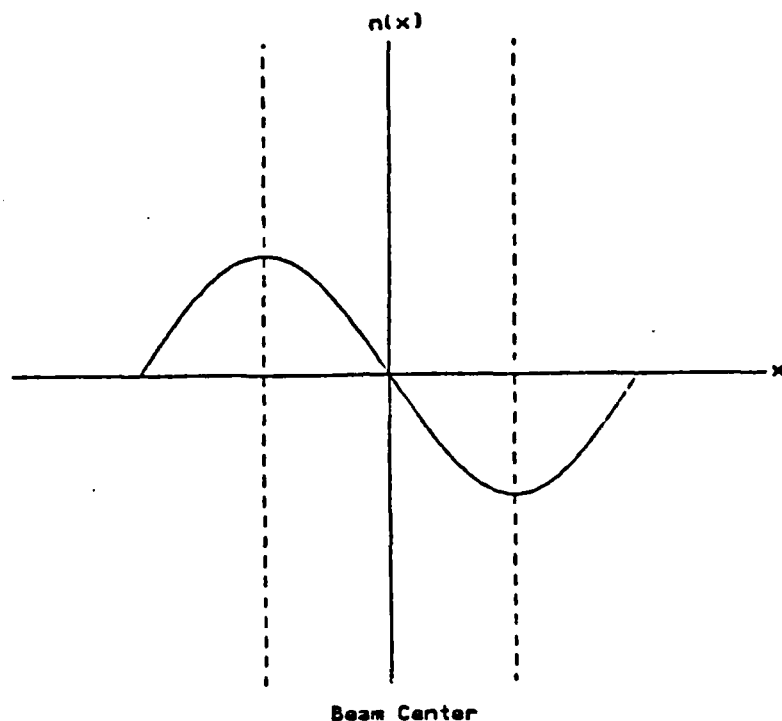


Figure 3.2 Nonlinear profile with possible divisions.

refraction gradient across the piece is the same as when it was part of the entire beam. This *may* be a proper assumption if the beam was continuous during fanning; however, as can be seen in Figure 2.4 and many others presented here, there are often portions of the beam which leave the major portion of the incident beam entirely. Under the condition of a complete disconnection it is possible that the total index gradient should be based on  $\Delta n_{\max}$  and not on the index gradient as it was calculated when the wavefront piece was within the incident beam; this was not programmed into the model. There are presently no data available indicating the effect of a detached piece of a beam in contrast to the continuous case. This problem is circumvented when a profile such as that shown in Figure 3.1 is used so that only one wavefront piece is considered.

#### D. RESULTS

As noted above, the output of the simulation is dependent on the index profile, the beam/crystal ratio, the angle of incidence and the position on the crystal where the incident beam enters. The criteria for success (of possible SPPC) of a given

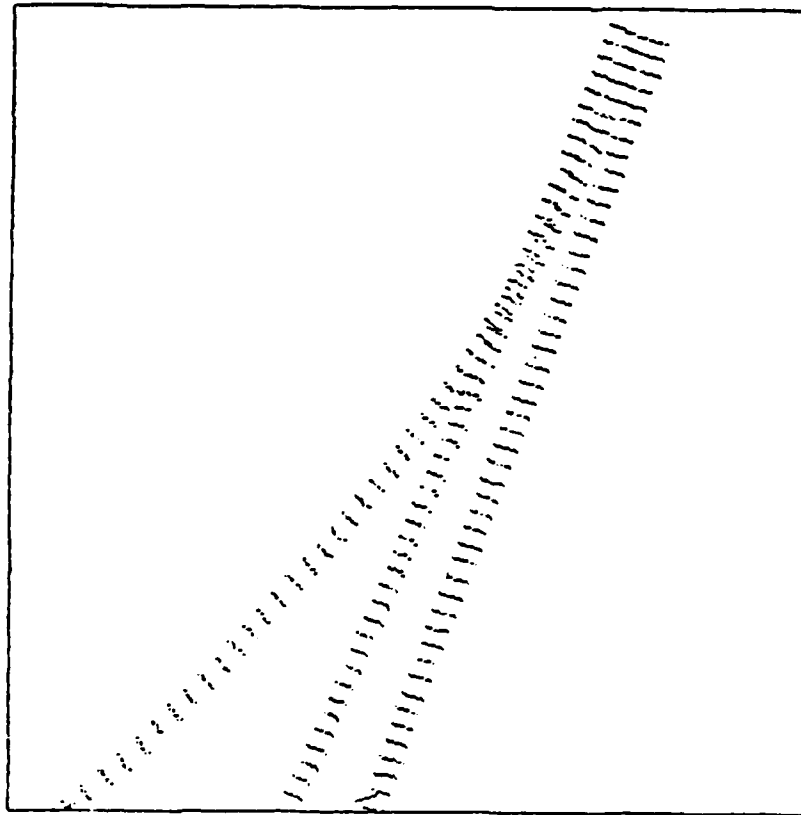


Figure 3.3 PSIM output for profile shown in Figure 3.2.

configuration was taken to be the ability of a portion of the beam to reflect off the crystal corner in such a way as to reintersect itself. This would allow for the production of auxiliary beams which are a prerequisite to SPPC. Therefore, a result such as that seen in Figure 3.5 would be considered capable of SPPC, and one such as that seen in Figure 3.6 would not.

Since the purpose of this investigation is to model beam fanning, the most important parameter is the index profile. To concentrate on this parameter, a beam/crystal ratio and angle of incidence that matched one of the configurations seen in the laboratory were chosen. The configuration chosen was an often used configuration with a beam/crystal ratio of 0.064 and an incident angle of  $40^\circ$ . The incident beam entered the crystal at a point  $\frac{3}{5}$  way across the face of the crystal. This corresponds to a crystal observed in the laboratory of 5.0 mm on a side with a beam of size 0.32 mm, incident 3 mm from the front side of the crystal.

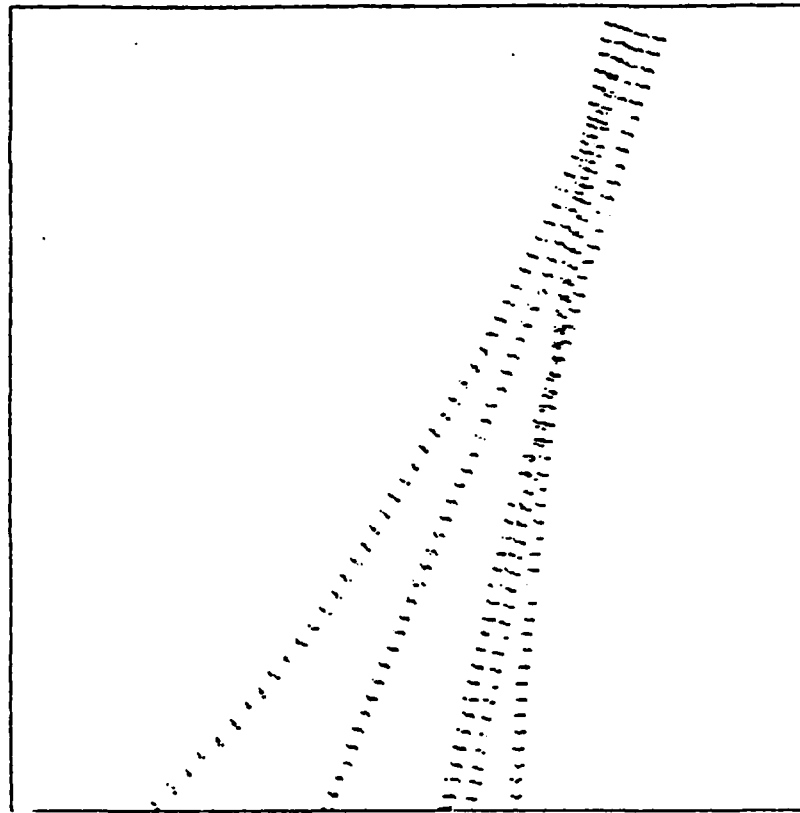


Figure 3.4 PSIM output for profile shown in Figure 3.2 but broken into five separate pieces.

Modeling was run with three index profiles. The rationale behind the use of the profiles will be explained in Section E of this chapter. In each case the values of  $\Delta n_{\max}$  which caused successful SPPC due to beam fanning are presented.

Following the theory of Feinberg [Ref. 2], the first index profile used was that shown in Figure 2.5. Successful SPPC from beam fanning was seen (Figure 3.8), however, note the beam fanning in the direction opposite the  $c$ -axis: this is never observed in practice.

The second beam profile used is shown in Figure 3.1. A typical successful run is shown in Figure 3.9. Although this approximates some observations of beam fanning, note the lack of a continued incident beam as one often (but not always) observes.



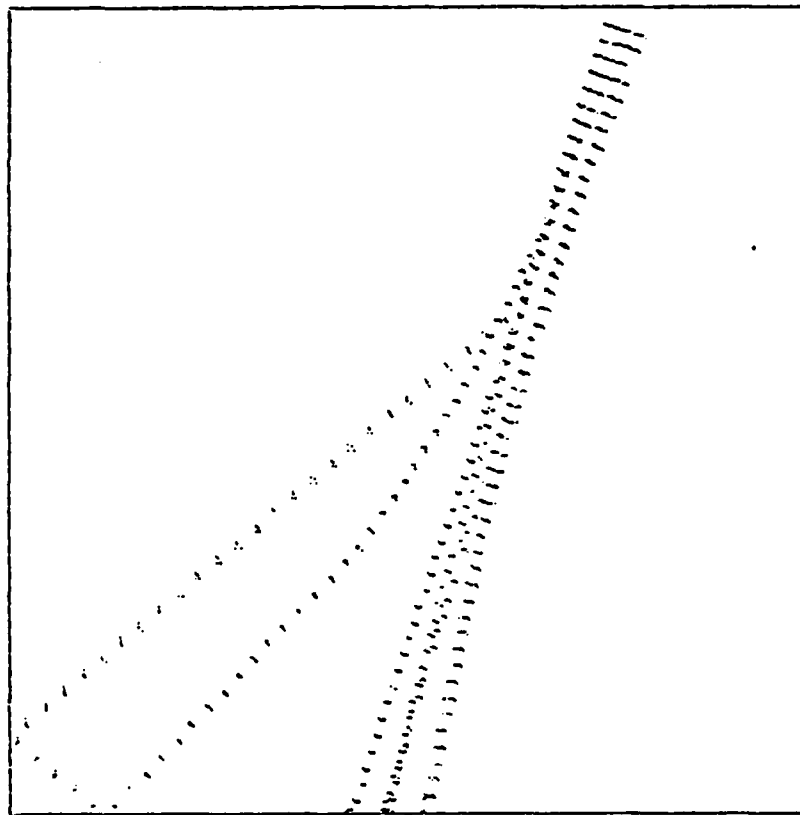


Figure 3.5 Beam fanning resulting in successful SPPC.

The final profile used is shown in Figure 3.7. SPPC due to beam fanning was exhibited as is seen in Figure 3.10. It was this configuration which exhibited results closest to those observed in the laboratory.

### E. DISCUSSION

The first index profile is taken directly from Feinberg [Ref. 2]. To arrive at a profile such as this it is necessary to assume that charge migration in the photorefractor is symmetric, resulting in a net charge distribution such as shown in Figure 2.5. The beam pattern predicted by the simulation is shown in Figure 3.8. The major problem with this profile is the fanning of the beam in the direction opposite the c-axis due to the tail of the index profile. In his original work Feinberg only considers the central region since it is the most intense part of the beam, ignoring the tails of the profile. As can be seen from the model, the tails of the profile cannot be totally

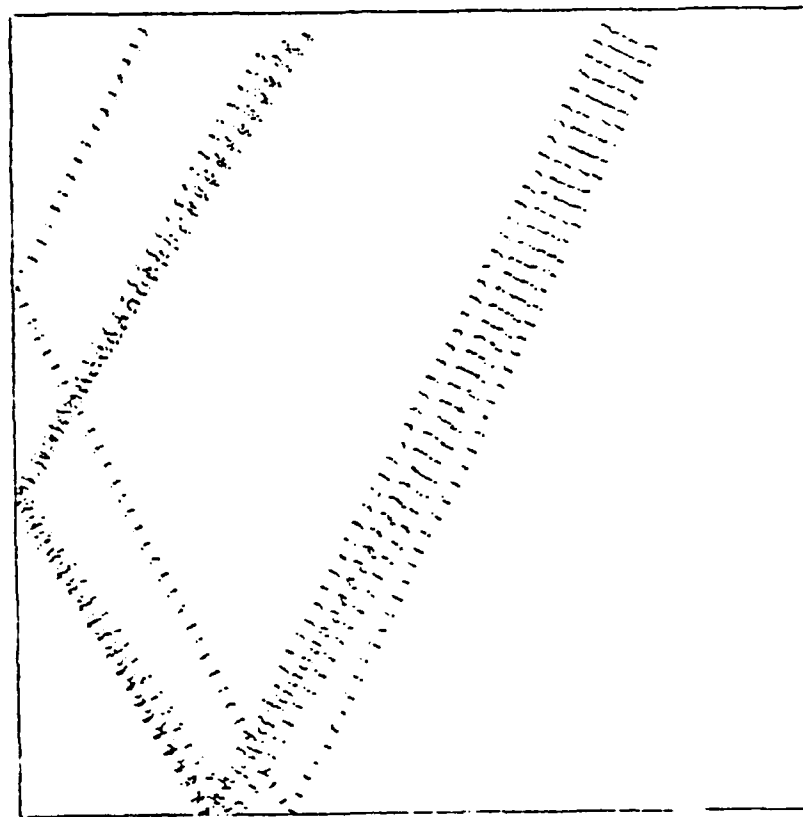


Figure 3.6 Beam fanning not resulting in successful SPPC.

ignored. To arrive at the observed effect with the index profile of Figure 2.5 it is necessary to assume that barium titanate exhibits asymmetric self-focusing (i.e. self-focusing only in the direction of the  $c$ -axis). If asymmetric self-focusing was present, then the (less intense) light subject to the profile of the tails would be unable to fan against the  $c$ -axis. To date there has been no reported evidence of self-focusing of any kind in  $\text{BaTiO}_3$ ; however, this does not preclude the possibility since it would only affect a weak portion of the beam and may not be obvious to the casual observer. Note that the fanning against the axis on the left-hand side of the beam would be abated by two beam coupling and might not be readily discerned.

An alternative explanation is that the crystal response to the beam is not characterized by the curves shown in Figure 2.5. Instead, all available charge may be totally excluded from all portions of the beam, resulting in the profiles shown in Figure 3.11.

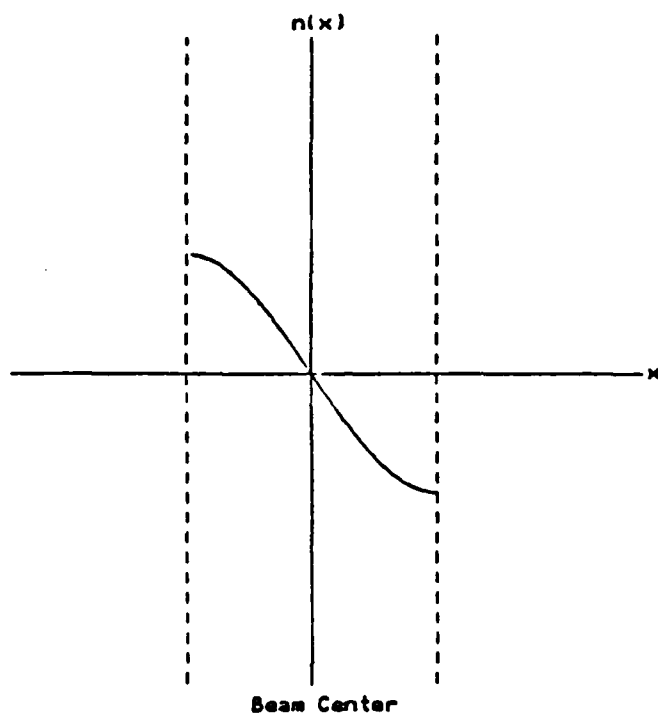


Figure 3.7 Index profile for simulation of beam fanning in BaTiO<sub>3</sub>.

In an effort to approximate an index profile which would exhibit the necessary behavior, the profile shown in Figure 3.1 was used. This beam profile was arrived at by making the important assumption that there is a total exclusion of charge carriers within the illuminated section of the crystal. This is an easy profile to work with since the outcome is independent of the number of pieces considered in the wavefront, as previously mentioned. The result of the simulation with this profile is shown in Figure 3.9. However, there are two major problems with this profile. The first one is the lack of extension of the incident beam as mentioned above. Note that in *most* of the photographs presented in Appendix A there is an extension of the incident beam. This is almost universally, though not exclusively, true (see Figure A.5 for example). Second, it is unrealistic in its sharp transitions. Both of these problems are solved with the introduction of the third index profile.

The final index profile (Figure 3.7) resulted in a beam geometry which exhibited all of the requisite properties. This profile was arrived at by the rounding of the discontinuities of the prior profile; specifically, a sine function was used to arrive at the configuration shown in Figure 3.7. The results of the simulation are presented in

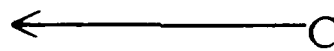
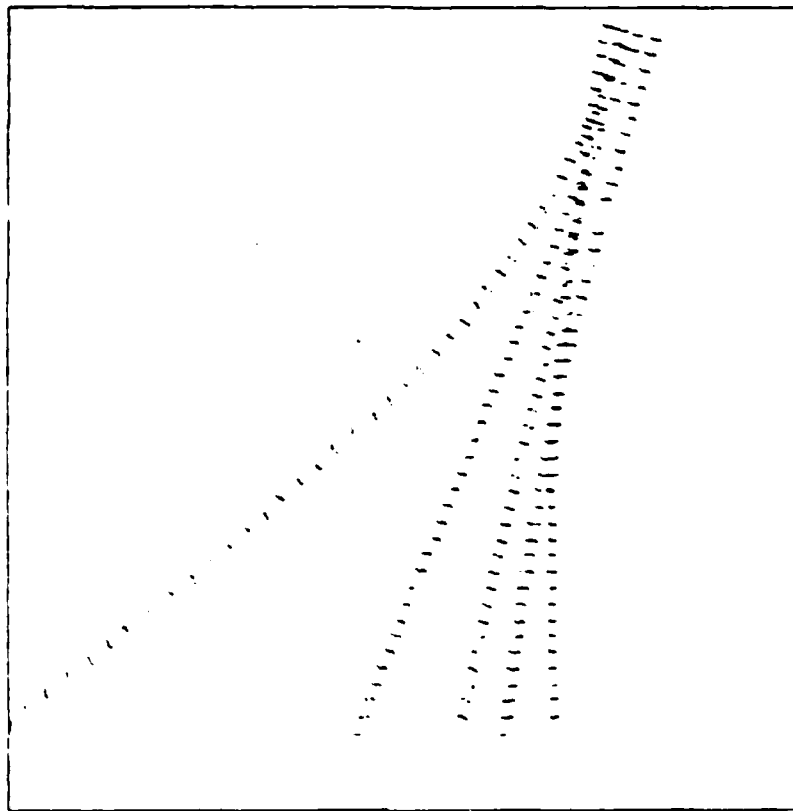


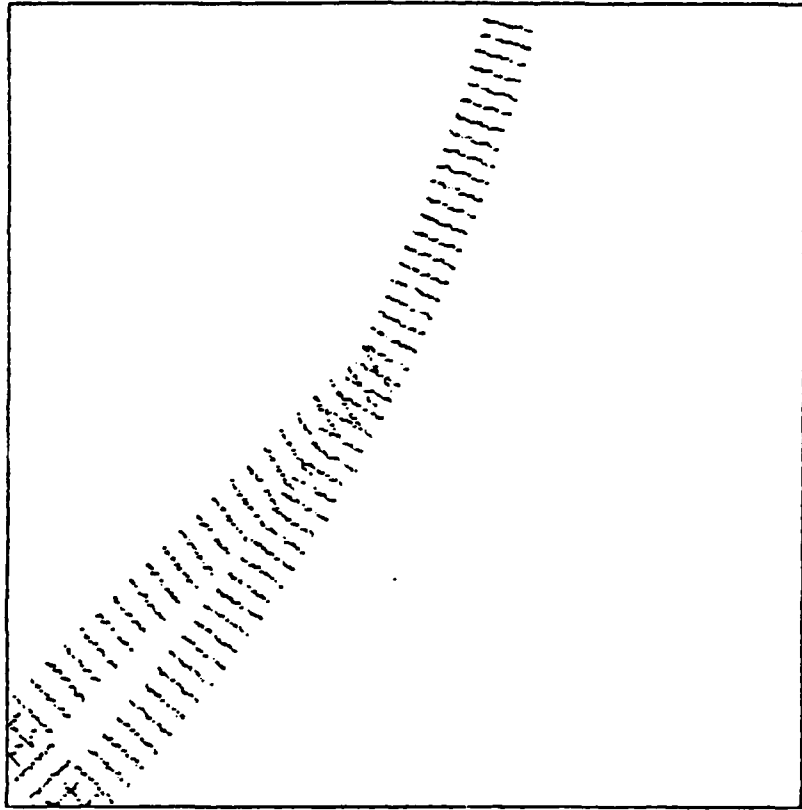
Figure 3.5 PSIM output using the index profile of Figure 2.5.

Figure 3.10. To arrive at this profile it would be necessary for diffusion of the charge carriers almost completely out of the incident beam path. The eventual diffusion of charge carriers completely out of the path may actually be expected since any light of intensity above ambient will cause any charge carriers to eventually be totally liberated<sup>4</sup>. The graphs of Figure 3.11 show the necessary charge, electric field and intensity profile of the incident beam necessary to arrive at an index profile similar to that used in this instance. It is assumed that the continuation beam in the left would be assumed to be a constant intensity of 1000 units, causing the appearance of the continued beam.

<sup>4</sup>Feinberg shows however, that the electric field may be proportional to the gradient of the incident beam intensity. [Ref. 27]

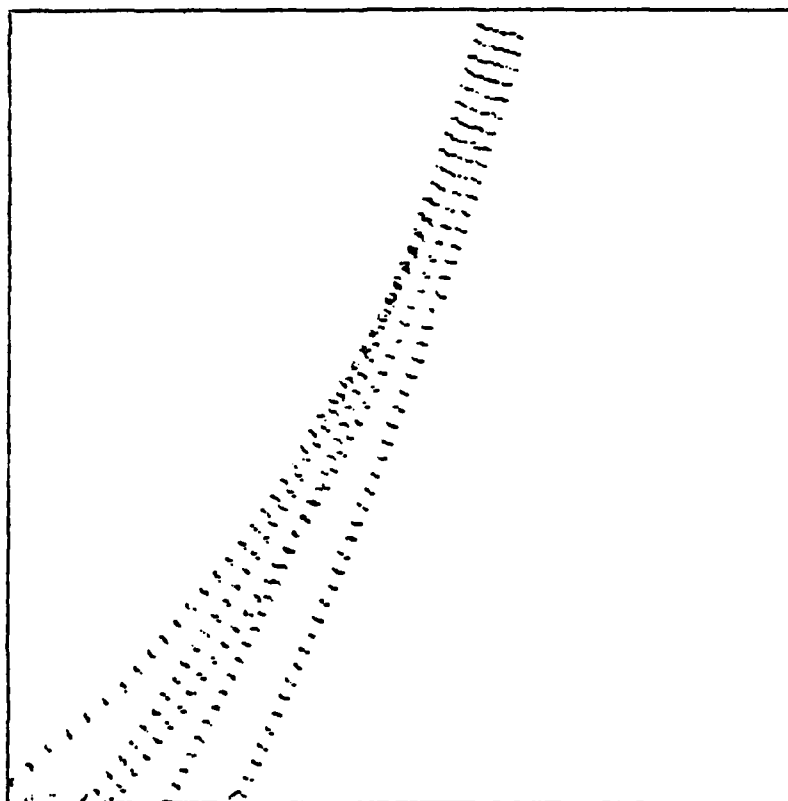
To arrive at the configuration of Figure 3.9 a value of  $\Delta n_{\max} = 0.03$  was used. In Figure 3.10  $\Delta n_{\max} = 0.02$ . Regardless of the profile used, these values of  $\Delta n_{\max}$  are characteristic of the value necessary to account for the observed beam fanning in  $\text{BaTiO}_3$ . For successful SPPC with the configuration chosen,  $\Delta n_{\max}$  must be greater than  $10^{-3}$ . Reducing the beam size will obviously reduce the necessary value of  $\Delta n_{\max}$ , but values on the order of  $10^{-2}$  to  $10^{-3}$  are typical.

Thus, the simulation has predicted the necessary change in index of refraction across the beam path, and the necessary profile of that change. In Chapter V the results of the necessary value for  $\Delta n_{\max}$  will be compared to those possible for the crystal. Also, the physical implications of the necessary profile of the index of refraction within the beam path, as determined by the simulation, will be discussed. The comparison of the information derived from the simulation to that experimentally derived from the crystal, will show that the necessary conditions cannot be met in  $\text{BaTiO}_3$ .



← C

Figure 3.9 PSIM output using the index profile of Figure 3.1.



← C

Figure 3.10 PSIM output for index profile shown in Figure 3.7.

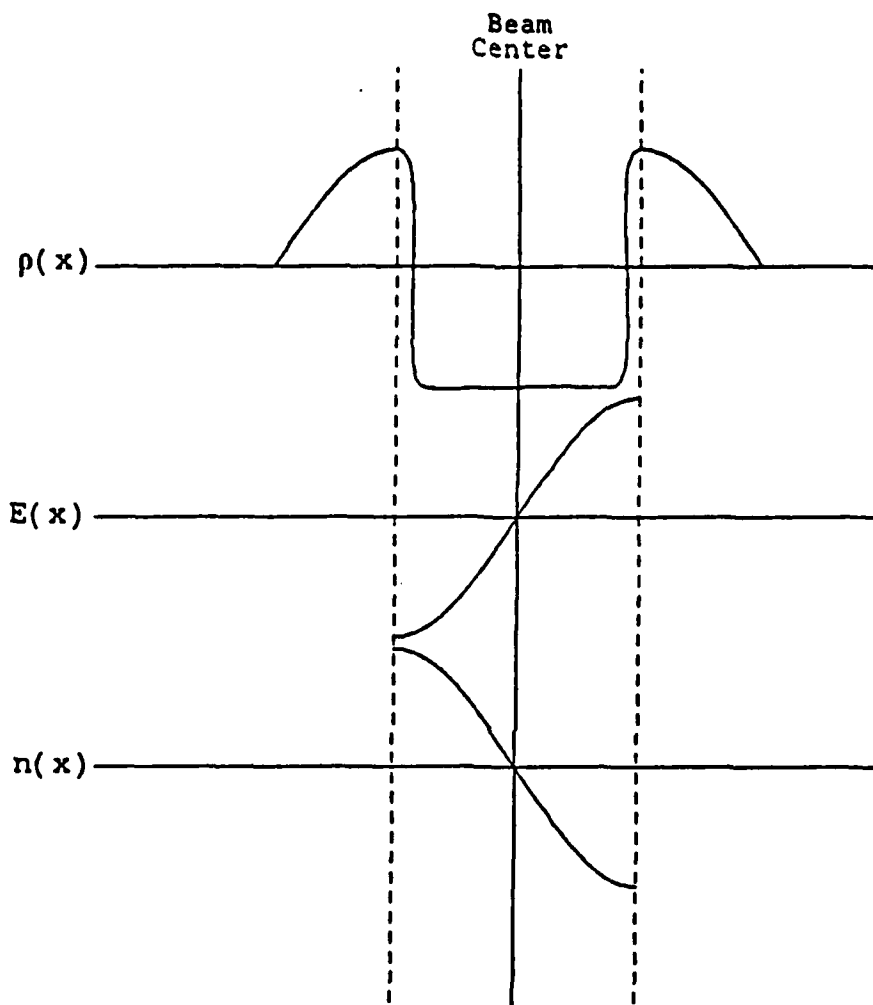


Figure 3.11 Necessary charge distribution and electric field to produce the index profile of Figure 3.7.



## IV. EXPERIMENTS

### A. INTRODUCTION

In order to investigate beam fanning in  $\text{BaTiO}_3$ , an experiment was designed to measure the influence of a change in the incident beam diameter on the fanning process. If fanning increases with a decrease in beam diameter, it could be concluded that beam fanning is a direct result of the change in index of refraction within the beam path, as predicted in Equation 2.25. If, however, the fanning decreases with a decrease in incident beam diameter, it could be concluded that beam fanning is actually forward-scattering due (probably) to SPS, since, as shown in Equation 2.28, the gain per unit length will decrease with a decrease in spot size.

### B. EXPERIMENTAL APPARATUS

The apparatus used for this work is shown in Figure 4.1. The laser was a Spectra Physics  $\text{Ar}^+$  variable power (20 mW maximum), multimode laser, model #162A-07. During the experimentation the laser was operated at all of the visible lines and was not optically isolated from the experiment. Upon leaving the laser, the beam was directed into a polarization rotator in order to rotate the beam from the ordinary to the extraordinary polarization in the crystal. To ensure that only extraordinarily polarized light was used, the beam was then directed through a Glan-Thompson polarizer. Following the polarizer was a beam splitter, to enable the observation of any phase-conjugate reflection, and a variable aperture of the type common in photographic lenses. This aperture acted as a spatial filter, reducing the amount of scattered light reaching the crystal. The beam was then focused onto the crystal by uncoated lenses of either 34 cm or 16 cm focal length.

The crystal was one of four single crystals of  $\text{BaTiO}_3$  manufactured by Sanders Associates and poled into a single domain. Two of the crystals (on loan from the Los Alamos National Laboratories) measured approximately 5 x 5 x 5 mm and were transparent with a slight yellow tint. Two of the crystals (belonging to the Naval Postgraduate School) measured approximately 5 x 5 x 2.5 mm and had no noticeable tint to them. The crystal was mounted on a rotatable platform capable of being translated 12 cm along the axis of the optical bench on which all of the components were mounted. Following the crystal, and connected to the mounting table, was a

knife edge. The knife edge was coated with black tape to ensure that a resonating cavity was not formed with the crystal. Behind and to the side of the knife edge, also connected to the translation table, was a silicon photodiode connected to an electrometer measuring the short circuit current.

### C. EXPERIMENTAL PROCEDURE

To measure the amount of beam fanning quantitatively, the knife edge was aligned in such a way that the beam transmitted through the crystal was blocked from the detector. To ensure that the blockage of the transmitted beam was sufficient, the table was translated rapidly along its entire range of motion and the detector output was monitored to ensure that there was little or no change in the recorded intensity. The vibration inherent in the movement and the changing beam diameter of the incident beam ensured the lack of significant beam fanning, so that a lack of change in the recorded intensity indicated that the transmitted beam was completely blocked from the detector for all observed beam diameters.

Once the crystal, knife edge and detector were in position, the beam was blocked and the crystal was flooded with light from a 75 watt incandescent lamp located approximately 12 cm away. After approximately one minute the light was turned off and the laser beam was unblocked. The intensity of the light reaching the detector was then monitored and the peak and steady-state intensities were recorded. Once the intensity had reached a steady-state value the beam was again blocked, the crystal was translated and flooded with white light, and the procedure was repeated.

The flooding of the crystal with white light effectively homogenized the charge distribution within the crystal and ensured that one reading was not affected by the previous one. Special care was taken to ensure that the beam was parallel to the crystal table and that all components were mounted on the optical axis of the optical bench. The precision translation mechanism on which the crystal table was mounted ensured that the beam was incident on the crystal with the same center for all measurements. These precautions effectively compensated for any surface inconsistencies on the crystal face except at very small laser beam diameters.

Both peak and steady-state values of the fanned beam intensity were recorded; however, only the peak values were used for final analysis. This decision was made because, although the steady state values generally correlated with the peak values, the steady state values could be affected by numerous variables. One obvious problem with steady-state readings is the possibility of phase conjugation, thus reducing the

amount of fanning recorded in the steady state. Also, due to the orientation of the detector, it was possible (even likely) that the beam would fan across the detector, eventually coming to rest past the area it can record; sometimes the fanning was observed to exit the face perpendicular to the face the detector was monitoring. To reduce all of these effects, the incident beam was originally allowed to enter at only small angles to the c-axis ( $\sim 2^\circ - 5^\circ$ ) and, although alignment was tedious, consistent results were obtained for various crystals, lens focal lengths, laser lines and incident angles. Eventually larger incident angles were used ( $\sim 20^\circ - 40^\circ$ ) with similarly consistent results.

To ensure that the observed effect is not influenced by scattering initiated by small (e.g. molecular size) crystal inhomogeneities, one configuration was chosen in which there was moderate fanning and the fanned intensity was recorded for each of the available visible lines of the laser. The result was a mean ratio of incident intensity to fanned intensity that was constant across all available wavelengths, thus indicating no resonances and no dependence of scattering on wavelength at the available laser lines.

After the data were collected, the beam diameter at each point was measured with an Aeronca Electronics *Laser Blade* and the direct laser intensity was recorded. Here, the beam diameter is defined as twice the distance from the center of the beam to the point of 10% intensity. For analysis purposes the beam diameter could be divided by the cosine of the angle of incidence so that the beam diameter would be that actually along the y-axis of the crystal.

Measurements were also made by placing the detector above the crystal as the incident beam diameter was changed. This gave an indication of the total amount of scattering, not just asymmetric scattering. In this case, the front surface of the crystal was shielded from the detector with black tape to keep specular reflection off of surface irregularities from influencing the measurements. Transmission measurements were also made by replacing the knife edge with an aperture, thus allowing only the transmitted portion of the incident beam to reach the detector.

#### D. RESULTS

Typical results of the fanning measurements are shown in Figure 4.2. In this case the crystal was at an angle of  $< 5^\circ$  so the beam diameter need not be adjusted for  $\cos\theta$ . All intensity recordings have been normalized for comparison purposes. The shape of the curves is insensitive to the laser line used, beam angle, choice of crystal,

and the divergence or convergence of the incident beam (i.e. whether the crystal is placed in front of or behind the focal point of the focusing lens).

Figure 4.3 is a plot of the intensity seen from above the crystal for various beam diameters for converging light. There are two important things to note here. First, there is less scattering for smaller beam diameters and second, the sharp discontinuity at about three micron beam diameter. This discontinuity is noticeable as the crystal goes through the focal point of the focusing lens. Figure 4.4 is a plot of the scattering as viewed from above the crystal for diverging light. Note the initial decrease in the scattering within the first four microns. This is only apparent with diverging light and is seen in all crystals I used. Note also that there is a much broader dynamic range in the intensity for diverging light than for converging light.

Although all of the scattering data are generally insensitive to which crystal is used (i.e. the general shape of all the curves for a given situation is the same for all crystals), the same cannot be said for the transmitted beam. Figures 4.5 and 4.6 show the transmitted intensity for all four crystals plotted together. Crystal #2 is the only one which does not exhibit SPPC and is the only crystal in which the transmitted beam intensity increases with beam diameter as a general trend. However, note that all of the curves exhibit some inflection point around six micron diameter for diverging light. This inflection is not a consistent maximum or minimum; it depends on the crystal. Presently I cannot explain the cause of these dissimilar curves. Generally it may be noted that the transmitted intensities map the same characteristics as the scattered intensity, but inverted, as would be expected. All of these various features will be addressed later, but the important aspect of all of the data is obvious; *increased* beam diameter results in *increased* beam fanning.

Although these data alone are a strong indication of the lack of index change within the beam path due to the photorefractive effect, there exists even stronger evidence. By removing the knife edge and detector from behind the crystal, the image of the transmitted spot could be observed on a screen approximately three meters away. Figure 4.7 shows the image of the spot, which was projected directly onto photographic film at different times after the beam was allowed to enter the crystal, and prior to the onset of phase conjugation. Figure 4.7a is an image of the beam immediately after turn on; notice the spot is generally undistorted. Figure 4.7b is a photograph between turn on and steady-state, and Figure 4.7c is a photograph at steady-state. By viewing these images it is clear that the energy of the beam is first extracted from the *outside* of the beam and not from the inside.

In addition to the above measurements, the index of refraction of the crystal was estimated by measuring Brewster's angle. At  $\lambda = 514$  nm the published value for the extraordinary index of refraction is  $n_e = 2.424$  [Ref. 22], however, my measurements consistently resulted in  $n_e = 2.26 \pm 0.02$ . This large discrepancy is still unexplained. It is also interesting to note that, although there was a distinct minimum at Brewster's angle, the reflection did not disappear entirely. The minimum was so slight that it was quite difficult to find, and eventually a photodetector had to be used to accurately locate it. It is possible that both of these observations may be explained by the presence of impurities on the surface of the crystal. Specifically, an oil film from the hands of the experimenter may be at fault. Additionally, there is the possibility that heating at the surface of the crystal due to the high energy density of the incident beam may be responsible. Since measurements by others [Ref. 30] of the index of refraction of  $\text{BaTiO}_3$  using Brewster's angle have resulted in indices consistent with the reported values, either one or both of these explanations may account for the observed anomalies.

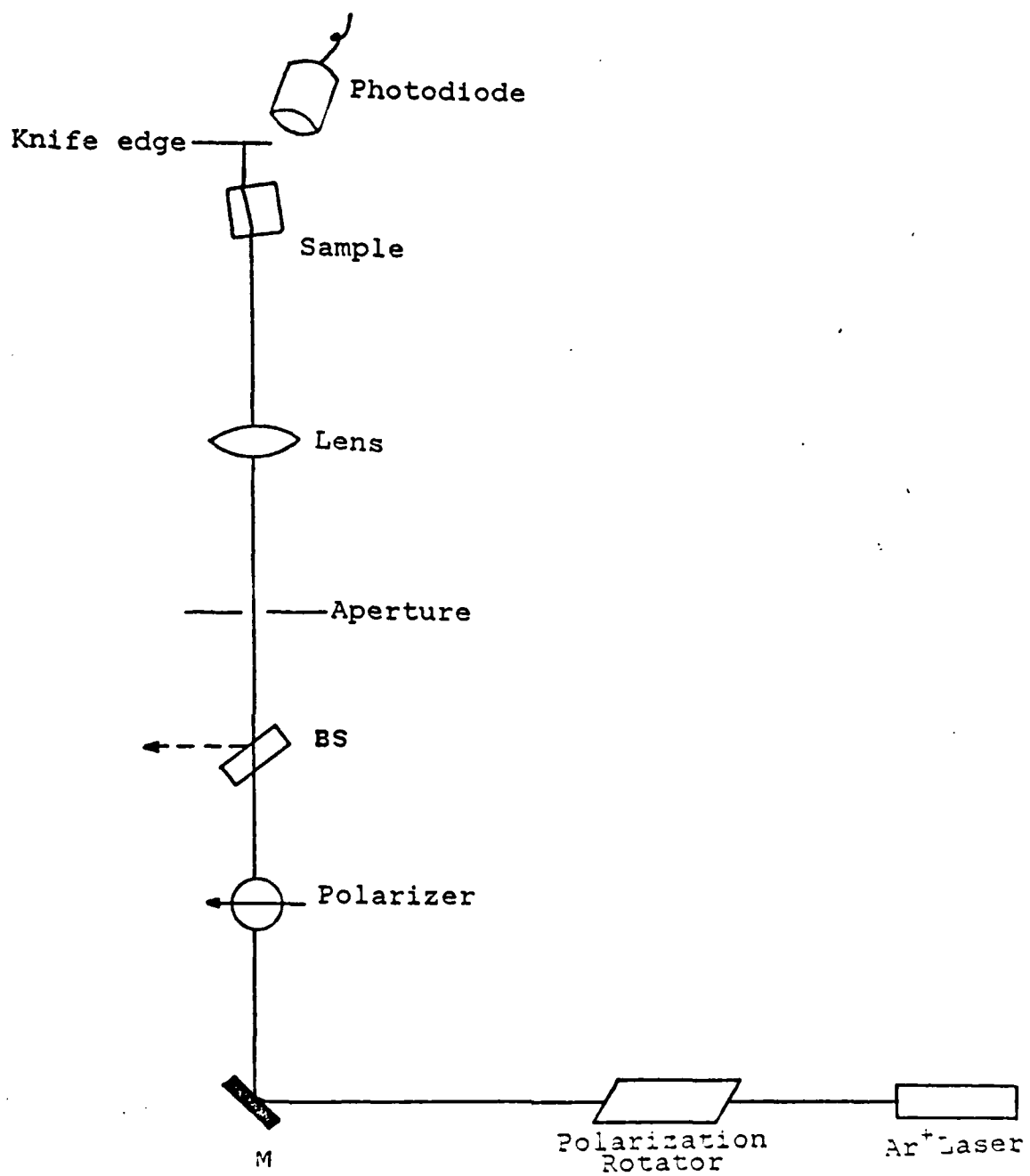


Figure 4.1 Experimental Apparatus.

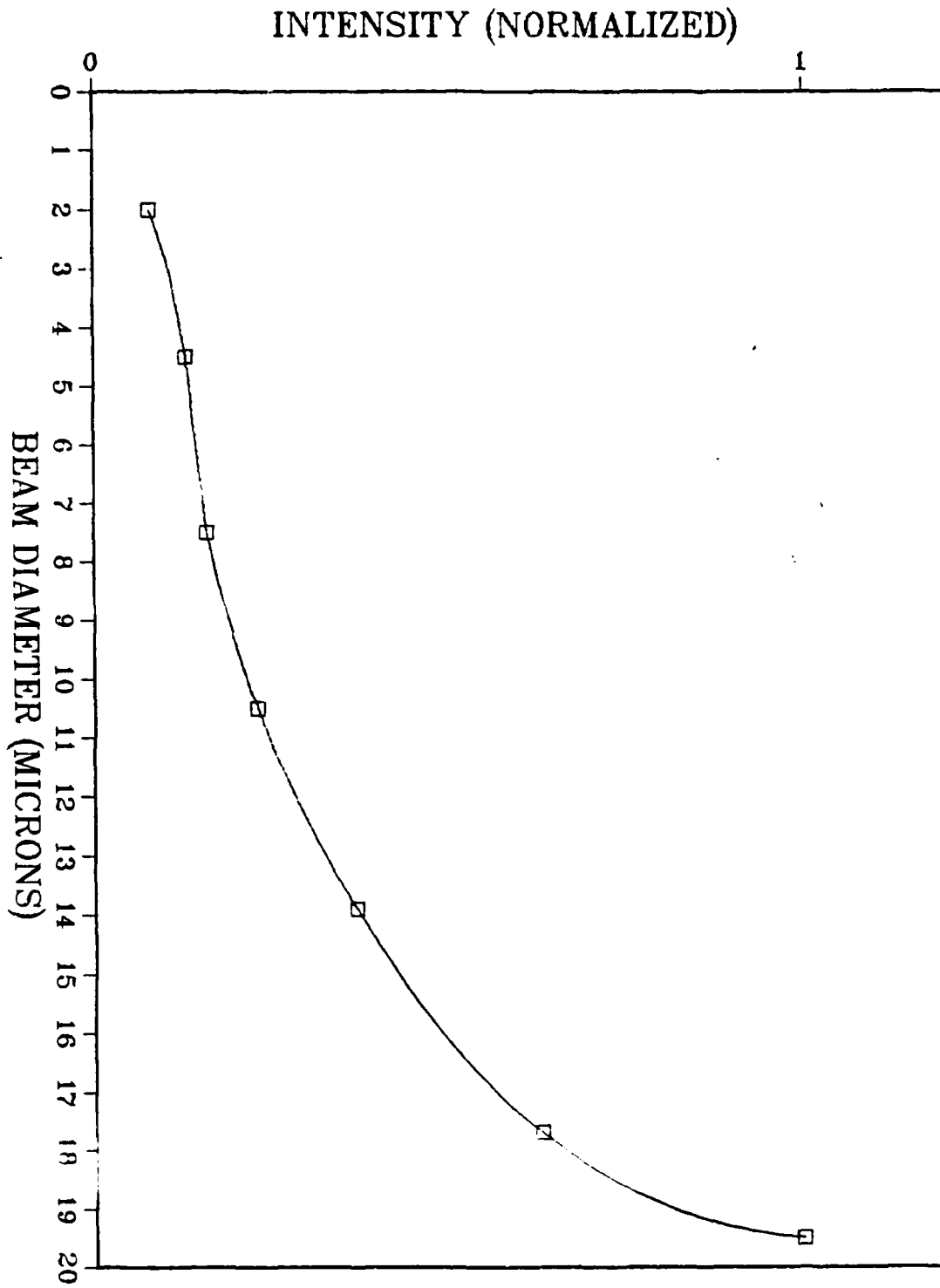


Figure 4.2 Dependence of fanning intensity on incident beam diameter.

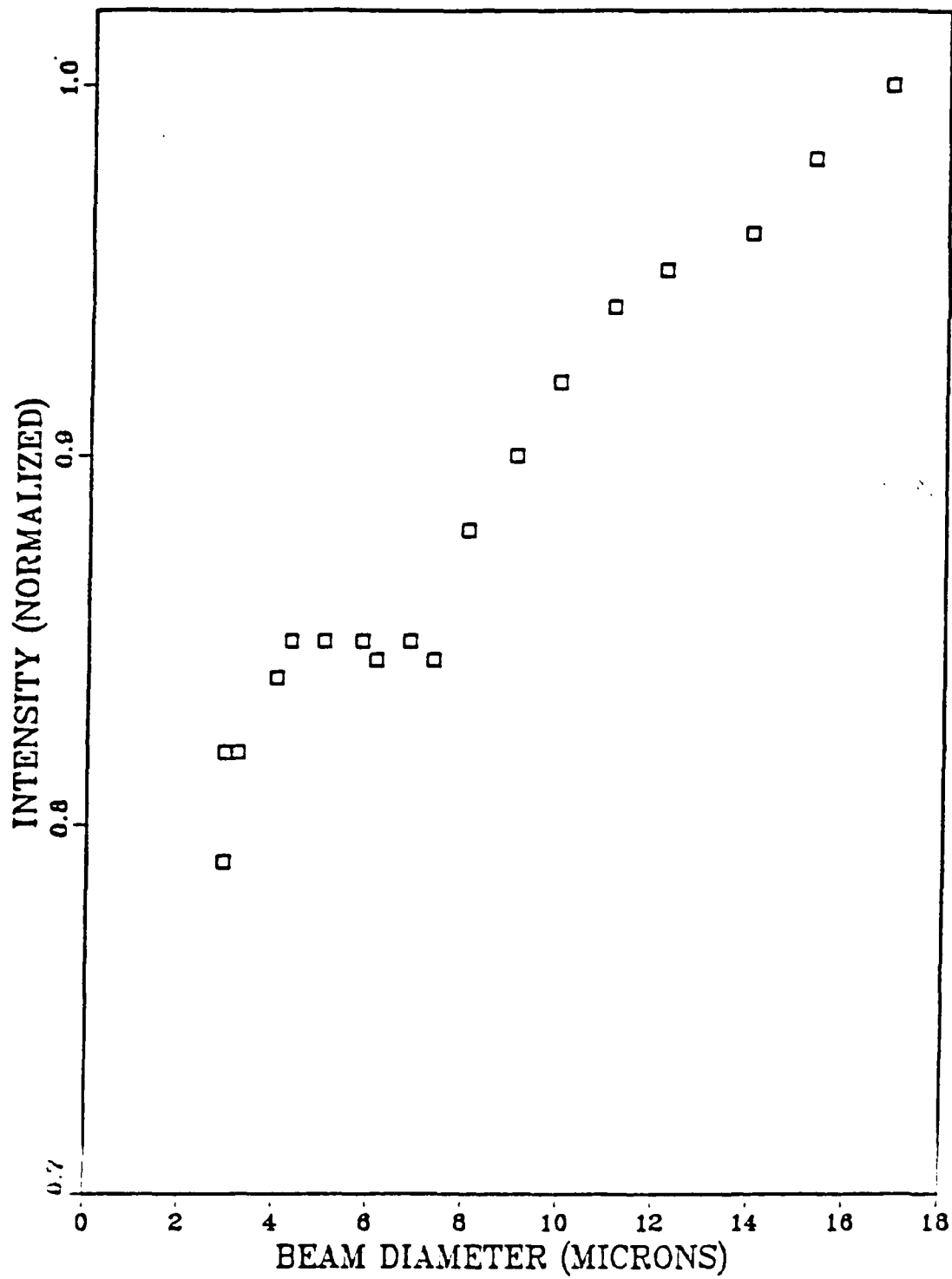


Figure 4.3 Typical dependence of scattered intensity on beam diameter as measured from above for converging light.



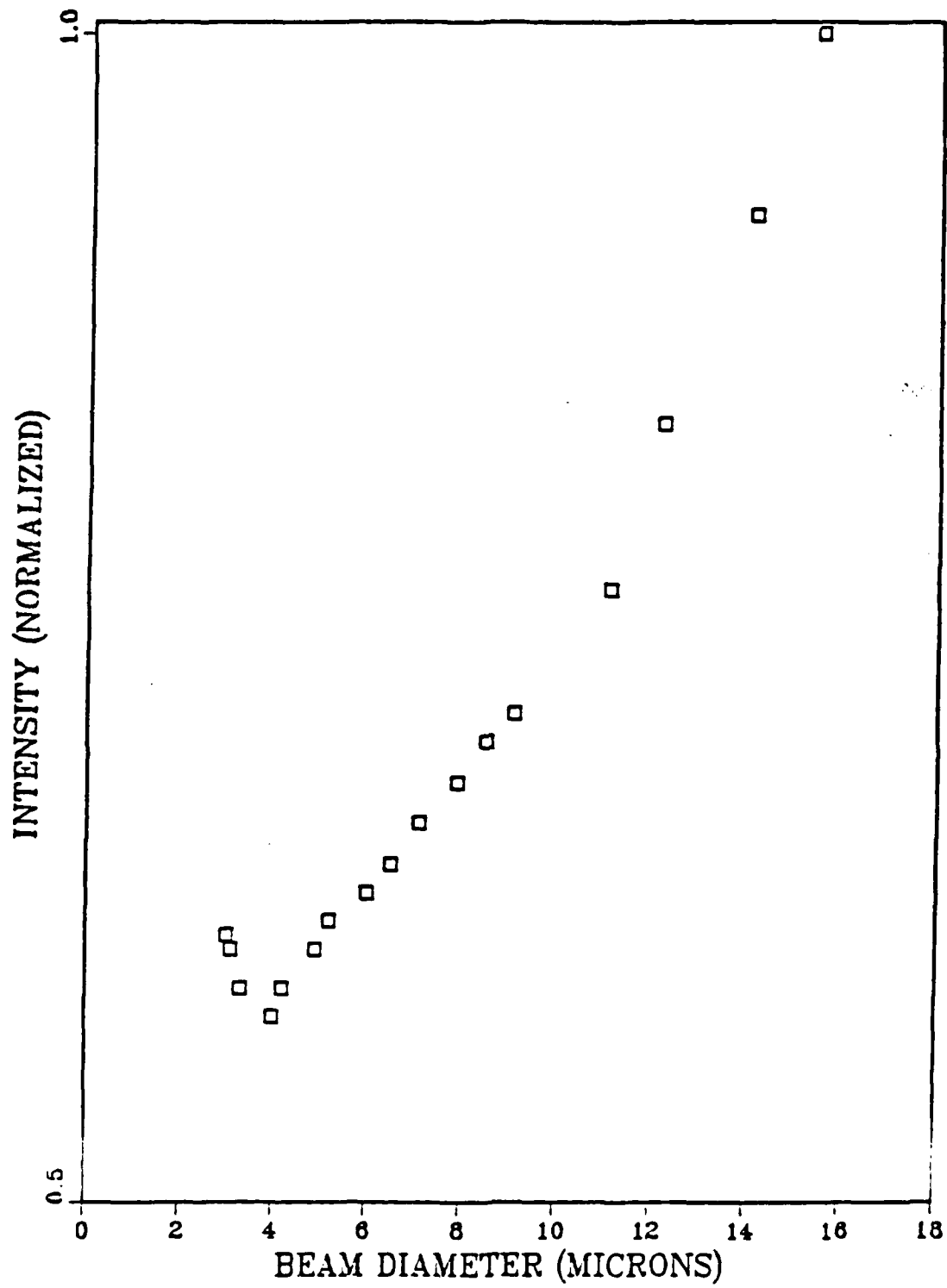


Figure 4.4 Typical dependence of scattered intensity on beam diameter as measured from above for diverging light.

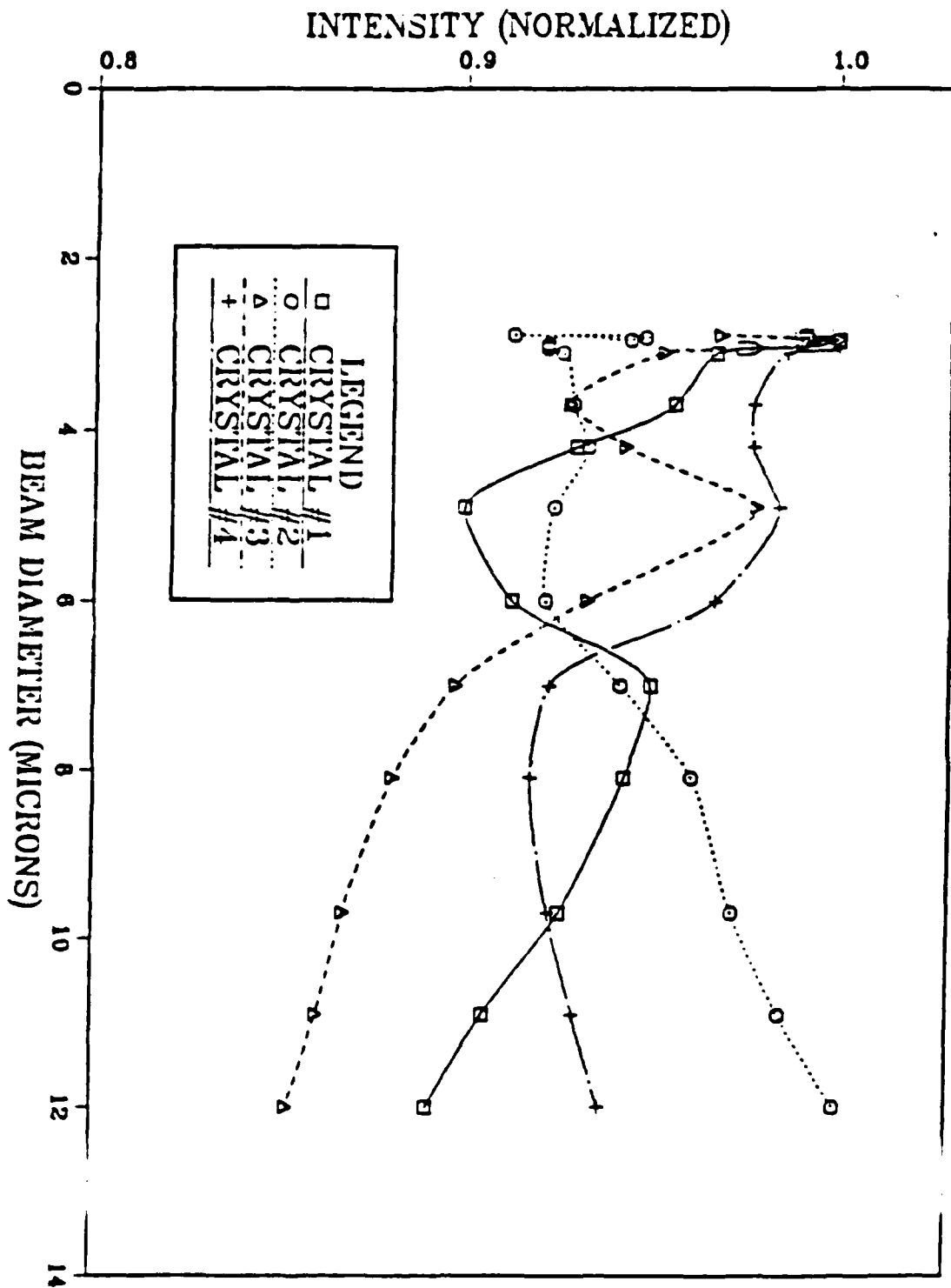


Figure 4-5 Transmitted intensity is a function of beam diameter for diverging light.

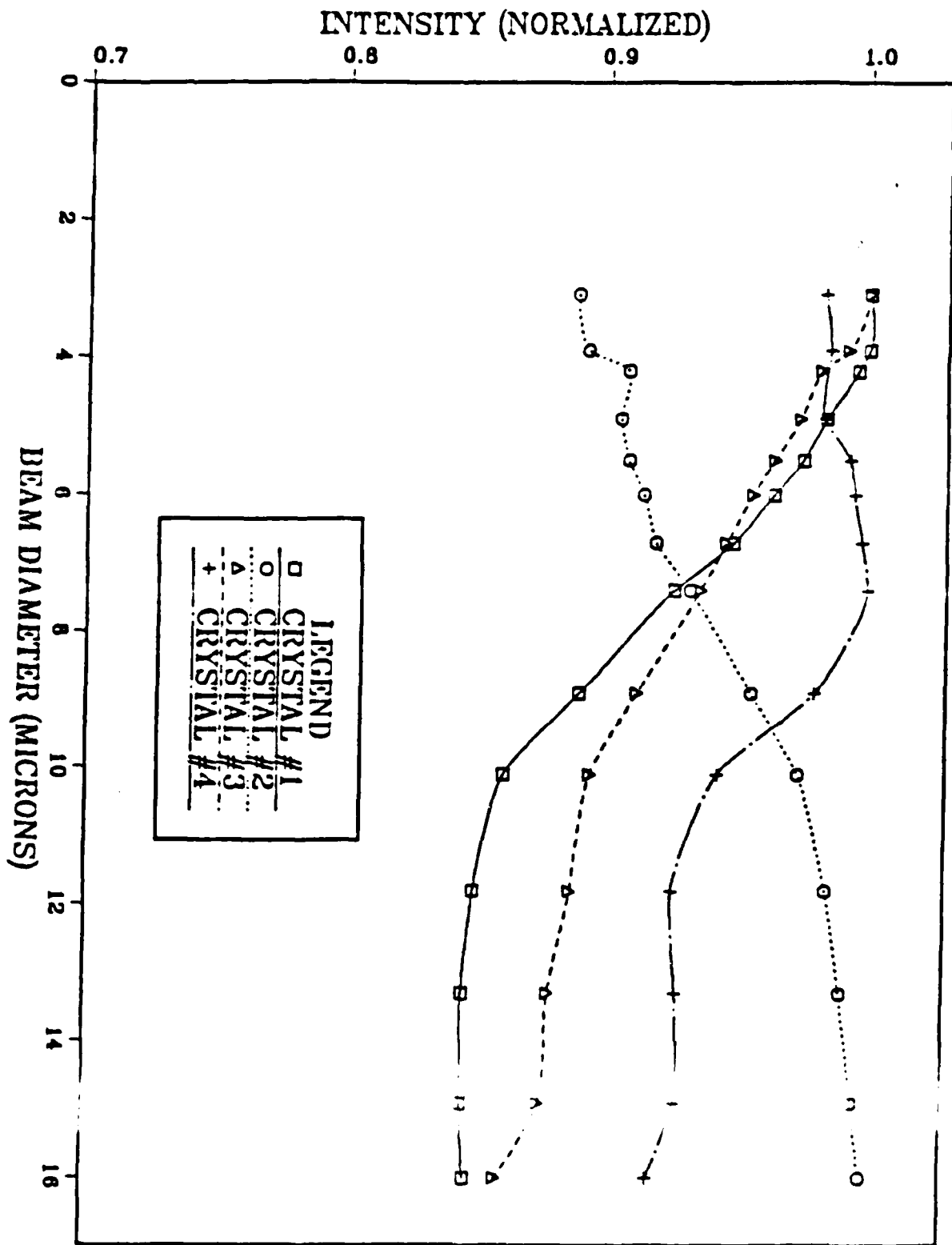


Figure 4.6 Transmitted intensity as a function of beam diameter for converging light.

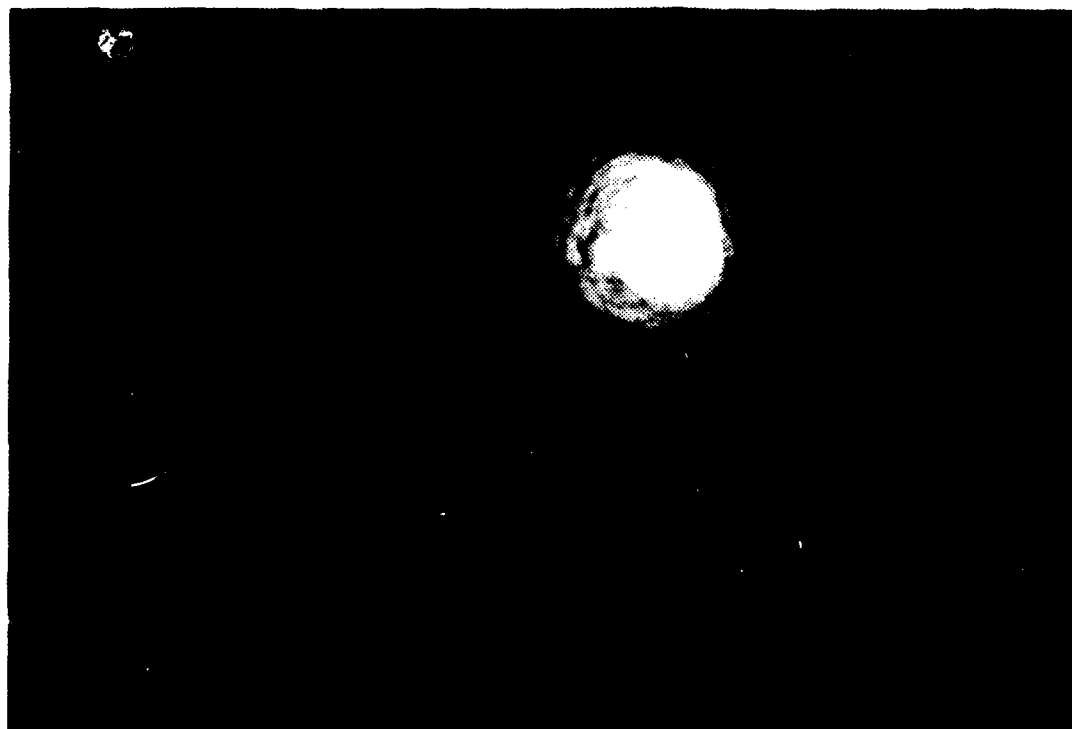


Figure 4.7a Photograph of projected spot immediately upon turning on the incident beam.

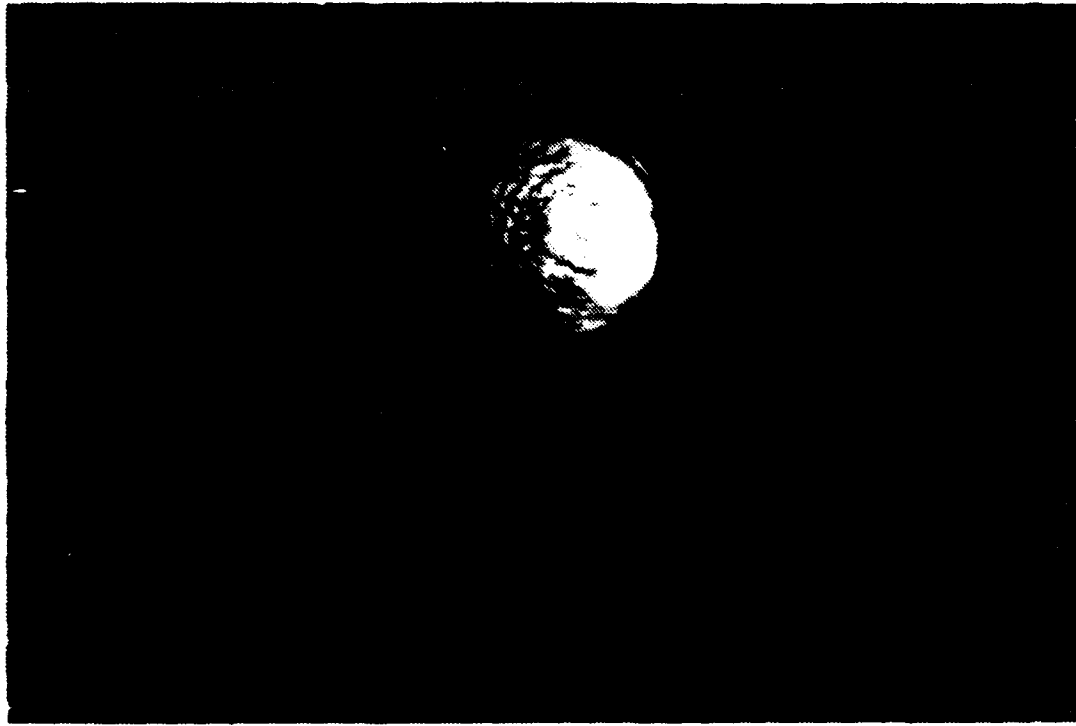


Figure 4.7b Photograph of projected spot after the onset of beam fanning.

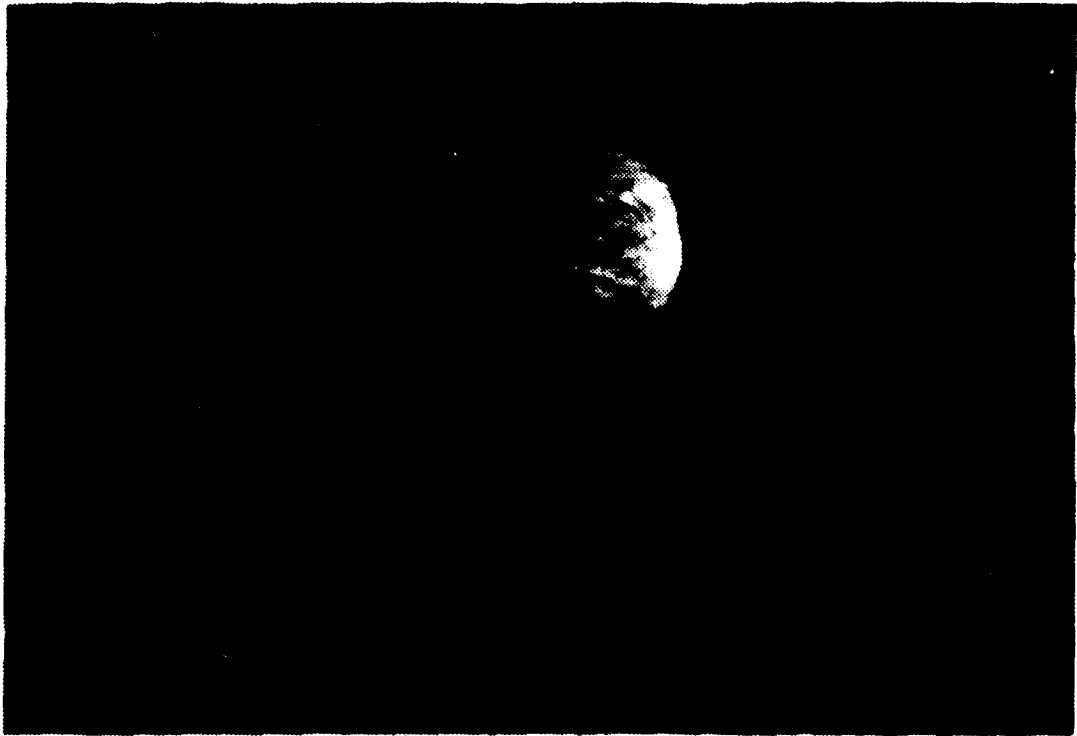


Figure 4.7c Photograph of projected spot in the steady state.

## V. ANALYSIS

### A. DISCUSSION OF RESULTS

The simulation in Chapter III and the experiments described in Chapter IV clearly show that asymmetric self-defocusing cannot be due solely to a change in index of refraction along the beam path within the crystal. Even with the changes of the profile for the change in index of refraction proposed in Chapter III, the necessary value of  $\Delta n_{\max}$  is too large according to the published maximum values for BaTiO<sub>3</sub>. Inspection of the necessary values of  $\Delta n_{\max}$  from the simulation shows that values on the order of  $10^{-2}$  are necessary to account for the observed fanning within the crystal; however, previously calculated values place an *upper bound* of  $\sim 10^{-4}$ , and a value of  $\sim 10^{-5}$  is probably more reasonable<sup>5</sup> [Ref. 11].

This discrepancy may be accounted for only by assuming that the index gradient is limited to a very small portion (in some cases as small as  $1/10$  the size of the input beam) of the center of the beam, or by assuming that the observed effect is a result of another process. It is impossible to justify the first assumption and still achieve the necessary index profile, since charge carriers must be liberated from the entire region where the brightness of the incident beam exceeds ambient. Therefore, by Laplace's equation, the gradient of the electric field within the beam path must be uniform. This leaves only the possibility that another process is responsible for beam fanning.

The results of the experiments of Chapter IV reinforce the conclusions made from the simulation portion. Figure 4.2 shows that beam fanning *decreases* with a decrease in beam diameter. From Equation 2.25 it is clear that this behavior cannot be explained by a change in the index of refraction within the beam path due to the photorefractive effect. If this type of change were responsible for beam fanning, the amount of fanning would have to increase with a decrease in beam diameter. Additionally, as shown in Figure 4.7, beam fanning begins on the periphery and the light is scattered progressing from the *outside* of the beam toward the center. Noting the index profile as shown in Figure 2.2, this is impossible if the fanning is due to an asymmetric change in index of refraction across the beam path, as was originally predicted.

---

<sup>5</sup>Feinberg does, however, calculate a possible maximum value on the order of  $10^{-3}$  [Ref. 27].

One may argue that all of the observed qualities of beam fanning may be explained by assuming "small-scale" self-focusing of the incident beam within the crystal. That is, the incident beam may experience a breakup into spots which are of diameters small enough to create index gradients of the magnitude shown necessary by the simulation in Chapter III. This type of self-focusing has been known for over two decades, and is common in materials whose dielectric constant increases with field intensity [Ref. 31]. If small-scale self-focusing occurred in BaTiO<sub>3</sub>, it could explain many of the effects that are observed during SPPC (e.g. the presence of small filaments, beam fanning, etc.). However, there are serious problems with a small-scale self-focusing theory. First, the breakup of optical beams due to self-focusing has been shown to be spatially periodic, with the periodicity being dependent upon intensity [Ref. 32]. As is demonstrated in Figure 4.7, there is no indication of spatial periodicity in the beam as it is transmitted through a BaTiO<sub>3</sub> crystal. Also, even in good self-focusing mediums at very high beam intensities ( $\sim 10^7$  W/cm<sup>2</sup>), it is necessary for the beam to have a long path length (on the order of tens of centimeters) within the medium before self-focusing is observed [Ref. 33]. Even with a very large change in the dielectric constant, it is unlikely that self-focusing could occur within a medium of only 5 mm in length. Finally, there is no evidence in the literature that the dielectric constant of BaTiO<sub>3</sub> changes significantly with the intensity of the incident light (although it does change with an intensity gradient, as discussed in Chapter II). It is interesting to note however, that the dielectric constant of BaTiO<sub>3</sub> does change with temperature [Ref. 25], and this may cause self-focusing at very high powers and very small beam diameters, given a long enough path within the medium.

From the evidence presented here it follows that asymmetric self-defocusing in BaTiO<sub>3</sub> cannot be due to an asymmetric change in index of refraction along the path of the incident beam due to the photorefractive effect. Attributing this phenomenon to some other process however, is not so easy.

## B. SCATTERING

As noted in Chapter II, the only other theory that is currently available to explain asymmetric self-defocusing in BaTiO<sub>3</sub>, besides the theory just discussed, is the theory involving scattering (SPS) [Ref. 24]. Although I have not conclusively demonstrated that beam fanning in BaTiO<sub>3</sub> is due to SPS, there are a number of observations which indicate that this type of scattering maybe the origin of the effect.



As may be seen in Equation 2.28, if near-forward scattering is the origin of beam fanning, then there should be a decrease in fanning with a decrease in incident beam diameter, an observation borne out in our experiments. Also, the diversion of energy from the incident beam could progress from the periphery toward the center, since noise photons originating from outside the beam must interact with the first portion of the beam they encounter (Figure 4.7).

Another interesting and important discovery is that although the shape of the fanned intensity curves is similar regardless of convergence or divergence of the incident beam (in front of or behind the focal point of the focusing lens), the absolute intensity of the scattered light is always observed to be greater for the diverging case. This is not perplexing when considering near-forward scattering. One would expect more scattering from diverging light than converging because the size of the beam increases as it progresses through the crystal for diverging light, thus increasing the amount of scattering. Also it is noted that individual intensity readings are not consistent, even if there is no movement of the apparatus between readings. This is expected since the scattering process begins with noise photons, and no two situations can be exactly alike, even for similar configurations. This inability to exactly reproduce any given measurement suggests that the scattering may begin with random index changes within the crystal, caused by the stochastic distribution of charge carriers.

Finally, if stimulated scattering is responsible for beam fanning, then one would not expect continuous fanning, but fanning only along paths from which an incident photon interacted with the incident beam, thus creating a set of filaments emanating from the incident beam. A close examination of any of the photographs of Appendix A shows that this is indeed the case. Fanning is a set of discrete small beams all emanating from the incident beam. We must now discuss curved appearance of the dominant-scattered beam during self-pumped phase conjugation, a phenomenon not explained by SPS.

A very close examination of many photographs of SPPC (e.g. Figure A.5) reveals that beams which appear to curve often have a series of discontinuities within them. Generally, a filament, or set of filaments, leaves the incident beam along the direction of the c-axis. After a certain distance (usually about halfway to the crystal edge) these filaments enter a region where they become fuzzy, and often two become indistinguishable. The filaments exit this fuzzy region at an angle different than their entrance angle. This type of behavior is explainable by assuming that within this fuzzy

region there is stimulated scattering due to SPS. Forward scattered beams enter into a region where scattering occurs due to photons arriving from a different angle. The beams which continue on at a new angle are the forward scattered beams from this second scattering. It is therefore a series of this type of scattering discontinuities which gives the characteristic curved appearance of a filament during SPPC. However, this is not always the case.

There exist configurations where this series of discontinuities does not appear to account for the curved filaments (i.e. Figure A.6). In a majority of these cases a close examination reveals that a large filament originates at the incident beam or a series of filaments leave the incident beam very close together. The curved appearance comes from the coupling of energy to the filament, or portion of the filament, in the direction of the c-axis as the filaments progress through the crystal. Therefore the beam doesn't actually curve; it simply appears to do so because it is losing energy from one side and transferring it to the other. The process is actually a form of self-focusing due to two beam coupling.

I have observed a very few instances where it appears that neither of these processes can fully account for the curved appearance of the fanned filaments. In these cases one would expect the effect to be due to true beam fanning from the change in index of refraction within the filament path. Although the simulation PSIM shows that it is impossible for this phenomenon to fully account for the observed fanning effect, it would be surprising not to find some evidence of a change in index of refraction on the order of  $10^{-5}$  across a beam of diameter less than a few microns.

### C. SELF PUMPED PHASE CONJUGATION

From the discussion of the previous section we may conclude that a change in index of refraction within the incident beam path is not responsible for asymmetric self defocusing in  $\text{BaTiO}_3$ . It is probable that SPS is responsible for the effect. Therefore one may say that the true origin of SPPC in  $\text{BaTiO}_3$  is scattering, probably SPS. The cause of the final phase conjugate reflection is not as clear.

Phase conjugation by stimulated scattering in  $\text{BaTiO}_3$  has been demonstrated [Ref. 23], and recently it has been shown how backscattering may dominate forward scattering in SPS [Ref. 24]. Additionally, the investigations reported here indicate that scattering is responsible for the phenomenon of beam fanning. Therefore one might incorrectly conclude that phase conjugation in  $\text{BaTiO}_3$  is due to stimulated scattering. With the onset of backward scattering in the crystal there begins a competition of the

scattered waves. As the modes begin to build, a mode showing high gain can usurp power from one showing less gain. In this way only the modes showing the highest gain eventually survive. It is this competition between configurations having high gain which is responsible for the amplitude oscillations often seen in a phase conjugate reflections (see [Ref. 34,35] or Appendix A).

If a filament, arising from near forward scattering, has a configuration such that it can reflect off the corner of the crystal (i.e. a CAT corner) to create a situation where degenerate four wave mixing (DFWM) is possible in addition to SPS, then one would expect that filament to have a gain advantage. This then would be the filament to eventually win the competition. So it actually would be expected that both DFWM and SPS should contribute to SPPC.

A review of the conditions of the only published report of phase conjugation due solely to SPS [Ref. 23] shows that special precautions were taken to ensure maximum coupling. Specifically, an index matching liquid was used which preserved as much of the phase conjugate return as possible. Additionally the crystal was surrounded by a glass cuvette (containing the index matching liquid) which increased the amount of scattered light available for SPS to begin. Even with these advantages, a phase conjugate reflection of only  $\sim 10\%$  was obtained. This is quite small compared to the 30% to 50% usually seen from SPPC in  $\text{BaTiO}_3$  in air. This indicates that DFWM from the internal corner reflection is the most significant contributor to the phase conjugate return observed in SPPC, as was originally proposed [Ref. 2].

## VI. CONCLUSIONS

Experimental evidence does not support the theory that asymmetric self defocusing in BaTiO<sub>3</sub> is a result of an asymmetric change in the index of refraction within the path of the incident beam. Instead, forward stimulated scattering, probably Stimulated Photorefractive Scattering (SPS), is found to be a more likely explanation.

Simulation has shown that for an index change to be responsible for the phenomenon of beam fanning, the necessary change in the index of refraction across the beam must exceed the theoretical maximum, based on the maximum possible space charge field. A change in the index of refraction on the order of  $10^{-2}$  is necessary to account for the observed effects, whereas the accepted maximum is on the order of  $10^{-4}$  to  $10^{-5}$ .

Experimental results do not support a theory which requires a change in index of refraction across the incident beam as the cause of beam fanning. The magnitude of fanning is observed to increase with an increase in beam diameter. Also, observations of the manner in which the beam fans show that energy is scattered out of the beam path beginning with the periphery and not beginning in the center. Neither of these observations is consistent with the results expected if a purely photorefractive effect were responsible for asymmetric self defocusing.

Close observations of the process of beam fanning in BaTiO<sub>3</sub> indicate that beam fanning can be explained by a stimulated scattering theory. The presence of filaments rather than continuous fanning, scattering beginning with the periphery of the incident beam, and discontinuous filaments during phase conjugation are all explicable when beam fanning is attributed to stimulated scattering.

Future experiments in this area should include probing the "fuzzy" regions of the observed filaments from above with a low power laser to search for the presence of additional index gratings. Also, the actual change in the index of refraction across the incident beam path within the crystal remains to be determined experimentally. Additionally, further research into the size, type and spacing of scattering centers within the crystal is necessary to fully explain the observed difference in scattering of diverging and converging light.

## APPENDIX A

### INTERNAL BEAM PRODUCTION

#### 1. INTRODUCTION

The production of internal beams in  $\text{BaTiO}_3$  has, to my knowledge, never been systematically investigated. A search of the available literature indicates that the cause for this oversight may be that, in general, millimeter sized, collimated beams have been used. In all available photographs of  $\text{BaTiO}_3$  used as a SPPCM, the beam has not been focused onto the crystal. If the beam is not focused, then the diameter of the beam upon entering the crystal is at best the same as when it leaves the laser. It appears that when a beam is not focused onto the crystal, auxiliary beams are eliminated or obscured by the strong input beam since its diameter is large compared to the dimensions of the crystal (sometimes being more than half the size of the crystal). However, if the input beam is focused, the beam diameter is small compared to the crystal and the immediate effects of the input beam stay localized within the crystal, thus allowing the formation and observation of auxiliary beams. There is also an immense increase in the energy density of the beam within the crystal upon focusing.

It was using a focused beam that we first discovered the ability of barium titanate to support internal auxiliary beam patterns. Extensive investigation by A. V. Nowak and myself at Los Alamos National Laboratories indicated that there is a plethora of internal beams which may be generated by the nonlinear effects of barium titanate during phase conjugation. It appears that phase conjugation is necessary to sustain these beams since no auxiliary beams were observed in the absence of phase conjugation. In many cases it seems that the beam is initiated by the reflection of the phase-conjugate beam off of the face of the crystal as it exits, but this is not always true.

What follows in this chapter is an attempt to report, categorize, and explain many of the observed internal beam patterns and anomalous effects. It is important to note that often it is difficult or impossible to recreate some of the observed effects. It appears that not only position and beam profile are important, but also the short term history of the crystal. This means that possibly one effect may not be observable unless another has (or has not) immediately preceded it.

## 2. EXPERIMENTAL APPARATUS

All investigations presented in this chapter were performed at Los Alamos National Laboratory on an air floated optical bench in free air that was maintained at a temperature of  $22 \pm 1^\circ\text{C}$ . The apparatus used is shown schematically in Figure A.1.

During all experimentation the light source was a Spectra Physics 2020-03 argon ion laser, prism-tuned to 514.5 nm and operated in a single longitudinal mode by means of an intercavity etalon. The beam at the laser had a diameter of 0.88 mm at the  $1/e$  of peak intensity.

After leaving the laser, the beam was directed through a half-wave plate that served as a beam attenuator when necessary. Following the half-wave plate was an apparatus for isolation of the laser from the phase-conjugate beam. The apparatus used was a faraday rotator, manufactured by Optics For Research Inc., consisting of a 25mm long rod of Hoya FR5 glass surrounded by a set of permanent magnets. The isolator was set for optimal rotation of the plane of polarization of the beam at  $45^\circ$  and placed between two polarizers with axes oriented at  $45^\circ$  to each other. This configuration gave a backward attenuation of approximately 500. Without the isolator the phase-conjugate beam entered the laser cavity and caused large fluctuations in power output as well as mode hopping. The polarization of the beam upon leaving the isolator was such that it would enter the crystal extraordinarily polarized, which is required for the formation of a SPPCM.

After passing through the isolator the beam was expanded by a factor of 6.25 with an expanding telescope. This allowed the insertion of transparencies into the beam when desired, enabling the verification that an observed beam is a phase-conjugate beam. Also included in the telescope apparatus was a 0.05 mm pinhole that could be removed at will. This pinhole provided the ability to make observations with a Gaussian beam (pinhole inserted) or with what was eventually termed a mottled Gaussian beam (without the pinhole). The mottled Gaussian was so named because, although the beam without the pinhole was generally Gaussian, it had a mottled appearance.

Following the telescope, the beam was directed through a beamsplitter with 67% transmission at 514 nm. This beamsplitter not only provided the means for viewing the phase-conjugate signal as it returned along the incident path, but also provided a reference beam that was used to look for frequency shifts of the phase-conjugate beam. To look for a frequency shift the phase-conjugate return was reflected from the

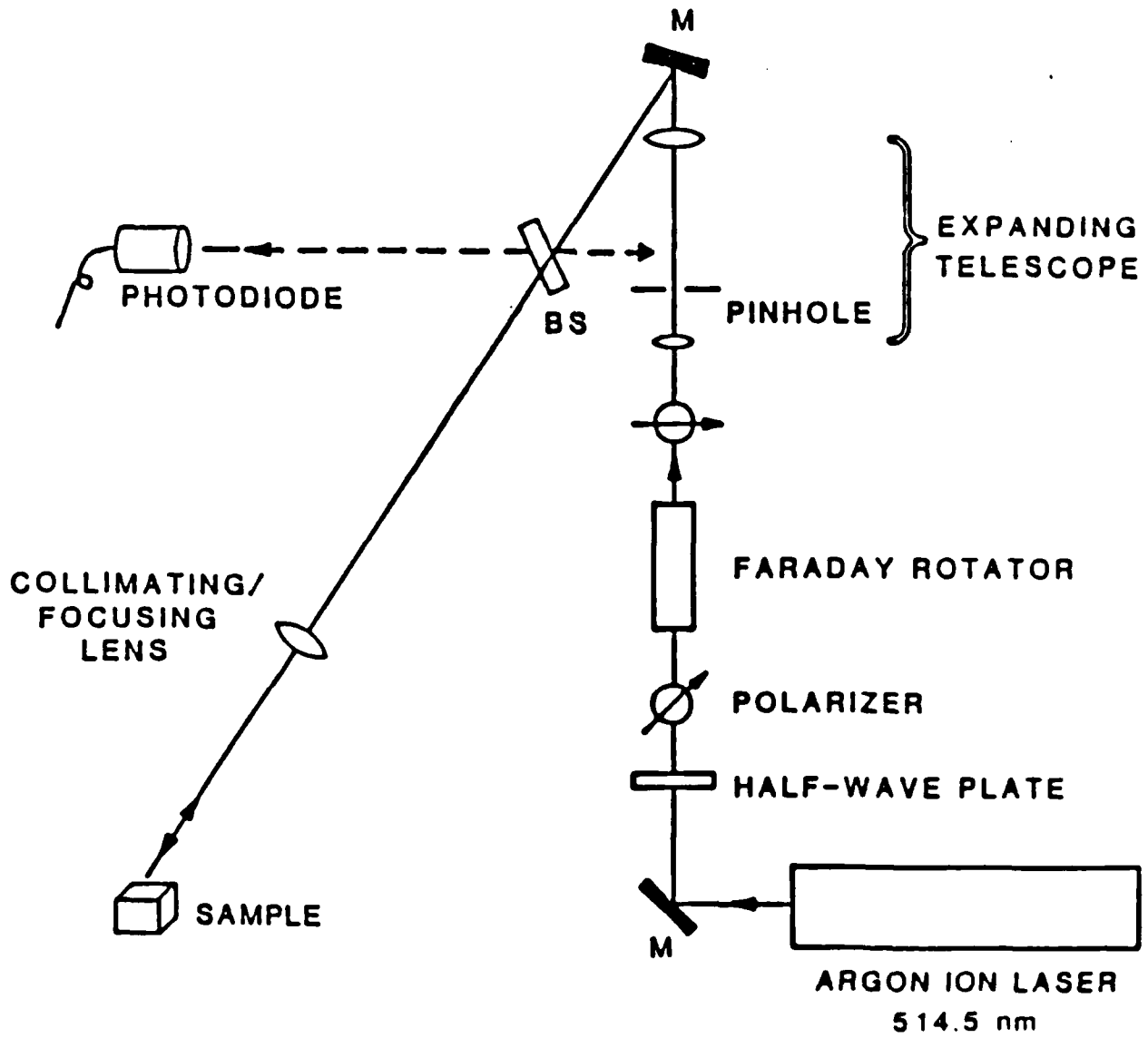


Figure A.1 Experimental Apparatus.

beamsplitter and redirected to interfere with a portion of the incident beam reflected from the front side of the beamsplitter. The resulting interference pattern was then observed for evidence of movement.

Upon passage through the beamsplitter, the beam, with power of  $75 \pm 5$  mW, was either modified by a lens, slit, knife-edge or a combination thereof, or simply collimated and directed toward the crystal. As the phase-conjugate beam returned along the incident path, the beamsplitter reflected a portion of it and directed it to a large area silicon PIN photodiode reverse biased at 22 volts and terminated with a 100 ohm resistor. The output of the detector was sent to a digital millivolt meter, an oscilloscope and a chart recorder. When an image was placed in the beam the detector was removed and replaced with a white screen for viewing. When frequency shift information was desired, the detector was replaced with a mirror and the two beams were directed toward a white screen for observation of the resulting interference pattern.

The crystal was any one of four nearly cubic single crystal of  $\text{BaTiO}_3$  measuring  $5 \pm 0.2$  mm on a side. The sides of the crystals were polished, but it is important to note that the sides were not exactly the same size and therefore the sides were not exactly orthogonal. The crystals were mounted on a platform that could be raised, lowered, rotated and tilted. Observations of internal beams were made visually from above and were recorded by film or video tape. Both the still and video cameras used a  $f = 35$ mm Cannon FL lens mounted on a single track bellows extended to provide a full frame view of the crystal.

Many of the photographs presented here were taken from the video tape directly off of a television screen using a 6x7 cm format still camera. The desired frame of the video was digitized and placed on a hard disk for recall and photographing, the numbers displayed in the photographs are a result of the equipment used to do this final photography and are not pertinent to the investigation. When this method was used, it was possible to make negative images of the desired photographs, which are the better quality than are some of the photographs presented in this report. The original photographs are available from the author upon request.

In this and in the following sections any reference to phase-conjugate reflectivity is the percent return of the beam actually incident on the crystal. The amount of specular reflection off of the face of the crystal (which can vary [Ref. 36]) is not subtracted from the calculation. All reflectances have an experimental tolerance of



$\pm 3\%$ . In the photographs presented, except where noted otherwise, the incident beam enters vertically from the top and is visible only upon entering the crystal.

### 3. RESULTS AND ANALYSIS OF DATA

#### a. Experimental variables

The number of variables involved in SPPC is immense, however I have tried to concentrate on those which have emerged as the most important. The most important factors in the production of various beams differ, but they generally may be considered as dependent on beam profile or the geometry of the beam-crystal interface.

Lenses, knife-edges, slits and pinholes were used to change the profile of the incident beam prior to the beam entering the crystal. The effect of these modifications of the incident beam is especially obvious when the beam profile has a large gradient, such as when a knife-edge is inserted into the beam, since this creates a very clear delineation in the lighted and unlighted areas of the crystal and introduces new wave vectors into the beam. The effect of the lens to crystal distance on phase-conjugate reflectivity has been studied by A. V. Nowak and is still not well understood [Ref. 37].

The geometry of the beam-crystal interface is probably the most important of all variables in the system. Changes in angle of less than one degree and lateral shifts in the beam of less than 0.5 mm can cause drastic differences in internal beams configurations. The following examples are presented to indicate the drastic effects observed with these type of changes.

The configuration shown in Figure A.2 is a typical experimental configuration that produced a phase-conjugate signal from the  $\text{BaTiO}_3$  crystal. The phase conjugate reflectivity was 33%. Note the fanned beams at the lower left corner of the crystal.

Figure A.3 demonstrates the extreme effects made possible when changing the beam profile by placing a knife-edge in the incident beam. Unless otherwise indicated, the knife-edge always intercepted the beam on the right side and was placed behind any lenses. Note the extreme curvature of the internal beam observed when blocking half the beam with a knife-edge. This also reduced the phase-conjugate reflection to zero. At other angles and intersection points, the introduction of a knife-edge produced a phase-conjugate reflection where there was none before.

A large effect is also seen when relocating the beam entrance position by a lateral shift in the beam-crystal intersection. As the beam is moved across the face of the crystal, the phase-conjugate reflectivity will change, beginning with no phase conjugation at one end and ending with the same result at the other. In between the

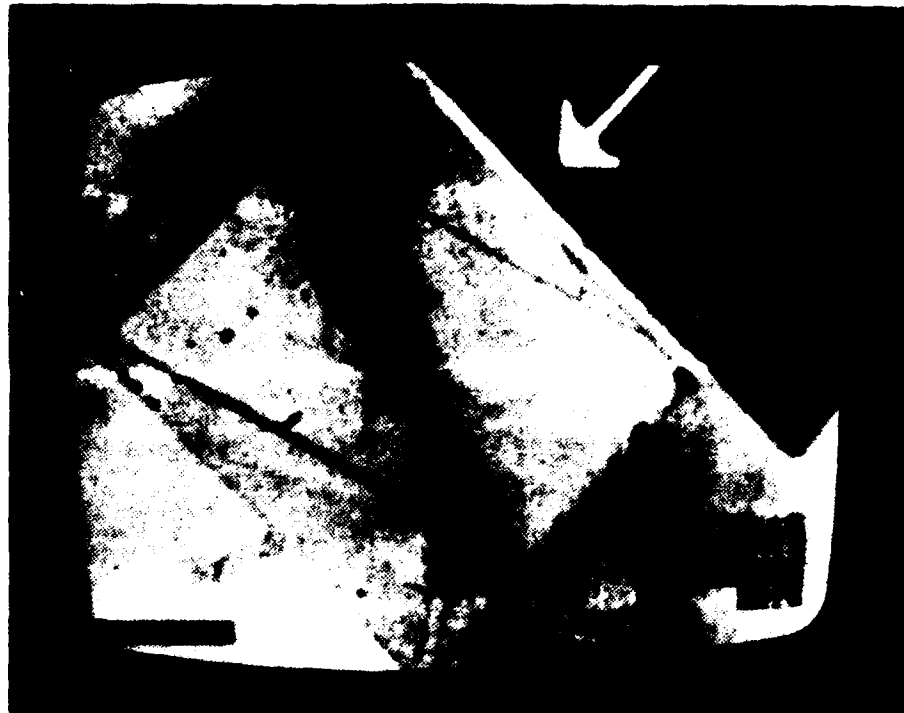


Figure A.2 Normal configuration for  $\text{BaTiO}_3$  exhibiting SPPC.

two extremes, the phase-conjugate reflectivity may range as high as 60% or be nonexistent depending on other factors. Similarly, a change in the angle of the beam entering the crystal will have a drastic effect on the phase-conjugate reflectivity and beam pattern. It is generally unpredictable and small changes in angle ( $\sim 4^\circ$ ) have been observed to have no effect, to destroy a pattern and eliminate all phase-conjugate reflectivity, or to increase the phase-conjugate reflectivity as much as 500%.

#### b. Complex Auxiliary Beam Patterns

##### 1. *The Total Internal Reflection (TIR) Ring*

One of the most interesting effects discovered was the TIR ring. Figure A.4 shows the first example, to my knowledge, of a totally internally pumped ring oscillation within a  $\text{BaTiO}_3$  crystal. This effect was achieved using a knife-edge to obscure half of the mirror Gaussian beam that was then focused through a lens, 29.5 cm from the face of the crystal. The beam was incident at  $40^\circ$  to the axis of the crystal and the knife-edge was placed on the side of the beam nearest the crystal. The effect was occasionally obtained while obscuring the other half of the beam, and was once obtained with a vertically aligned slit. A. V. Nowak once obtained the ring

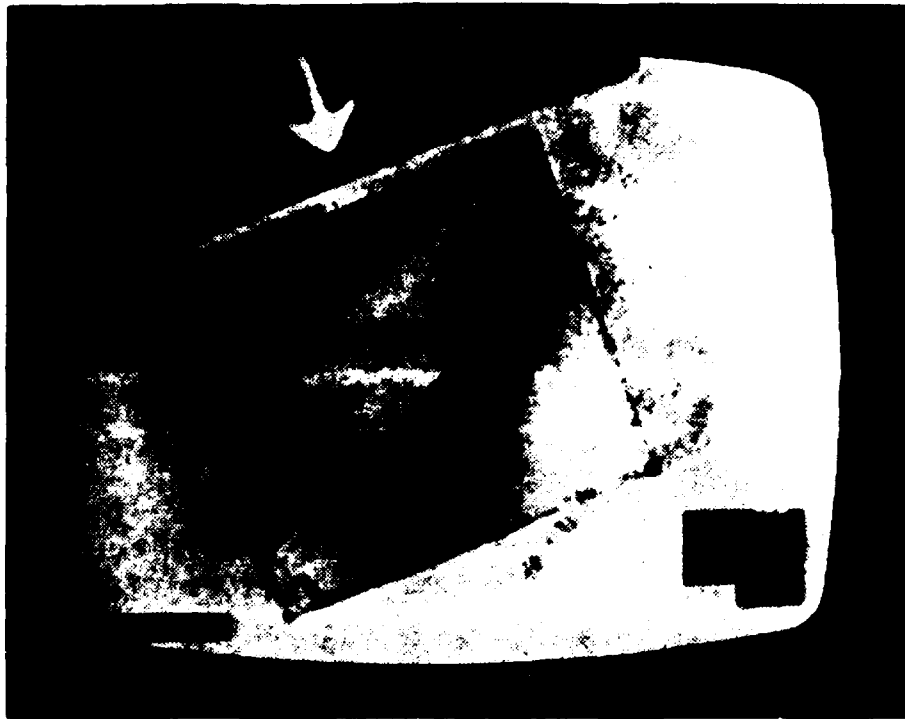


Figure A.3 Effect of placing a knife edge in the incident beam.

with just the focusing lens, indicating that the TIR ring may be dependent more on the availability of light scattered at a certain angle than on the incident beam profile.

In the case shown in Figure A.4 the phase-conjugate signal took about 30 seconds to appear. The beam within the crystal slowly moved to the corner until the configuration of the beam arrived as shown, but without the ring. Then, slowly, the ring appeared over a three second interval. As the ring appeared, the phase-conjugate reflectivity dropped from 76% to 67%. A drop in phase-conjugate reflectivity was observed in all examples of ring formation for those cases where the reflectivity was measured. In some cases, several nearly overlapping rings were observed, as in Figure A.4. The ring in Figure A.4 was steady, fading occasionally (on the order of once every five minutes) but always returning. It was not overly sensitive to translation. Translation parallel to the ring centerline would destroy the ring but if the rotation was under  $1^\circ$  then the ring would reappear. Translation along the crystal on the order of 0.5 mm in either direction did not disturb the ring, further translation would destroy it. For other configurations, the ring was only preserved for one direction of crystal motion (see Section 4).



Figure A.4 The TIR Ring.

The direction of circulation within the rings was determined by extracting some of the light out of the ring into a second crystal of  $\text{BaTiO}_3$ . After producing the ring in one crystal, a drop of index matching liquid (methylene iodide ( $\text{CH}_2\text{I}_2$ ) diluted 1:1 with 2-propanol,  $n \sim 1.6$ ) was placed onto the surface of a second crystal and the second crystal was moved into contact with the first. Since the loss into the second crystal was too great to allow the continuation of the ring, the operation was recorded by the video camera and the frame of the instant of contact was studied at a later time. Study of the video revealed that the light within the ring could propagate counterclockwise, or both ways simultaneously depending on the particular ring. However, in the majority of cases, only the counterclockwise direction was observed. Figure A.5 clearly shows this counterclockwise propagation and is representative of the majority of observations.

The ring within the crystal is probably produced by two-beam coupling between the main beam and scattered light that finds a closed loop via internal reflections around the crystal. This somewhat lossy TIR ring takes power from the incident beam, which explains the drop in phase-conjugate reflectivity seen immediately

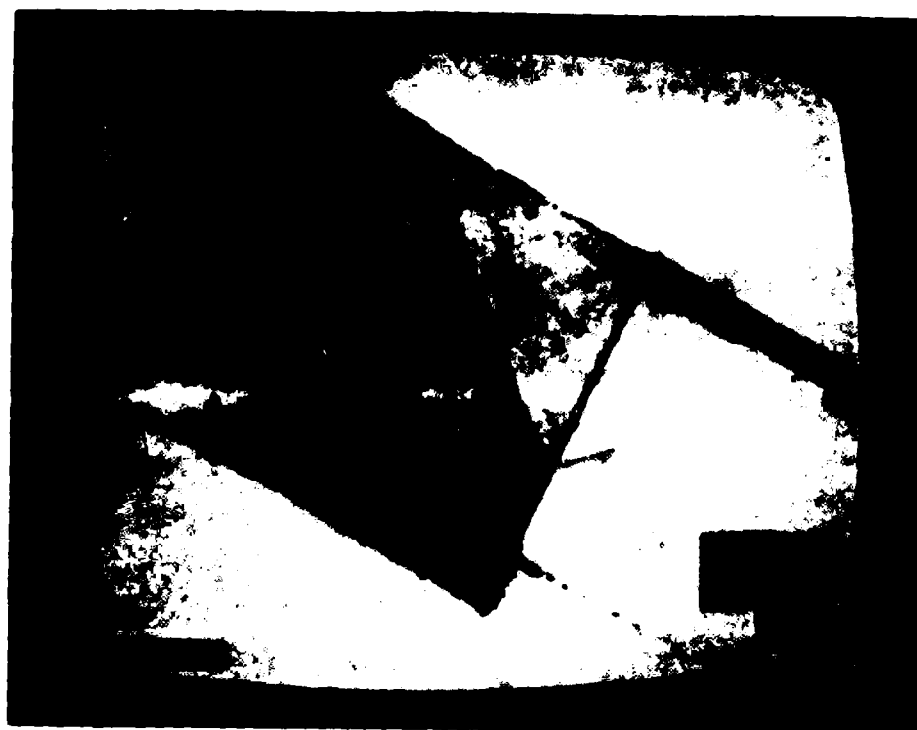


Figure A 5 Determination of the direction of the TIR ring by extraction of light with another crystal

upon its appearance. Of interest also is the difficulty in finding the TIR ring, in some crystals the ring pattern could be found in minutes. In others it would take many hours. Nowak discovered that in many cases, however, formation of the ring was promoted by a slight forward or backward tilt of the crystal (out of the plane of the film).

The effect of crystal motion on the TIR ring was also investigated by Nowak (Ref. 38) and it is interesting to note that the TIR ring appears to seek a square shape. It was observed that the ring will go from rectangular to square upon translation but not from square to rectangular. Also discovered were configurations in which the ring exhibited both shape invariance under translation.

#### *The Diamond*

The diamond is a very common phenomenon which is easily observed. It is considered to be easier to obtain than the TIR ring and has been produced with a variety of input beam profiles and orientations. It is thought to be a simple case of two beams coupling between the main beam and an internal reflection. Usually after the



Figure A.6 The Diamond configuration.

sharp diamond appears in the crystal the phase-conjugate signal increased considerably (up to 50 times what it is just prior to its appearance). The sharp diamond probably begins as a specular reflection of the phase-conjugate signal, which reflects back to the incident beam by internal reflection. Since a second point for DFWM is created, one would expect the observed increase in the phase-conjugate signal upon the appearance of the diamond.

A fascinating and unexplained variation of the sharp diamond is the diffuse diamond. The diffuse diamond, shown in Figure A.7, begins in a configuration similar to the diamond shown in Figure A.6, but as the crystal is laterally moved, a portion of the incident beam composing the sharp diamond stays to create a diamond in the right part of the crystal. The diffuse diamond is very weak compared to the sharp diamond. The diffuse diamond is a result of the same physical processes that create the sharp diamond effects which will be discussed later.

### ***3. Internal Specular Reflection***

Often the specular reflection of the incident beam within the crystal behaves in unexpected ways. Figure A.8 shows a case where there is visible specular



Figure A.7 The Diffuse Diamond configuration.

reflection of the input beam within the crystal creating a diamond but there is no reflection of the secondary beam off of the rear face of the crystal. Absorption of the reflected beam by two-beam coupling with the incident beam within the first few micrometers of the crystal edge is probably responsible for the lack of specular reflection in this and other similar cases. There is a similar theory which accounts for the lack of specular reflection of the phase-conjugate beam off of surfaces such as the input face of the crystal. Pepper [Ref. 36] proposes that the lack of a reflection of the phase-conjugate beam is due to destructive interference between the incident beam reflection, and a beam created by the phase conjugation of the reflection of the original phase-conjugate beam. This has been borne out in experiment. However, as Figure A.9 demonstrates, at certain angles the specular reflection is sufficiently intense to cause multiple internal reflections. The boundary conditions associated with the lack of a reflection have yet to be fully determined.

#### 4. *Diagonals*

Figure A.10 illustrates the diagonals. The diagonals faded in and out as the phase-conjugate reflectivity oscillated from 12% to 21% with a period on the order of



Figure A.8 Example of lack of reflection of the incident beam within the crystal.

5 seconds. The reflectivity was strongest when the diagonals were brightest. When the angle of incidence was increased to  $56^\circ$  a similar configuration appeared, but with the phase-conjugate reflectivity oscillating from one to 15% and specular reflection off of the back face fading as the diagonals became brighter. At another angle of incidence in this configuration ( $62^\circ$ ) it was noted that increasing the power of the input beam could eliminate all oscillations of the phase-conjugate reflection while eliminating the diagonals. This configuration has also been seen without any measurable phase-conjugate reflection.

#### Temporal Effects and Frequency Shifts

Up to this point this work has considered only examples of the main temporal effects of the phase-conjugate reflection. The effects of the phase-conjugate reflection on the phase-conjugate amplitude and on frequency shifts between the phase-conjugate signal and the incident beam will now be addressed.





Figure A.9 Example of multiple reflections within the crystal.

### *1. Amplitude Oscillations*

Frequently, amplitude oscillations were observed in the phase-conjugate signal of many of the previously discussed examples. These include Figures A.2, A.4, A.6, A.8, A.9. The oscillations, probably similar to those reported by Valley and Dunning in an external resonating cavity [Ref. 39], were most obvious when a mottled beam was focused into the sample, but they also appeared in some configurations with all beam profiles. The observed oscillations often appeared to be chaotic, and much work has been reported recently concerning the observation of chaotic oscillations in  $\text{BaTiO}_3$  [Ref. 34,35]. However, some of the observed oscillations were very nearly periodic (periodic within 10% of some mean period) with periods ranging from 0.01 to 1.0 seconds.

Figure A.11 shows the amplitude of the phase-conjugate signal as a function of time with a focused Gaussian beam incident on the center of the crystal  $40^\circ$  to the c-axis. These oscillations appeared immediately upon the initiation of phase conjugation. These were maintained as shown for a period of about one minute and then abruptly changed to the oscillations shown Figure A.12. Within a few minutes the original

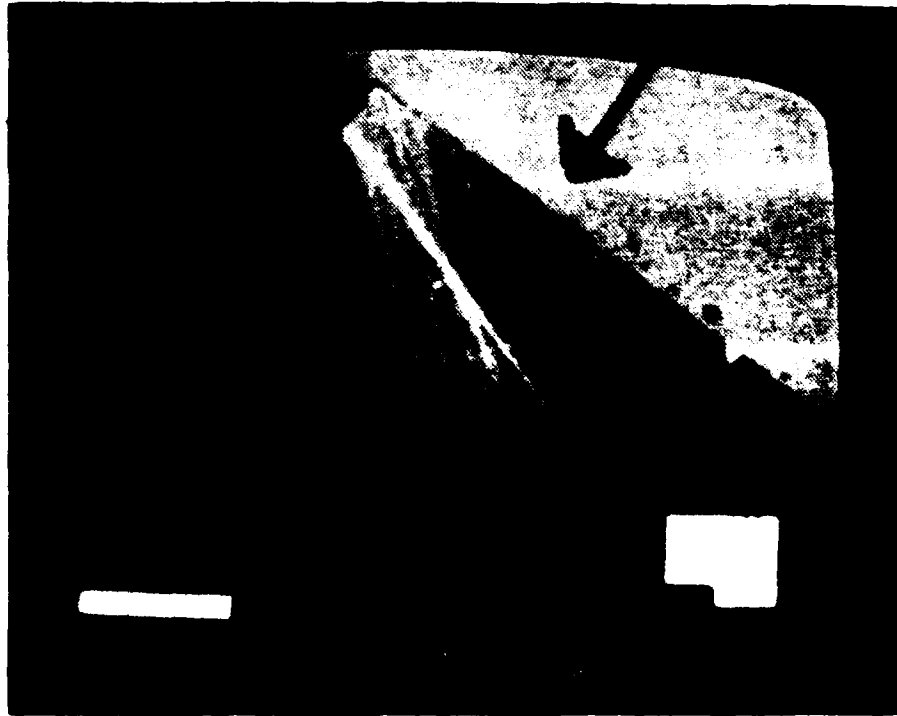


Figure A.10 The Diagonals configuration.

oscillations reappeared. Fast oscillations ( $\sim 10$  Hz) amplitude modulated by slower oscillations ( $\sim 0.5$  Hz), and oscillations with faster beats superimposed on them were also observed. Nowak has shown that the frequency of these amplitude oscillations is proportional to the intensity of the incident beam [Ref. 37] and this has been confirmed by others [Ref. 30].

These amplitude oscillations of the phase-conjugate signal are probably a result of frequency shifts of those auxiliary beams that account for the formation of the grating. Frequency shifts of the auxiliary beams were proposed by Feinberg and Bauner [Ref. 40] to explain observed frequency sweeping in the output of a ring resonator using  $\text{BaTiO}_3$  and in an unisolated  $\text{Ar}^+$  laser producing phase conjugation in  $\text{BaTiO}_3$  [Ref. 41]. Thus, it is expected that the phase-conjugate reflectivity will be reduced for large frequency differences between the auxiliary beams, since the four-wave mixing signal is reduced for large frequency differences, as shown by MacDonald and Feinberg [Ref. 42]. The nature of and reasons for this frequency shifting within the crystal has yet to be explained.

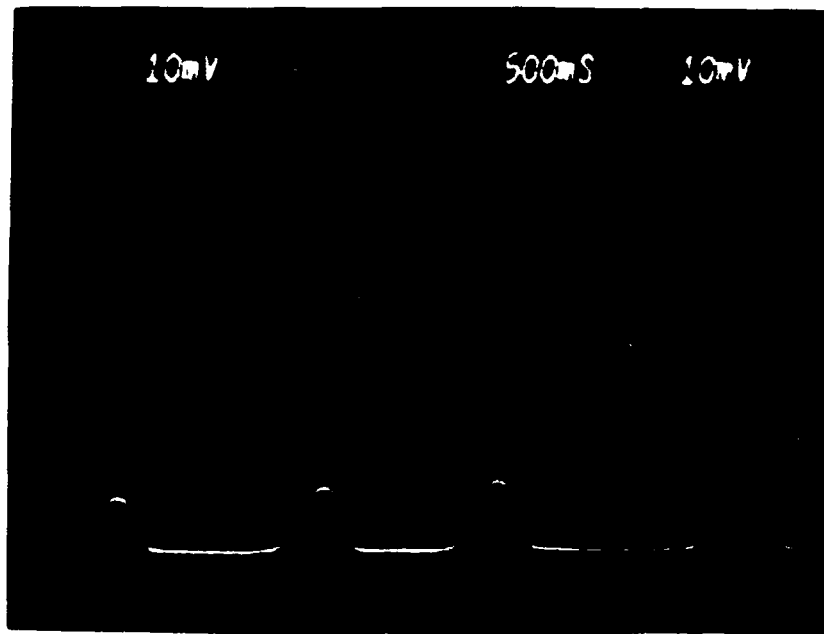


Figure A 11: Example of quasi-periodic amplitude oscillations in  $BaTiO_3$ .

## 2. Frequency Sweeping

To determine the difference in frequency of the phase-conjugate light, a Michelson interferometer arrangement was used. A part of the phase-conjugate light interfered with the phase-conjugate light itself, while the other part interfered with the reference light. A signal of the interference pattern was observed. The signal is a function of the normal lateral displacement of the interference fringes. In contrast to the case of a stable phase-conjugate light, oscillating amplitude oscillations (e.g. Figures A 11 and A 12) cause a variation of the lateral displacement of the fringes between the two cases.

Let us assume that the phase-conjugate light is a plane wave with the wave vector  $\vec{k}_c$  and the reference light is a plane wave with the wave vector  $\vec{k}_r$ .

Assuming that the phase-conjugate light is a plane wave with the wave vector  $\vec{k}_c$  and the reference light is a plane wave with the wave vector  $\vec{k}_r$ , the interference pattern is a function of the lateral displacement of the fringes. In contrast to the case of a stable phase-conjugate light, oscillating amplitude oscillations cause a variation of the lateral displacement of the fringes between the two cases.

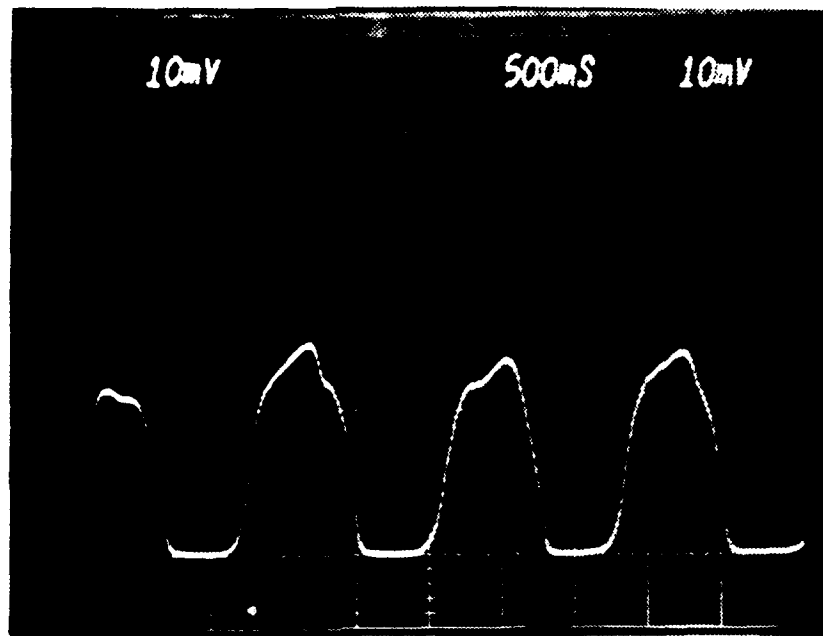


Figure A.12 Amplitude oscillations which progressed from those of Figure A.11.

correlation of amplitude and frequency shift of the phase-conjugate beam may have been explained by MacDonald and Feinberg when they showed that the four-wave mixing signal falls off smoothly as the frequency difference between the reflected and incident beam becomes larger than  $\sim 1$  Hz. Although the mechanism for this frequency shifting is still under investigation, Lam [Ref. 3] has proposed that the bulk photovoltaic effect gives rise to an intensity-dependent frequency shift. This implies that the frequency is dependent on the amplitude instead of vice versa. Another explanation may be that there is consistent movement of the grating when the reflected pumpwave forms a loop (see Figure A.2 for example). In this case each circuit around the loop will Doppler-shift the pumpwave and the observed effect may be expected.

There was only one observed instance where the frequency difference between the two beams was non-zero and constant (no photograph available). The phase-conjugate return was frequency-shifted from the input beam, but there was no sweeping. That is, there was obvious movement of the interference fringes at a constant velocity. This effect resulted from a mottled Gaussian beam incident on the

crystal at an angle of  $35^\circ$  to the c-axis. However this is an anomalous effect that has yet to be repeated or explained.

### **3. Influence of Returning the transmitted Beam**

This effect is similar to that reported by Feinberg [Ref. 27] and was discovered while trying to stabilize the amplitude oscillations of the phase-conjugate signal discussed above. The effect was seen using an arrangement that produced nonperiodic amplitude oscillations of the phase-conjugate reflection ranging from 20% to 46%. In this configuration a 100% reflectance mirror was placed behind the crystal directing the transmitted beam back through the crystal, but not directly along the incident path. All oscillations stopped, leaving the phase-conjugate reflection steady at 10%.

The explanation for this effect is probably found in the competition between beam patterns. In any instance, the observed beam pattern is the one which exhibits the maximum gain. When oscillation occurs between two competing beam patterns it is apparent that, for some reason, the gain of one is falling above and then below the possible gain of another. The input of a beam of light from any source with brightness on the order of the internal beams will cause a change in the gain of the system due to some or all of the possible nonlinear effects. In the case of returning the transmitted beam, it appears that the gain of one of the competing patterns is sufficiently reduced to eliminate it from the possible patterns.

#### **d. The Free Standing Auxiliary Beam Pattern**

This section presents an occasionally observed result due to a small crystal motion. Here the crystal was translated at right angles to the beam path while the internal beam pattern was carefully observed for any changes.

Note the beam configuration seen in Figure A.13. When the crystal was shifted slightly to the left, the auxiliary beam pattern moved with the crystal as shown in Figure A.14 instead of changing to adapt to the new crystal orientation. Note, however, that some slight distortion of the pattern did occur. In this case the phase-conjugate reflectivity was originally 32% with small amplitude oscillations on the order of 5%. There was no evidence of frequency shifting of the phase-conjugate beam. Upon translation of the crystal, the phase-conjugate reflectivity diminished to 23% with oscillations of the same amplitude as before the translation.

After translation, any rotational motion of the crystal destroys the auxiliary beam and a new one appears that is similar to the original pattern (i.e. Figure A.13).



Figure A.1. BaF<sub>2</sub> prior to translation.

A 1000 W laser beam is directed in the opposite direction, causing the input beams to meet in the center of the beam pipe, inside the last cathode and a few pellets. A 1000 W laser beam is directed in the opposite direction, causing the input beams to meet in the center of the beam pipe, inside the last cathode and a few pellets. A 1000 W laser beam is directed in the opposite direction, causing the input beams to meet in the center of the beam pipe, inside the last cathode and a few pellets.

The 1000 W laser beam is directed in the opposite direction, causing the input beams to meet in the center of the beam pipe, inside the last cathode and a few pellets. A 1000 W laser beam is directed in the opposite direction, causing the input beams to meet in the center of the beam pipe, inside the last cathode and a few pellets. A 1000 W laser beam is directed in the opposite direction, causing the input beams to meet in the center of the beam pipe, inside the last cathode and a few pellets.



Figure A.14 Free standing beams created by translating the crystal  $\sim 0.5\text{mm}$  from the configuration of Figure A.13.

## APPENDIX B PSIM LISTING

```

10      | PSIM_3
20      |
30      | A SIMULATION OF INTERNAL BEAM RESPONSE IN BARIUM TITANATE
40      |
50      |
60      |
70      |
80      |
90      |
100     | IBEAM = SIZE OF INPUT BEAM
110     | IBEAMF = ACTUAL NUMBER OF POINTS IN WAVEFRONT AFTER
120     |         DESIGNATION OF ANGLE PHI
130     | ISIZE = SIZE OF CRYSTAL
140     | ICRYS () = CRYSTAL GRID
150     | KEEP() = ARRAY TO KEEP TRACK OF CURRENTLY OCCUPIED SPACES IN THE
160     |         GRID, 2=COL, 1=ROW
170     | IPHI = INPUT ANGLE OF INCIDENCE
180     | PHI = ANGLE OF INCIDENT BEAM (REAL)
190     | PHIC = ANGLE OF INCIDENT BEAM AFTER ENTERING CRYSTAL
200     | IX = NUMBER OF COLUMN POINTS ACROSS WAVEFRONT
210     | IY = NUMBER OF ROW POINTS ACROSS WAVEFRONT
220     | ADD() = AMOUNT TO ADD TO Y FOR EACH X MOVED
230     | IROW = ROW NUMBER
240     | ICOL = COLUMN NUMBER
250     | ITOP = HIGHEST INDEX OF REFRACTION
260     | IBOT = LOWEST INDEX OF REFRACTION
270     | GRAD = GRADIENT OF INDEX OF REFRACTION ACROSS THE BEAM
280     | CRYST = REAL VALUE OF INDEX OF REFRACTION (BEFORE FIXING)
290     | IMDEX = INDEX OF REFRACTION OF LOCATION
300     | REALX = PLACE FOR KEEPING TRACK OF AMOUNT TO ADD TO COLUMN
310     |         (OR ROW FOR REALY) WHEN MOVING DOWN THE BEAM
320     |         THIS ENSURES THAT ALL FRACTIONS OF A GRID SPACE
330     |         ARE NOT LOST
340     | REALY = SEE REALX
350     | REALAD () = SAME AS REALX ABOVE BUT ONE SPACE FOR EACH POINT.
360     |         USED DURING ACTUAL WAVEFRONT MOVEMENT
370     | IPERMC() = STARTING COLUMN FOR WAVEFRONT POINT
380     | IMARKB = MARKER TO KNOW WHEN REFLECTION OFF OF BOTTOM HAS OCCURRED
390     | IMARKS = MARKER TO KNOW WHEN REFLECTION OFF OF SIDE HAS OCCURRED
400     | ICHECK = INDEX OF TIME PERIODS
410     | RSTOP = NUMBER OF TIME PERIODS IN SIMULATION
420     | IDIR = NUMBER OF TIME PERIODS BETWEEN COMPUTATIONS
430     |         OF DIRECTION OF WAVEFRONT
440     | MDIR = COUNTER FOR CHECKING AGAINST IDIR
450     | XX = HORIZONTAL DISTANCE BETWEEN END POINTS OF WAVEFRONT
460     | YY = VERTICAL DISTANCE BETWEEN END POINTS OF WAVEFRONT
470     | ICHNG = VARIABLE USED TO CHANGE DIRECTION AFTER REFLECTION
480     | ITRACK = MATRIX USED TO MARK THE INCIDENT BEAM PATH SO THAT
490     |         THE INDICES SET UP BY THE INCIDENT BEAM DOMINATE
500     | MEAN = MEAN VALUE OF THE INDEX OF REFRACTION
510     | REF = ACTUAL INDEX OF REFRACTION OF THE PHOTOREFRACTOR BEING
520     |         SIMULATED
530     | IPLACE = POINT THAT BEAM STARTS IN CRYSTAL
540     | IGRAPH = MARKER FOR POINTS TO BE PLOTTED (SET FOR 100 POINTS)
550     | IGRMAX = NUMBER OF ITERATIONS BETWEEN PLOTTING WAVEFRONTS
560     | CAXIS = FRACTION OF TOTAL INDEX CHANGE DUE TO ANGLE BEAM
570     |         MAKES WITH THE C-AXIS IN THE CRYSTAL
580     | CINDEX = REAL VALUE OF INDEX OF REFRACTION USED TO COMPUTE

```



```

590      !           THE CHANGE DUE TO THE ANGLE TO C-AXIS
600      ! IOUT() = MATRIX FOR HOLDING VALUES OF PLOTTED POINTS
610      ! ICOUT = COUNTER FOR PLACE OF POINT IN OUTPUT FILE
620      ! ISKIP = MARKER TO CHECK IF WAVEFRONT IS UNDERGOING REFLECTION
630      ! REFLCHKB =MARKER TO KNOW WHEN REFLECTION OF WAVEFRONT STARTS/ENDS
640      ! REFLCHKs = SAME BUT FOR SIDE
640      ! OP1 = NUMBER OF POINTS IN WAVEFRONT TO LOOK AT FOR RECALCULATION
650      !           THIS EQUALS IBEAMF/PIECE
660      ! ISETMARK = MARKER TO TELL WHEN TO STOP LOOKING FOR REFLECTION
670      ! PIECE = NUMBER OF PIECES OF WAVEFRONT
680      ! ADDY() = FRACTION OF ONE BOX THAT EACH POINT STARTS OUT AHEAD OF
690      !           ITS ROW
700      !
710      !
720      !
730      !
740      !
750      INTEGER Ibeam, Ibeamf, Isize, Icrys(500,500)
760      INTEGER Keep(2,50), Iphi, Ix, Iy, Irow, Icol, Itop, Ibot, Reflchks(50)
770      INTEGER Reflchkb(50), Ikfac, This, That
780      INTEGER Imdex, Imdex(50), Ipermc(50), Imarkb(50), Itime(50), Iskipb
790      INTEGER Imarks(50), Idir, Mdir, Ichng, Icout, Iskips, Itemp, Op1, Piece
800      INTEGER Itrac(500,500), Mean, Iplace, Igraph, Iout(1,50,101), Isetmark
810      REAL Phi, Phic, Add(50), Grad, Crys, Realx, Realad(50), Rstop, Grmax
820      REAL Xx, Yy, Ref, Caxis(50), Cindex, Rcheck, Kfac, Realy, Addy(50)
830      !
840      !
850      !           NOTE THAT IF BEAM SIZE EXCEEDS 50 YOU MUST REDIMENSION
850      !
870      ON ERROR GOSUB 5430      ! WRITES FILE TO DISK IF ERROR
880      PRINTER IS 1      ! SET TERMINAL OUTPUT
890      GRAPHICS OFF
900      OUTPUT KBD; K;      !CLEARS SCREEN
910      ON KEY 2 LABEL SAVE      &STOP GOSUB 5430
920      PRINT TO STOP PROGRAM AND SAVE DATA PRESS f2
930      !
940      !
950      !
960      !           INPUT FACTORS
970      !
980      !
990      INPUT NAME OF DATA FILE TO BE USED ,Name$
1000     PRINT DATA FILE: ,Name$
1010     INPUT SIZE OF CRYSTAL TO BE USED ,Isize
1020     PRINT CRYSTAL SIZE IS ,Isize, ON A SIDE
1030     INPUT BEAM SIZE IS ,Ibeam
1040     PRINT WITH A BEAM OF SIZE , Ibeam
1050     INPUT PLACE ON CRYSTAL FOR BEAM TO ENTER IS , Iplace
1060     PRINT ENTERING AT , Iplace
1070     INPUT HIGH VALUE OF INDEX IS , Itop
1080     PRINT LOW VALUE OF INDEX IS ,Ibot
1090     PRINT INDICES RANGE FROM ,Itop, TO ,Ibot
1100     INPUT INITIAL ANGLE IN DEGREES IS (89 DEG MAX) , Iphi
1120     !
1130     T1=TIMEDATE
1140     !
1150     !
1160     !           INITIALIZE VARIABLES
1170     !
1180     Rcheck = 0
1190     Mdir=0
1200     Ref=2.4
1210     Icout=0
1220     Isetmark=0
1230     Piece=5 ! REM TO CHANGE KK IF YOU CHANGE PIECE
1240     !
1250     !
1260     !
1270     !
1280     !

```

```

1290 PRINT NUMBER OF PIECES IN WAVEFRONT , Piece
1300 !
1310 !
1320 !
1330 ! PUT FACTORS IN OUTPUT FILE
1340 !
1350 Iout(0,0,0)=Isize
1360 Iout(0,1,0)=Ibeam
1370 Iout(1,0,0)=Iplace
1380 Iout(1,1,0)=Itop
1390 Iout(0,0,101)=Ibot
1400 Iout(0,1,101)=Iphi
1410 Iout(1,0,101)=Piece
1420 Igraph=0
1430 Rstop=Itop*2 !SET TIME TOTAL PERIODS
1440 Rstop=Rstop*Isize !USE TWO LINES TO KEEP FROM INTEGER PROBLEMS
1450 PRINT TOTAL TIME = , Rstop
1460 Grmax=Rstop/100 ! SET FOR 100 WAVEFRONTS PLOTTED
1470 GOSUB 5170 !SET UP GRAPHICS DISPLAY
1480 !
1490 ! TIME BETWEEN NONLINEAR CALCULATIONS
1500 Idir=5*Itop
1510 !
1520 !
1530 ! INITIALIZE ARRAY
1540 !
1550 FOR I=1 TO Ibeam
1560 Keep(1,I)=0
1570 Keep(2,I)=0
1580 Itime(I)=0
1590 Reflchks(I)=0
1600 Reflchkb(I)=0
1610 NEXT I
1620 !
1630 !
1640 !
1650 ! CONVERT PHI FROM DEGREES TO RADIANS AND FIND ANGLE INSIDE CRYSTAL
1660 Phi=Iphi
1670 Phi=Phi*(2*PI/360)
1680 Phic=(SIN(Phi)/Ref)
1690 Phic=ASN(Phic)
1700 !
1710 !
1720 ! CHANGE SIZE OF BEAM DEPENDENT ON THE INPUT ANGLE
1730 !
1740 !
1750 X=Ibeam*COS(Phic)
1760 Y=Ibeam*SIN(Phic)
1770 Iy=Y
1780 Ix=X
1790 Ibeamf=Ix
1800 Opl=Ibeamf/Piece !SIZE OF PIECE TO LOOK AT WHEN CALCULATING DIRECTION
1810 Add(1)=Y/X
1820 Add1=Add(1)
1830 IF Iplace>(Isize-Ibeamf) THEN ! MAKE SURE IPLACE IS NOT TOO LARGE
1840 Iplace =Isize-Ibeamf
1850 END IF
1860 !
1870 !
1880 !
1890 !
1900 !
1910 !
1920 !
1930 Irow=0
1940 Realy=0
1950 Icol=Iplace
1960 !
1970 ! FILE WAVEFRONT COORD
1980 !

```

```

1990 FOR I=1 TO Ibeamf
2000     Keep(2,I)=Icol
2010     Realy=Realy+Add(1)
2020     Add(I)=Add(1)
2030     IF Realy>Irow+1 THEN Irow=Irow+1
2040     Addy(I)=Realy-Irow
2050     Keep(1,I)=Irow
2060     Icol=Icol+1
2070 NEXT I
2080 !
2090 !
2100 !
2110 !
2120 !
2130 ! *****SET UP INDEX OF REFRACTION FOR PATH OF INCIDENT BEAM *****
2140 !
2150 !
2160 !
2170 ! SET UP CRYSTAL TO MEAN INDEX
2180 !
2190 Mean=ABS((Itop+Ibot)/2)
2200 FOR I=1 TO Isize
2210     FOR J=1 TO Isize
2220         Icrys(I,J)=Mean
2230         Itrac(I,J)=0
2240     NEXT J
2250 NEXT I
2260 !
2270 !
2280 !
2290 Grad=(Itop-Ibot)/2 !INDEX OF REFRACTION GRADIENT
2300 FOR I=1 TO Ibeamf
2310     Irow=Keep(1,I)
2320     Icol=Keep(2,I)
2330     Crys=Grad*SIN(((Ibeamf/2)-(I-1))*(PI/Ibeamf))
2370     Crys=Crys+Mean
2380     Icrys(Irow,Icol)=Crys
2390 NEXT I
2400 !
2410 !
2420 !
2430 ! SET UP VALUES DOWN THE BEAM PATH
2440 !
2450 FOR I=1 TO Ibeamf
2460     Icol=Keep(2,I)
2470     Irow=Keep(1,I)
2480     Imdex=Icrys(Irow,Icol)
2490     Imdexp(I)=Imdex
2500     Itemp=Icol
2510     Realx=0
2520     FOR J=Irow TO Isize
2530         Icrys(J,Itemp)=Imdex
2540         Itrac(J,Itemp)=1
2550         Realx=Realx+Add(I)
2560         Itemp=Icol-Realx
2570         IF Itemp>Isize THEN Itemp=Isize
2580         IF Itemp<0 THEN Itemp=0
2590     NEXT J
2600 NEXT I
2610 !
2620 !
2630 !
2640 !
2650 ! SET THE STARTING COLUMNS FOR THE WAVEFRONT AND
2660 ! INITIALIZE FLAGS
2670 !
2680 !
2690 FOR I=1 TO IBEAMF
2700     Ipermc(I)=Keep(2,I)
2710     Imarkb(I)=0

```

```

2720     Imarks(I)=0
2730 NEXT I
2740 !
2750 !
2760 !
2770 !
2780 !
2790 ! *****BEGIN MOVEMENT *****
2800 !
2810 !
2820 ! MAKE SURE BEAM IS STILL IN CRYSTAL
2830 !
2840 FOR I=1 TO Ibeamf
2850     IF Imarkb(I)=1 THEN
2860         IF Keep(1,I)<2 THEN GOTO 5140
2870     END IF
2880     IF Imarks(I)=1 THEN
2890         IF Keep(2,I)>Isize-10 THEN GOTO 5140
2900     END IF
2910 NEXT I
2920 !
2930 ! *****MOVEMENT *****
2940 !
2950 !
2960 WHILE Rcheck<Rstop
2970 !
2980 !
2990 FOR I=1 TO Ibeamf
3000     Icol=Keep(2,I)
3010     Irow=Keep(1,I)
3020     Imdex=Icrys(Irow,Icol)
3030 !
3040 !
3050 ! MARK REFLECTION IF NECESSARY
3060 !
3070     IF Icol<=1 THEN
3080         IF Imarks(I)=0 THEN
3090             Imarks(I)=1
3100             Realad(I)=1
3110         END IF
3120     END IF
3130     IF Irow =Isize THEN
3140         Imarkb(I)=1
3150     END IF
3160 !
3170 !
3180 ! MOVE IF IT IS TIME
3190 !
3200     IF Itime(I)<Imdex THEN
3210         Itime(I)=Itime(I)+1
3220     ELSE
3230         Itime(I)=0
3240         Realad(I)=Realad(I)+Add(I)
3250         IF Imarks(I)=0 THEN
3260             Icol=Ipermc(I)-Realad(I)
3270             IF Icol<0 THEN Icol=0
3280         ELSE
3290             Icol=Realad(I)
3300         END IF
3310         Keep(2,I)=Icol
3320         IF Imarkab(I)=0 THEN
3330             Keep(1,I)=Irow+1
3340         ELSE
3350             Keep(1,I)=Irow-1
3360         END IF
3370     END IF
3380 NEXT I
3390 !
3400 !
3410 !

```

```

3420 |
3430 |           PUT POINTS IN FILE AND DISPLAY GRAPHICS
3440 |           IF IT IS TIME TO DO SO
3450 |
3460 |
3470 Igraph=Igraph+1
3480 IF Igraph>Grmax THEN
3490   Icout=Icout+1
3500   FOR L=1 TO Ibeamf
3510     Igraph=0
3520     Iout(0,L,Icout)=Keep(2,L)      !X COORD OF POINT
3530     Iout(1,L,Icout)=Isize-Keep(1,L) !Y COORD OF POINT
3540     PENUP
3550     PLOT Iout(0,L,Icout),Iout(1,L,Icout)
3560   NEXT L
3570 END IF
3580 |
3590 |
3600 |
3610 |
3620 |
3630 Rcheck=Rcheck+1
3640 |
3650 |   CHECK IF TIME TO RECOMPUTE DIRECTION *****
3660 |
3670 MDIR=Mdir+1
3680 IF Mdir>=Idir THEN
3690   Mdir=0
3700   PRINT TABXY(1,11), CURRENT TIME PERIOD = , Rcheck
3710 |
3720 |
3730 |
3740 |
3750 |
3760 |
3770 |
3780 FOR K=0 TO Piece-1
3790 |
3800 |   ***** SET FOR 5 PIECES *****
3810 |
3820 |   IF K=0 THEN Kk=0
3830 |   IF K=1 THEN Kk=4
3840 |   IF K=2 THEN Kk=1
3850 |   IF K=3 THEN Kk=3
3860 |   IF K=4 THEN Kk=2
3870 |   !IF K=5 THEN Kk=7
3880 |   !IF K=6 THEN Kk=3
3890 |   !IF K=7 THEN Kk=6
3900 |   !IF K=8 THEN Kk=4
3910 |   !IF K=9 THEN Kk=5
3920 |   This=Kk*Opl+1
3930 |   That=(Kk+1)*Opl
3940 |   IF Kk=Piece-1 THEN That=Ibeamf
3950 |
3960 |
3970 |   FIRST CHECK TO MAKE SURE THE FRONT IS NOT PARTIALLY REFLECTED
3980 |
3990 |
4000 |   Iskipb=0
4010 |   Isetmark=0
4020 |   IF Reflchkb(K)=0 THEN
4030 |   FOR M=This TO That
4040 |     IF Imarkb(M)=1 THEN
4050 |       Isetmark=1
4060 |       FOR N=This TO That
4070 |         IF Imarkb(N)=0 THEN Iskipb=1
4080 |       NEXT N
4090 |     END IF
4100 |   NEXT M
4110 |   END IF

```

```

4120 IF Isetmark=1 AND Iskipb=0 THEN Reflchkb(K)=1
4130 Iskips=0
4140 Isetmark=0
4150 IF Reflchks(K)=0 THEN
4160 FOR M=This TO That
4170 IF Imarks(M)=1 THEN
4180 FOR N=This TO That
4190     Isetmark=1
4200     IF Imarks(N)=0 THEN Iskips=1
4210     NEXT N
4220 END IF
4230 NEXT M
4240 !
4250 !
4260 !
4270 !
4280 !
4290 IF Isetmark=1 AND Iskips=0 THEN Reflchks(K)=1!SKIP THIS IF NOT NECESSARY
4300 !
4310 END IF
4320 !
4330 !
4340 !
4350 !
4360     IF Iskips=0 AND Iskipb=0 THEN !IF WAVEFRONT IS NOT PARTIALLY REFLECTE
4370 !
4380 !
4390 !
4400     SLOPE OF PIECE OF WAVEFRONT IS YY/XX
4410 !
4420 !
4430     Yy=(Keep(1,This)+Addy(This))-(Keep(1,That)+Addy(That))
4440     Y1=itime(This)/Icrys(Keep(1,This),Keep(2,This))
4450     Y2=itime(That)/Icrys(Keep(1,That),Keep(2,That))
4460     Yy=Yy+Y1-Y2
4470     IF Imarks(This)=0 THEN
4480         Xx=(Ipermc(That)-Realad(That))-(Ipermc(This)-Realad(This))
4490     ELSE
4500         Xx=Realad(That)-Realad(This)
4510     END IF
4520     IF Xx>1 THEN
4530     FOR G=This TO That
4540     Add(G)=ABS(Yy/Xx) !FIGURE NEW DIRECTION
4550     Caxis(G)=Xx/Opl
4560     IF Kk=Piece-1 THEN Caxis(G)=Xx/(Ibeamf-(K*Opl))
4570     NEXT G
4580     PRINT Add(G-1)
4590     END IF
4600 !
4610 !
4620 !
4630 !
4640     FOR I=This TO That
4650         Icol=Keep(2,I)
4660         Irow=Keep(1,I)
4670         Imdex=Imdexp(I)
4680 !
4690 !
4700 !
4710         Itemp=Icol
4720         Realx=0
4730 !
4740 !
4750         CHECK FOR REFLECTION
4760 !
4770         IF Imarkb(I)=0 THEN
4780             FOR J=Irow TO Isize
4790                 Icrys(J,Itemp)=Imdex
4800                 Realx=Realx+Add(I)
4810                 Itemp=Icol-Realx
4810                 IF Itemp<0 THEN Itemp=0

```

```

4820         IF Itemp>Isize THEN Itemp=Isize
4830         Itrac(J,Itemp)=1
4840     NEXT J
4850     !
4860     !
4870     ELSE !INCIDENT BEAM DOMINATES
4880     FOR J=0 TO Irow
4890         Ichng=Irow-J
4900         !
4910         IF Itrac(Ichng,Itemp)=0 THEN
4920             Icrys(Ichng,Itemp)=Imdex
4930         ELSE
4940             Icrys(Ichng,Itemp)=Icrys(Ichng,Itemp)
4950         END IF
4960         !
4970         Realx=Realx-Add(I)
4980         Itemp=Icol-Realx
4990         IF Itemp<0 THEN Itemp=0
5000         IF Itemp>Isize THEN Itemp=Isize
5010     NEXT J
5020     END IF
5030     NEXT I
5040     END IF
5050     NEXT K
5060 END IF
5070 !
5080 !
5090 !
5100 ! CHECK FOR END OF RUN *****
5110 END WHILE
5120 T2=TIMEDATE
5130 PRINT TOTAL RUN TIME = ,T2-T1
5140 GCSUB 5360 !WRITE FILE TO DISK
5150 STOP
5160 ! SUBROUTINE TO INITIALIZE GRAPHICS
5170 GRAPHICS ON
5180 GCLEAR
5190 SHOW 0,Isize,0,Isize
5200 PLOT 0,0,-2
5210 FOR Q=0 TO Isize
5220     PLOT Q,0,-1
5230 NEXT Q
5240 FOR Z=0 TO Isize
5250     PLOT Isize,Z,-1
5260 NEXT Z
5270 FOR Q=Isize TO 0 STEP -1
5280     PLOT Q, Isize,-1
5290 NEXT Q
5300 FOR Z=Isize TO 0 STEP -1
5310     PLOT 0,Z,-1
5320 NEXT Z
5330 PLOT 0,0,-2
5340 RETURN
5350 ! SUBROUTINE TO OUTPUT FILE TO DISK
5360 MASS STORAGE IS : ,700,0
5370 CREATE BDAT Names,10404,2
5380 ASSIGN Path_1 TO Names
5390 OUTPUT Path_1, Iout
5400 ASSIGN Path_1 TO *
5410 RETURN
5420 ! SUBROUTINE TO OUTPUT FILE IF ERROR OCCURS
5430 MASS STORAGE IS : ,700,0
5440 CREATE BDAT Names,10404,2
5450 ASSIGN Path_1 TO Names
5460 OUTPUT Path_1, Iout(*)
5470 ASSIGN Path_1 TO *
5480 PRINT ERROR! PROGRAM TERMINATED
5490 T2=TIMEDATE
5500 PRINT TOTAL RUN TIME = ,T2-T1
5510 STOP

```

5520 RETURN  
5530 end



## LIST OF REFERENCES

1. Zeldovich, B. Y., Popovich, V. I., Ragulski, V. V. and Faizullov, F. S., "Connection between the wave fronts of the reflected and exciting light in stimulated Mandelstam-Brikouin scattering," *Zh. Eksp. Teor. Fiz. Pisma Red.* **15**, 160 (1972). (English translation: *Sov. Phys. JETP Lett.* **15**, 109 (1972).)
2. Feinberg, J., "Self-pumped, continuous-wave phase conjugator using internal reflection," *Opt. Lett.* **7**, 486 (1982).
3. Lam, J. F., "Origin of phase conjugate waves in self-pumped photorefractive mirrors," *Appl. Phys. Lett.* **46**, 909 (1985).
4. Biedowski, A., "Model of a degenerate four-wave mixing phase-conjugate mirror without slowly varying envelope approximation," *Opt. Comm.* **52**, 231 (1984).
5. Fisher, R. A., ed., *Optical Phase Conjugation*, Academic Press, 1983.
6. Hellwarth, R. W., "Generation of time-reversed wave fronts by nonlinear refraction," *J. Opt. Soc. Am.* **67**, 1 (1977).
7. Yariv, A. and Pepper, D., "Amplified reflection, phase conjugation and oscillation in degenerate four-wave mixing," *Opt. Lett.* **1**, 16 (1977).
8. Bloom, D. M. and Bjorklund, C. G., "Conjugate wave-front generation and image reconstruction by four-wave mixing," *Appl. Phys. Lett.* **31**, 592 (1977).
9. Hellwarth, R. W., "Theory of phase conjugation by stimulated scattering in a waveguide," *J. Opt. Soc. Am.* **68**, 1050 (1978).
10. Cronin-Golomb, M., Fischer, B., White, J. O. and Yariv, A., "Theory and applications of four-wave mixing in photorefractive media," *IEEE J. Quant. Elec.* **QE-20**, 12 (1984).
11. Gunter, P., "Holography, coherent light amplification and optical phase conjugation with photorefractive materials," *Phys. Rept.* **93**, 201 (1982).
12. Ashkin, A., Boyde, G. D., Dziedzic, J. M., Smith, R. G., Ballman, A. A., Levenstein, J. J., and Nassau, K., "Optically-induced refractive index inhomogeneities in  $\text{LiNbO}_3$  and  $\text{LiTaO}_3$ ," *Appl. Phys. Lett.* **9**, 72 (1966).

13. Chen, F. S., "A laser-induced inhomogeneity of refractive indices in KTN," *J. Appl. Phys.* **38**, 3418 (1967).
14. Glass, A. M., "The photorefractive effect," *Opt. Eng.* **17**, 15 (1978).
15. Yariv, A., *Optical Electronics*. Holt, Rinehart and Winston, 1985.
16. Fisher, R. A., Los Alamos National Laboratory, private communication, 18 February to 28 March, 1986.
17. Chen, F. S., "Optically induced change of refractive indices in  $\text{LiNbO}_3$  and  $\text{LiTaO}_3$ ," *J. Appl. Phys.* **40**, 3389 (1969).
18. Amodei, J. J., "Analysis of transport processes during holographic recording in insulators," *RCA Rev.* **32**, 185 (1971).
19. Klein, M. B. and Schwartz, R. N., "Photorefractive effect in  $\text{BaTiO}_3$  microscopic origins," *J. Opt. Soc. Am. B* **3**, 293 (1986).
20. Ducharme, S. D. and Feinberg, J., "Altering the photorefractive properties of  $\text{BaTiO}_3$  by reduction and oxidation at  $650^\circ\text{C}$ ," *J. Opt. Soc. Am. B* **3**, 283 (1986).
21. Staebler, D. L. and Amodei, J. J., "Coupled-wave analysis of holographic storage in  $\text{LiNbO}_3$ ," *J. Appl. Phys.* **43**, 1042 (1972).
22. Feinberg, J. and Hellwarth, R. W., "Phase-conjugating mirror with continuous wave gain," *Opt. Lett.* **5**, 519 (1980).
23. Chang, T. Y. and Hellwarth, R. W., "Optical phase conjugation and backscattering in barium titanate," *Opt. Lett.* **10**, 408 (1985).
24. Valley, G. C., "Competition between forward- and backscattering photorefractive scattering in  $\text{BaTiO}_3$ ," *J. Opt. Soc. Am. B* **4**, 14 (1987).
25. Jona, F. and Shirane, G., *Ferroelectric Crystals*, Macmillan Co., New York, 1962.
26. Wemple, S. H., Didomenico, M. and Camphouse, J. D., "Optical properties of melt-grown  $\text{BaTiO}_3$ ," *J. Phys. Chem.* **70**, 29 (1966).
27. Feinberg, J., "Photorefractive phase conjugation and the photorefractive effect," *J. Opt. Soc. Am.* **72**, 15 (1976).
28. MacDonald, K. R. and Feinberg, J., "Photorefractive phase conjugation with two coupled internal gratings," *J. Opt. Soc. Am.* **72**, 15 (1976).

AD-A184 697

DETERMINATION OF THE ORIGIN OF SELF-PUMPED PHASE  
CONJUGATION IN BARIUM TITANATE (U) NAVAL POSTGRADUATE  
SCHOOL MONTEREY CA T R MOORE JUN 87

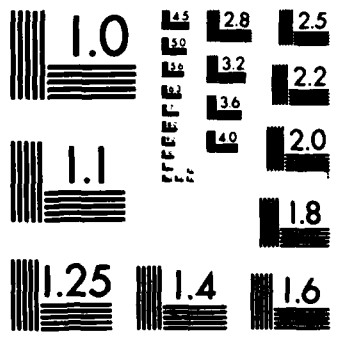
2/2

UNCLASSIFIED

F/G 20/2

NL





MICROCOPY RESOLUTION TEST CHART  
NATIONAL BUREAU OF STANDARDS-1963-A

29. Giuliano, C. R., Hughes Research Laboratories, private communication, March 3, 1987.
30. Pepper, D., Hughes Research Laboratories, private communication, May 18, 1987.
31. Chiao, R. Y., Garmire, E. and Townes, C. H., "Self-trapping of optical beams," *Phys. Rev. Lett.* 13, 479 (1964).
32. Campillo, A. J., Shapiro, S. L. and Suydam, B. R., "Periodic breakup of optical beams due to self-focusing," *Appl. Phys. Lett.* 23, 628 (1973).
33. Campillo, A. J., Shapiro, S. L. and Suydam, B. R., "Relationship of self-focusing to spatial instability modes," *Appl. Phys. Lett.* 24, 178 (1974).
34. Gunter, P., Voit, E., Zha, M. Z. and Albers, J., "Self-pulsation and optical chaos in self-pumped photorefractive BaTiO<sub>3</sub>," *Opt. Comm.* 55, 210 (1985).
35. Gauthier, D. J., Narum, P. and Boyd, R. W., "Observation of deterministic chaos in a passive nonlinear optical system," *Digest of the International Quantum Electronics Conference*, (Optical Society of America, Washington D.C., 1986) paper FHH4.
36. Pepper, D., "Observation of diminished specular reflectivity in self pumped photorefractive conjugators," *J. Opt. Soc. Am. B* 3, 33 (1986).
37. Nowak, A. V., Moore, T. R. and Fisher, R. A., "Variegated internal beam production in BaTiO<sub>3</sub> phase conjugators," *to be published*.
38. Moore, T. R., Nowak, A. V. and Fisher, R. A., "Internal beam patterns in barium titanate phase conjugators: Ring oscillations, half-rings, and translation-invariant patterns," *Digest of the International Quantum Electronics Conference*, (Optical Society of America, Washington D.C., 1986) postdeadline paper PD12-1.
39. Valley, G. C. and Dunning, G. J., "Observation of optical chaos in a phase-conjugate resonator," *Opt. Lett.* 9, 513 (1984).
40. Feinberg J. and Bacher, G. D., "Self-scanning of a continuous-wave dye laser having a phase-conjugating resonator cavity," *Opt. Lett.* 9, 420 (1984).
41. Whitten W. B. and Ramsey, J. M., "Self-scanning of a dye laser due to feedback from a BaTiO<sub>3</sub> phase-conjugate reflector," *Opt. Lett.* 9, 44 (1984).
42. MacDonald, K. R. and Feinberg, J., "Enhanced Four-Wave mixing by use of frequency-shifted optical waves in photorefractive BaTiO<sub>3</sub>," *Phys. Rev. Lett.* 55, 821 (1985).

## INITIAL DISTRIBUTION LIST

	No. Copies
1. Defense Technical Information Center Cameron Station Alexandria, VA 22304-6145	2
2. Library, Code 0142 Naval Postgraduate School Monterey, CA 93943-5002	2
3. CPT Thomas R. Moore P.O. Box 1205 Merritt Island, FL 32952	7
4. Professor D. L. Walters, Code 61We Naval Postgraduate School Monterey, CA 93943-5004	4
5. Professor K. E. Woehler, Code 61Wh Naval Postgraduate School Monterey, CA 93943-5004	1
6. Dr. R. A. Fisher Route 5 Box 230 Santa Fe, NM 87501	2
7. Mr. Robert T. Moore P. O. Box 1205 Merritt Island, FL 32952	1
8. Dr. Otis Peterson CLS-6 Los Alamos National Laboratory Los Alamos, NM 87545	1

END

10-87

DTIC